

**STRUCTURAL CONTROLS OF AURIFEROUS QUARTZ VEINS IN
THE KARIBIB AREA, SOUTHERN CENTRAL ZONE OF THE
PAN-AFRICAN DAMARA BELT, NAMIBIA**

by

Shawn Kitt

*Thesis presented in partial fulfillment of the requirements for the degree
of*



Master of Science
at Stellenbosch University

Supervised by Prof. Alex Kisters

December 2008

Declaration

By submitting this thesis electronically, I declare that the entirety of the work contained therein is my own, original work, that I am the owner of the copyright thereof (unless to the extent explicitly otherwise stated) and that I have not previously in its entirety or in part submitted it for obtaining any qualification.

Date: 22 December 2008

Copyright © 2008 Stellenbosch University

All rights reserved

ABSTRACT

Detailed geological mapping and a structural analysis of auriferous quartz veins were undertaken in the Karibib region of the Pan-African Damara belt in central Namibia. The study focuses on the formation and controls of quartz-vein sets and associated lode-gold mineralization in heterogeneous, siliciclastic- and marble- dominated amphibolite-facies host rocks around the Navachab gold mine and adjacent areas. Two main arrays of shallowly-dipping quartz veins can be distinguished that form a conjugate set. Steep, bedding-parallel and high-angle cross-cutting veins also occur, but play a subordinate role for mineralization. The orientation of the main conjugate set and progressive deformation of these quartz veins indicate that veining occurred during the late stages of the main phase of NW-SE directed, subhorizontal shortening (D2) and associated NW-verging folding and top-to-the-NW thrusting. Cross-cutting relationships with plutonic rocks indicate a timing of ca. 540 Ma for the mineralization.

The quartz veins sets show a consistent orientation irrespective of their location with respect to NE-trending, NW-verging first-order fold structures that were previously considered to be pertinent for the mineralization. The quartz vein sets also cross-cut different lithologies at high angles. This suggests that the regional strain (D2) was the first-order control of quartz vein formation. More localized lithological and/or structural controls played, however, an important factor for the formation of economic-grade mineralization. Thick and closely spaced quartz veins in steeply dipping rocks of the Navachab open pit form a more than 150m thick economic-grade vein swarm. In this structural situation and during layer-normal subhorizontal shortening, the host rocks experienced high extensional strains in a vertical direction, favouring the formation of subhorizontal extension fractures. The detailed mapping of veins discloses a regular or anticlustered spacing of veins. Individual veins show remarkably high aspect ratios, (> 1:1000) and straight-parallel sided geometries that can be followed for > 300 m in a down-dip direction. This suggests that vein growth was a competitive process between the nucleation of veins along earlier formed veins and fracture nucleation outside the stress shadow of veins. In contrast, quartz veins in the adjacent area of the shallowly-plunging hinge of the Usakos dome only show thinner quartz-vein swarms of < 50 m in thickness. This may be explained by lower vertical extensional

strains during D2 shortening in the hinge of the first-order fold, where the vertical stretch can still be accommodated by further tightening and amplification of the fold.

Massive sulphide lenses in the banded MC unit of the Navachab open pit are the alteration products of intersecting shallowly dipping sheeted quartz veins cross-cutting the intercalated marbles and calc-silicates. The orientation of shallow NE plunging ore shoots identified by exploration and mining corresponds to the intersection of the shallow dipping quartz veins with the steeply dipping bedding and the intersection of conjugate sets.

This comparative study of quartz veins in structurally diverse settings of the Navachab district has shown that lode-gold mineralization is not necessarily controlled by the orientation and kinematics of regional structures such as folds or shear zones. In this case, it is the regional strain that determines quartz vein formation, although localized lithological and/or structural controls may upgrade the mineralization (quartz-vein density) to economic grades. This represents an important perspective for regional exploration.

UITTREKSEL

Gedetailleerde geologiese kartering en 'n strukturele analise van gouddraende kwarts are is onderneem in die Karibib gebied van die Pan-Afrikaanse Damara gordel in sentrale Namibia. Die studie fokus op die vorming en kontroles van kwarts aar stelle en geassosieerde ertsaar-goud mineralisasie in heterogene, siliklastiese en marmer gedomineerde amfiboliet fasies gesteentes rondom die Navachab goud myn en omgewing. Twee hoof slagordes bestaande uit vlak hellende kwarts are kan onderskei word wat 'n vervoegende stel vorm. Steil laevlak ewewydige en hoë hoek dwarsnyende are kom ook voor, maar speel 'n ondergeskikte rol in die mineralisasie. Die orientasie van die hoof vervoegende stel en progressiewe deformatsie van die kwarts are dui aan dat die are gevorm is tydens die laat fases van die hoof stadium van noordwes-suidoos gerigte, subhorizontale vernouing (D2) en geassosieerde noordwes-gekantelde plooi en bokant-na-die-noordwes stootverskuiwing. Dwarssny verhoudinge met plutoniese gesteentes dui daarop dat mineralisasie plaasgevind het rondom 540 miljoen jaar gelede.

Die kwarts aar stelle toon 'n vaste orientasie ten spyte van ligging ten opsigte van noordoos-strekkende, noordwes-gekantelde eerste-orde plooi strukture wat voorheen beskou was as geskik vir die mineralisasie. Die kwarts aar stelle dwarsny ook verskillende litotipes met steil hoeke. Dit dui aan dat die regionale drukrag (D2) die eerste-orde kontrole was op vorming van kwarts are. Meer gelokaliseerde litologiese en/of strukturele kontroles was egter 'n belangrike faktor vir die vorming van ekonomiese graad mineralisasie. Dik en naby gespaseerde kwarts are in steil duikende gesteentes in die Navachab oop groef vorm 'n meer as 150m dik ekonomiese-graad aar swerm. In die strukturele toestand en gedurende gelaagdheid-normale subhorizontale vernouing, ondervind die gasheer gesteentes hoë uitstrekkende kragte in 'n vertikale rigting, wat die vorming van subhorizontale uitstrek frakture bevoordeel. Gedetailleerde kartering van are dui op 'n reëlmatige of anti-gebondelde spasieering van are. Individuele are beskik oor merkwaardige hoë aspek verhoudinge, ($> 1:1000$) en reguit-parallel kantige geometries wat gevolg kan word vir > 300 m in duik rigting. Dit dui aan dat aar groei 'n mededingende proses was tussen die ontstaan van are langs vroëer gevormde are en fraktuur vorming buite die druk skaduwee van are. In teenstelling, kwarts are in die aanliggende vlak duikende skarnier van die Usakos

koepel vertoon dunner kwarts-aar swerms van < 50m in dikte. Dit kan dalk verduidelik word deur laer vertikale uitstreckende kragte gedurende D2 verkorting in die koepel van die eerste orde plooi, wanneer die vertikale verlenging nog geakkomodeer was deur verdere digvouing en amplifikasie van die plooi.

Massiewe sulfied lense in die gebande MC eenheid van die Navachab oop groef is die veranderings produk van deurkruisende vlak duikende kwarts aar plate wat die tussengelaagde marmer en kalk-silikate dwarssny. Die orientasie van vlak noordoos duikende ertstroke wat deur eksplorاسie en mynbou geïdentifiseer is, stem ooreen met die deurkruising van vlak duikende kwarts are met steil duikende bedding en die interseksie van vervoegende stelle.

Hierdie vergelykende studie van kwarts are in strukturele uiteenlopende toestande in die Navachab distrik wys dat ertsaar mineralisasie nie noodwendig gekontroleer word deur die orientasie en kinetiesie van streek strukture soos plooië en skuifskere zones. In hierdie geval, is dit die drukkragte in die streek wat die kwarts aar vorming bepaal, alhoewel lokale litologiese en/of strukturele kontroles die mineralisasie (kwarts aar digtheid) mag opgradeer na ekonomiese grade. Dit verteenwoordig 'n belangrike perspektief vir eksplorاسie in die streek.

ACKNOWLEDGEMENTS

- Professor Alex Kisters, for basically, everything! For keeping the boat afloat, for never-ending enthusiasm, vision, inspiration, motivation, ideas, and meticulously reviewing every page. I owe you a lot of beer!
- Frik Badenhorst, for support, encouragement, discussions and keeping me on my toes. Thanks for generously giving me the time and logistical support from the start.
- Nick Steven, for many discussions in the field, office, “kegel bahn” and squash court. Your detailed geological maps are inspiring...your squash and kegel not so much.
- Bertie Roesener and Karl Hartmann, for many discussions and support in the field, office, and on the “kegel bahn”.
- Simon Brodie, for teaching me the tricks of his trade (Arcview).
- Gerald and Libania for never a dull moment.
- Everyone else, family and friends, who assisted in some way or another, thank you!
- “Hierdie een is vir my Ma”.

CONTENTS

DECLARATION	ii
ABSTRACT	iii
UITTREKSEL	v
ACKNOWLEDGEMENTS	vii
CONTENTS	viii
APPENDICES	ix
LIST OF FIGURES	xii
LIST OF TABLES	xiv
1. INTRODUCTION	1
1.1 Background and rationale	1
1.2 Location	2
1.3 Aims of this study	3
1.4 Methodology	4
2. REGIONAL GEOLOGICAL SETTING	6
2.1 The Damara Orogen	6
2.2 Geodynamic evolution of the Damara belt	6
3. LOCAL GEOLOGICAL SETTING	10
3.1 Lithostratigraphy	10
3.1.1 <i>Abbabis Metamorphic Complex</i>	11
3.1.2 <i>Etusis Formation</i>	11
3.1.3 <i>Chuosis Formation</i>	11
3.1.4 <i>Spes Bona Formation</i>	12
3.1.5 <i>Okawayo Formation</i>	12
3.1.6 <i>Oberwasser Formation</i>	12
3.1.7 <i>Karibib Formation</i>	13
3.1.8 <i>Kuiseb Formation</i>	13
3.2 Intrusive Rocks	13

3.2.1	<i>Syn-to post-tectonic granitoids in the area</i>	13
3.2.2	<i>Mafic rocks</i>	14
3.2.3	<i>Pegmatites and aplites</i>	14
3.3	Structure	15
3.3.1	<i>Fabric elements in the study area</i>	17
(a)	<i>Bedding (S0)</i>	17
(b)	<i>Secondary tectonic fabrics</i>	17
(c)	<i>Linear fabrics</i>	18
3.3.2	<i>Folding and transposition</i>	19
(a)	<i>F1 folding</i>	19
(b)	<i>F2 folding</i>	20
3.3.3	<i>Mon Repos Thrust Zone</i>	21
3.4	Metamorphism	21
4.	GEOLOGY OF THE NAVACHAB OPEN PIT	22
4.1	Structural geology of the Navachab open pit	29
4.2	Intrusive rocks in the Navachab open pit	30
4.2.1	<i>Metalamphyres</i>	30
4.2.2	<i>Pegmatites and aplites</i>	31
5.	QUARTZ VEINS IN THE NAVACHAB OPEN PIT	32
5.1	Data collection and analytical techniques	32
5.2	Sheeted quartz veins	39
5.2.1	<i>Geometry and morphology</i>	39
5.2.2	<i>Orientation of veins</i>	39
5.2.3	<i>Size of veins</i>	41
(a)	<i>Vein thickness</i>	44
(b)	<i>Vein spacing</i>	47
5.2.4	<i>Vertical extensional strain</i>	48
5.2.5	<i>Vein mineralogy and hydrothermal alteration</i>	48
5.2.6	<i>Vein textures</i>	51
5.2.7	<i>Massive sulphide veins</i>	53
5.3	Subordinate veins	56

5.4 Vein deformation	57
6. GEOLOGY OF THE NE PART OF THE USAKOS DOME	62
6.1 Structural geology of the NE part of the Usakos Dome	72
6.1.1 <i>Domain 1: The SE limb of the dome</i>	72
6.1.2 <i>Domain 2: The hinge of the dome</i>	73
6.1.3 <i>Domain 3: The NW limb of the dome</i>	75
7. QUARTZ VEINS IN THE NE PART OF THE USAKOS DOME	76
7.1 Data collection and analytical techniques	76
7.2 Sheeted quartz veins	77
7.2.1 <i>Geometry and morphology</i>	77
7.2.2 <i>Orientation of veins</i>	77
7.2.3 <i>Size of veins</i>	80
(a) <i>Vein thickness</i>	80
(b) <i>Vein spacing</i>	81
7.2.4 <i>Vein textures, mineralogy and hydrothermal alteration</i>	83
7.3 Subordinate veins	84
7.4 Vein deformation	85
8. DISCUSSION	87
8.1 Prerequisites for quartz veining: fluid pressures and effective stresses	87
8.2 Regional controls	88
8.3 Local controls	91
8.4 Controls on ore shoots	93
8.5 Quartz veins as strain markers	94
8.6 Previous models	96
8.7 Conceptual model	97
9. CONCLUSIONS	99

REFERENCES **102**

APPENDICES **108**

APPENDIX I Geological map of the NE part of the Usakos Dome.

APPENDIX II Navachab open pit sampling line vein data.

APPENDIX III Navachab open pit diamond drillhole data.

APPENDIX IV Anomaly 16 diamond drillhole data.

LIST OF FIGURES

1.1: Landsat TM7 image of the Usakos and Karibib domes	2
2.1: Simplified tectonostratigraphic map of the Damara Orogen	7
2.2: Schematic formline map of dome structures in the sCZ	9
4.1: View to the NNE of the Navachab Open Pit Mine	22
4.2: Plan map of the open pit showing the main lithological units	23
4.3: Detailed lithostratigraphic column through the lithologies in and around the Navachab open pit	24
4.4: Characteristics of the main rock types in the open pit	27
4.5: Photomicrographs of the main rock types in the open pit	28
4.6: Aplite and pegmatite dykes in the open pit	31
5.1: Plan map of the open pit, showing localities of mapped panels	33
5.2: Diagram of a typical line sample through shallow dipping sheeted quartz veins in the open pit	33
5.3: Simplified 3D panels of the northern, and parts of the eastern and western sidewalls of the Navachab open pit	35
5.4: Synoptic profile of the footwall schist in the open pit	36
5.5: Synoptic profile of the hangingwall schist and marbles in the open pit	37
5.6: Characteristics of sheeted quartz veins in the open pit	38
5.7: Profile of quartz veins and pegmatites in the Spes Bona Formation	40
5.8: Lower hemisphere, equal-area projection of conjugate quartz vein sets	42
5.9: Histogram of the thickness of sheeted veins in the open pit	45
5.10: Stick diagrams and staircase plots of sheeted quartz veins in the different lithological units of the open pit	46
5.11: Photomicrographs of alteration around veins in the open pit	50
5.12: Structural profile of the northern open pit wall showing quartz veining and alteration in the Okawayo Formation in the open pit	52
5.13: Massive sulphide alteration halos around quartz veins in the open pit	55

5.14: Isometric block diagrams illustrating the orientation and deformational behaviour of quartz veins in siliceous units	59
5.15: Isometric block diagrams illustrating the orientation and deformational behavior of quartz veins in marble units	60
5.16: Shallow northerly dipping and boudinaged quartz vein, showing well-developed necklines	61
6.1: Photograph of the NE hinge of the Usakos Dome	62
6.2: Geological map of the northeastern part of the Usakos Dome	63
6.3: Lithostratigraphic column of the SE limb of the Usakos Dome	64
6.4: Lithostratigraphic column of the NW limb of the Usakos Dome	65
6.5: Summary of the main rock types and styles of deformation in the NE part of the Usakos dome	69
6.6: Simplified structural formline map of the NE part of the Usakos Dome	70
6.7: Geological cross-sections (view to the NE) through the NE lobe of the Usakos dome	71
7.1: Lower hemisphere, equal-area projection of conjugate quartz vein sets measured in the Spes Bona Formation on the NE part of the Usakos Dome	77
7.2: Characteristics of quartz veins on the NE lobe of the Usakos Dome	79
7.3: Structural formline map of the Usakos dome with the relative abundance of quartz veins in the Usakos Dome	82
7.4: Photo and photomicrograph of alteration around vein in Spes Bona Formation schist and metapsammities	83
8.1: Simplified schematic sketch showing the proposed development of boudinaged shallowly dipping quartz veins and folding of subvertical dykes	95
8.2: Schematic sketch illustrating the conceptual model for the formation of auriferous quartz veins on the NW limb of the Karibib dome and NE hinge of the Usakos dome	98

LIST OF TABLES

3.1 Stratigraphy of the Damara Sequence in the study area	10
3.2 Summary of main fabric elements in the study area	16
5.1 Summary of vein data from sampling lines and drillcores from the open pit	43
7.1 Summary of vein data from drillcores from Anomaly 16	80

1. Introduction

1.1 Background and rationale

The term 'orogenic gold deposits' describes a deposit type characterized by structurally controlled gold-bearing quartz- and quartz-carbonate vein systems of hydrothermal origin (e.g. Groves et al., 1998, 2003; Kerrich et al., 2000). These deposits show a close temporal and spatial association to deformation and metamorphism during crustal convergence and collisional tectonics along Andean- or Himalayan-type plate margins (Goldfarb et al., 2001). Most of the auriferous quartz-vein systems of orogenic lode-gold deposits have formed in the brittle-ductile regime and under greenschist-facies or higher-grade metamorphic conditions. This corresponds to crustal depths where rock permeabilities are very low and the quartz-vein systems testify to the mainly fracture-controlled transport of fluids under these conditions (Sibson, 1996, 2001; Sibson and Scott, 1998). This also explains the significance of regional-scale and associated second- and third- order structures for the formation of the vein systems (e.g. Sibson et al., 1988; Hodgson, 1989; Cox et al., 1991, 1995; Ridley, 1993; Groves et al., 1998, 2003; Kerrich et al. 2000; Robert and Paulsen, 2001).

In the past two decades, or so, numerous studies have shown that the geometric and structural analysis of veins and vein systems in orogenic gold deposits is vital for our understanding of the evolution of hydrothermal vein systems and lode-gold deposits (e.g. Windh, 1995; Ridley and Mengler, 2000; Robert and Poulsen, 2001, and references therein; Schaub and Wilson, 2002). Most of these studies have demonstrated an intricate link between the formation of the vein systems and the regional and local structural evolution (Robert and Poulsen, 2001). Today, it is generally accepted that vein systems commonly comprise low-displacement faults or shears, interlinked by hydraulic extension fractures that originated from the infiltration of overpressurized fluids of metamorphic, magmatic and/or meteoric origin (Sibson and Scott, 1998). The vein systems represented high-permeability conduits that allowed for the episodic circulation and discharge of large volumes of fluids, also highlighting the interdependence between suprahydrostatic or lithostatic fluid pressures and deformation in the commonly mid-crustal environments (Etheridge et al., 1983; Cox et al., 1991; Sibson and Scott, 1998). In order to identify paleoplumbing systems that have

potentially channeled fluids, it is therefore crucial to establish the (1) structural setting, (2) orientation, distribution and kinematics of host structures such as faults, shear zones, lithological contacts or folds, and (3) veins and vein sets associated with these controlling structures.

1.2 Location

The Navachab gold mine (NGM), situated to the southwest of the small town of Karibib, is currently the only gold producing mine in Namibia (Fig. 1.1). Geologically, it is situated in rocks of the Damara Supergroup of the south Central Zone (sCZ) in the Pan-African Damara Belt, comprising a shelf- to continental slope-type host-rock sequence that is metamorphosed at amphibolite-facies conditions. The structural architecture of the area around the NGM is controlled by two doubly plunging anticlines, the Karibib and Usakos domes (Fig. 1.1).

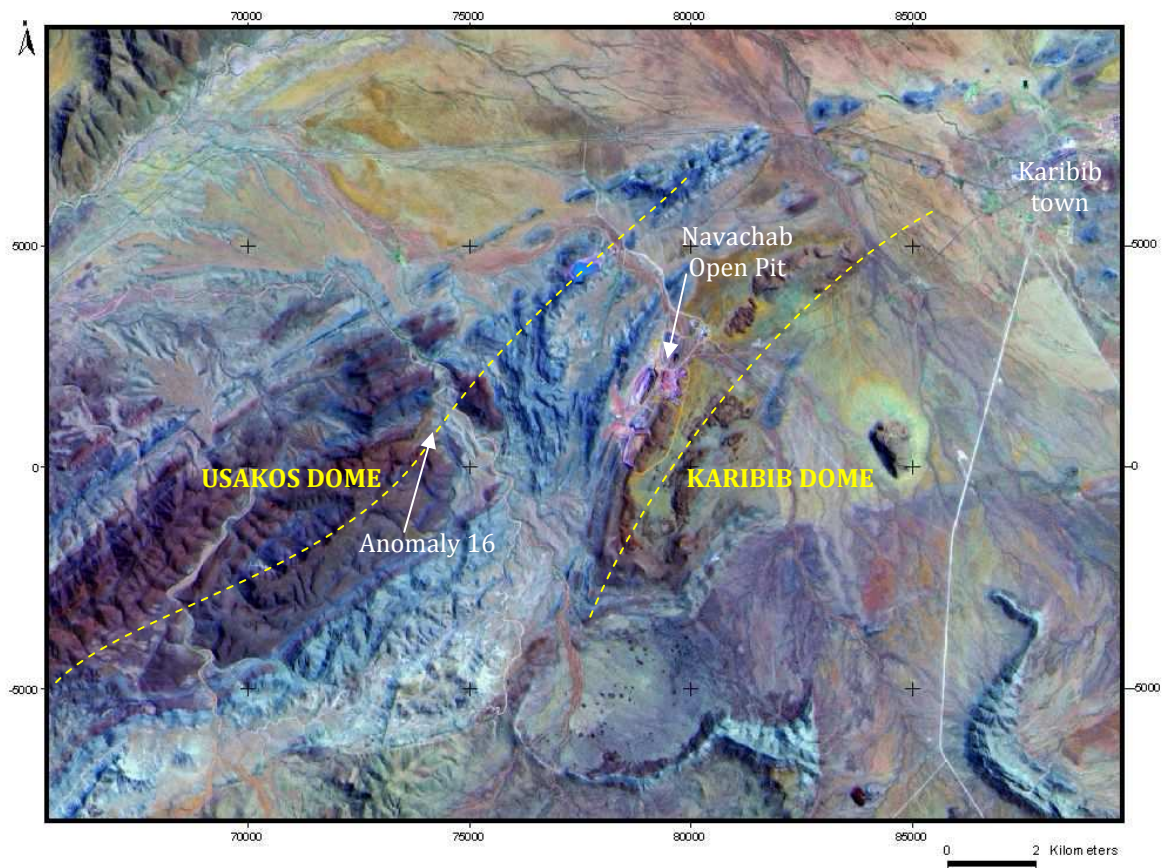


Fig. 1.1 Landsat TM7 image of the Usakos and Karibib domes showing the locations of the study areas. The axial traces of the domes are outlined in yellow.

Gold mineralization is hosted by a discordant system of sheeted quartz veins, as well as stratabound quartz-sulphide lenses. Earlier genetic concepts favoured a stratabound skarn model for the mineralization (e.g. Pirajno and Jacob, 1991; Nörtemann et al., 2000), but in recent years, most workers have agreed upon the discordant sheeted quartz veins being the main mineralizing system that show many similarities with orogenic lode-gold deposits (Moore and Jacob, 1998; Moore et. al., 1999; Steven and Badenhorst, 2002; Kisters, 2005). There are a number of prospects located in this area, centered around the Navachab Mine. This study focuses on two areas on the farm Navachab 58, including:

1) The open pit of the Navachab Gold Mine ($21^{\circ} 58' S$; $15^{\circ} 35' E$). The mine is situated approximately 8 km southwest of Karibib, on the steep northwestern limb of the Karibib dome.

2) The broad northeastern hinge of the Usakos dome centered around the prospect of Anomaly 16 ($21^{\circ} 59' S$; $15^{\circ} 43' E$). This area is situated approximately 15km southwest of Karibib, covering an area of roughly 5km by 7km that can only be accessed via small unpaved farm roads or dry river beds.

1.3 Aims of this study

The main aim of this study is to identify the controls of quartz veining in the region. In order to do this, the Navachab open pit and Anomaly 16 and surroundings were studied for their quartz-vein inventory. The Navachab open pit provides an almost complete 3D outcrop of the Damara Sequence and different quartz-vein geometries and sets. This allows for a comprehensive and semi-quantitative description of the quartz-vein system and its controls. Since Anomaly 16 and its surroundings are situated in a different structural setting compared to the Navachab open pit, a comparison between the quartz-vein inventories of the two should help to identify and distinguish regional from local controls of quartz veining and, thereby, contribute to a better understanding of the fluid-flow system on a regional scale.

In detail, the main aims of this study can be summarized as follows:

- a) To map and document the different lithologies and structures at (1) the Navachab open pit, and (2) Anomaly 16, documenting the lithological and structural inventory, also in order to establish the geological evolution of the two areas.
- b) Previous studies of quartz veining in the area (e.g. Steven and Badenhorst, 2002; Kisters, 2005) have mainly been descriptive. This study intends to present a semi-quantitative account of quartz veins by documenting their occurrence and orientation, density distribution (spacing, clustering, overlap of veins, etc.), the presence and controls of linear ore shoots, and the progressive deformation of auriferous quartz veins at the two selected localities.
- c) To determine the relative timing of the veins with respect to regional deformation by relating the local and regional controls to the formation and progressive deformation of quartz veins.
- d) To compare the evolution of auriferous quartz veins at the Navachab open pit with Anomaly 16. Both areas are found in different structural sites with respect to regional first-order structures so that similarities and/or differences in the quartz-vein inventory will hopefully allow a distinction between regional and local structural and lithological controls. The main questions to be addressed are: What are the main controls of quartz vein formation? Do lithological controls play a role, i.e. is there a difference in quartz-vein geometries and densities between different lithologies? Alternatively, are the controls mainly of a structural nature determined by (1) the regional strain/stress field, and/or (2) controlled by the location of quartz veins with respect to first- and second-order structures?

1.4 Methodology

Mapping in the open pit was done over a period of several months, but depended on and was often interrupted by the ongoing mining activities. Mapping of the different panels in the pit was done using detailed 1:200 scale base maps supplied by the Navachab survey department. Maps and panels presented here represent the status of the mining progress as by the 31 January 2007. In addition 7 diamond drill boreholes were

analyzed for their quartz vein contents and quartz vein distribution. Detailed core data are presented in Appendix III.

Mapping at Anomaly 16 was undertaken over a period of 6 months on a 1:10,000 scale on the northeastern part of the Usakos dome (Appendix I). The regional mapping focused on lithological contacts, compositional variations within formations and the structural geology of the area. At all times, specific attention was given to the occurrence, orientation and deformation of quartz veins in the area.

Before field work started, several days were spent on remote sensing and interpretation of digital Landsat TM7 satellite images using Arcview GIS technology. Mapping of the NE part of the Usakos dome was done using printed topographic maps, aerial photographs, and satellite imagery as base maps. In the following, the field maps were digitised using Arcview GIS. A Breithaupt structural compass was used to record structural readings. Over 2000 readings were taken in the Navachab open pit and at Anomaly 16. All planar elements are given as dip and dip direction and all linear elements as plunge and plunge direction.

Surface and relatively fresh samples of the main lithological units and quartz veins were collected in the field for petrographic work in order to characterize the main lithotypes as well as alteration features around quartz veins.

2. Regional geological setting

2.1 The Damara Orogen

Following the break-up of Rodinia, the Damara orogen of Namibia is the result of the amalgamation of Gondwana during the late Proterozoic and early Phanerozoic (Prave, 1996, Trompette, 1997). It forms part of the much larger Pan-African orogenic system that surrounds and transects the African continent (Porada, 1989). In Namibia, the Damara orogen can be subdivided into the N-S-trending coastal branches of the Kaoko and Gariep belts, and the NE-trending inland branch of the Damara belt.

The intracontinental Damara belt represents the collisional suture between the Congo and Kalahari cratons and chronicles a complete history from rifting and associated rift sedimentation and volcanism, via an oceanic stage and marine sedimentation through to convergence and final collision (Miller, 1983; Porada, 1989; Gray et al., 2006). It comprises a 400km wide, asymmetric, doubly vergent orogen, and can be subdivided into several tectonostratigraphic zones based on lithologies, deformation, metamorphic grade, magmatism and geochronology (Miller, 1983). From north to south, these include: the Northern Platform, the Northern Zone, the Central Zone (CZ), the Okahandja Lineament Zone, the Southern Zone, the Southern Marginal Zone and the Southern Foreland (Fig 2.1)

2.2 Geodynamic evolution of the Damara belt

The following section is a summary of the evolution of the Damara orogen. Detailed accounts of the tectonic and lithostratigraphic evolution of the Damara belt can be found in for example, Miller (1983), Porada (1989), Stanistreet et al. (1991) and Gray et al. (2006).

The deposition of the Damara Supergroup was initiated by continental rifting along a triple junction between the Congo, Kalahari and Rio de la Plata Cratons (Miller, 1983; Porada, 1989). Rifting was already in progress by ~750Ma as is evident from radiometric ages of rhyolitic volcanics ($746 \pm 2\text{Ma}$) and quartz syenite plugs ($756 \pm 2\text{Ma}$) in the sedimentary sequence (Hoffman et al. 1996). In the CZ of the Damara belt, this led to the deposition of the basal continental sediments and volcanic rocks of the Nosib Group.

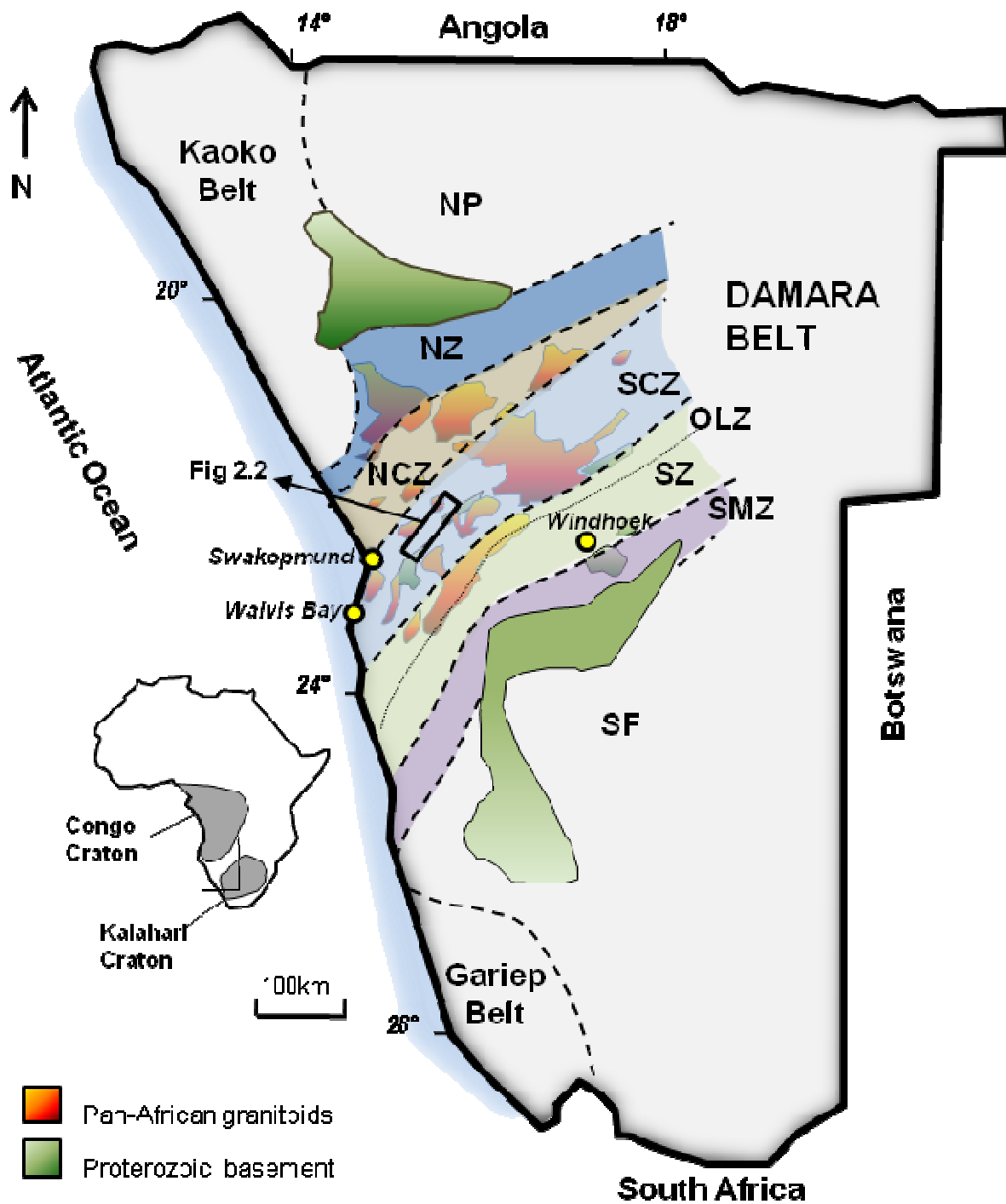


Fig. 2.1 Simplified tectonostratigraphic map of the Damara Orogen in Central Namibia (after Miller, 1983). NP: Northern Platform; NZ: Northern Zone; NCZ: Northern Central Zone; SCZ: Southern Central Zone; OLZ: Okahanja Lineament Zone; SZ: Southern Zone; SMZ: Southern Margin Zone; SF: Southern Foreland.

These rift-type siliciclastics and alkaline volcanics rest unconformably on mainly Mesoproterozoic, ca. 1.8-2.0 Ga gneisses of the Congo Craton (Jacob et al., 1983). Prolonged rifting led to the development of two deep-water basins and associated marine sedimentation in the proto-Atlantic Adamastor ocean, now preserved in the Kaoko and Gariiep belts, and the NE trending Khomas Sea between the Congo and Kalahari Cratons. Marine sedimentation continued until ca. 580-600 Ma when crustal convergence between the Congo and Kalahari Cratons led to the closure of the Khomas sea (Gray et al., 2006). In the Damara belt, convergence can be attributed to the N-ward subduction of the Kalahari craton underneath the Congo craton (Miller, 1983). Shallow- to deep-marine carbonate and turbidite sedimentation dominated along the southern margin of the Congo Craton, which led to the deposition of the thick, mixed carbonate-siliciclastic succession of Swakop Group in the CZ (see Table 3.1 for details on the Swakop Group). The Kalahari Craton continued to be a major source of siliciclastic sediments, now preserved as the thick succession of monotonous turbidite sequences of the Southern Zone that are interpreted to represent accretionary prism deposits lying above the downgoing plate of the Kalahari Craton (Stanistreet et al., 1991).

Crustal convergence between ca. 580-550Ma was associated with the development of a regional bedding-parallel (S1) fabric, and large-scale thrusting and recumbent folding (D1) (Miller, 1983). Numerous, though relatively small gabbroic, dioritic and syenitic plutons intruded throughout the central Damara belt during this phase of crustal convergence (Jacob et al., 2000; de Kock., 2000). The subsequent high-angle collision between the Kalahari and Congo Cratons led to the formation the main regional NE-trending structural grain in the Central Zone around 550-540Ma (Miller, 1983; Gray et al., 2006). The main phase of regional-scale fold-and-thrust tectonics (D2) can be attributed to this stage, resulting in the bivergent structure of the Damara belt. The characteristic regional-scale dome structures and intervening synclines of the CZ formed during this time (Fig 2.2). The collisional stage also marks the widespread intrusion of syntectonic granites, including the I- and S-type Salem-type granites as well as highly differentiated garnetiferous leucogranites (Miller, 1983; Jung et al., 2001; Johnson et al., 2006). Collisional tectonics were associated with a high-P, low- to medium T metamorphism (P: 6-8kbar, T: 400-600°C) in the Southern Zone, the accretionary wedge of the orogen, and a medium P, medium T metamorphic event (M1)

in the Central Zone (Nex et al., 2001), the timing of which is only poorly constrained between ca. 570-535 Ma.

The late- and post-collisional evolution of the Damara belt and the CZ, in particular, is characterized by a complex thermal history (Jung et al., 2001; Jung and Mezger, 2003). The thermal peak in the CZ of the Damara belt was reached well after the main phase of crustal thickening between ca. 535-500 Ma. This high-T, low-P metamorphism (M2) was episodic and resulted in late- to post-tectonic partial melting of parts of the CZ and the late- to post-tectonic emplacement of mainly S-type leucogranites over an area of > 70,000 km² in the CZ and Northern Zone. Ar-Ar geochronology records a differential uplift and cooling history for different parts of the orogen. In the CZ, cooling through ca. 300°C is recorded between 480-465 Ma, coinciding with the last phases of post-tectonic granite plutonism.

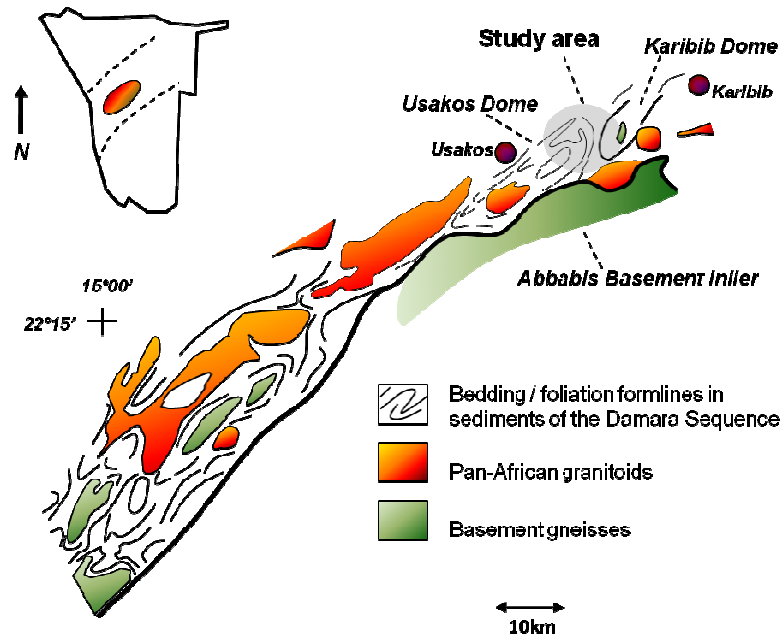



Fig.2.2. Schematic formline map showing the regional-scale northeast trending dome structures in the SCZ. Note how most of the domes are cored by basement gneisses or Pan-African granitoids, with the Damara sequence draped around the domes (after Kisters et. al., 2004).

3. Local geological setting

3.1 Lithostratigraphy

Both the Navachab open pit and Anomaly 16 are situated in rocks of the Neoproterozoic Damara Supergroup (Miller, 1983). This study follows the stratigraphy outlined by Badenhorst (1992) for this part of the sCZ in the Damara Belt shown as a simplified lithostratigraphic column in Table 3.1. The lithostratigraphic columns also show a general correlation of the main formations between the Navachab open pit and Anomaly 16, but with distinct facies and thickness variations so that the detailed lithostratigraphies of the two areas and petrography of rocks will be dealt with separately in chapters 4 and 6. This chapter provides a general overview of the lithostratigraphy.

Table 3.1 Stratigraphy of the Damara Sequence in the study area (modified from Badenhorst, 1992).

	Group	Formation	Lithologies	Age
DAMARA SEQUENCE	SWAKOP GROUP	Kuiseb	<i>Biotite-muscovite schists with cordierite porphyroblasts, metapsammites and intercalated biotite schists.</i>	
		Karibib	<i>Massive and banded, grey and white calcitic and dolomitic marbles with finely intercalated calc-silicates and marble breccia horizons.</i>	
		 Oberwasser	<i>Dark grey biotite and biotite-cordierite schists, calc-silicate felses, minor carbonate breccia horizons, including glaciomarine pelites and dropstone units of the Ghaub Formation and interbedded amphibolites of the Daheim Member in the upper parts of the unit.</i>	635.5±1.2 Ma (Hoffmann, 2004)
		Okawayo	<i>Calcitic and dolomitic marbles and intercalated calc-silicate felses, locally intruded by mafic sills and dykes</i>	
		Spes Bona	<i>Dark grey biotite and biotite-cordierite schists, calc-silicate felses with minor amphibolites, metapsammites and marbles.</i>	
		Chuosis	<i>Glaciomarine diamictite</i>	746±2 Ma (Hoffman et al., 1996)
	Nosib Group	Etusis	<i>Well-bedded reddish-pink feldspathic quartzites, arkoses, conglomerates and minor metavolcanics</i>	
Abbabis Basement			<i>Pink and grey quartzo-feldspathic augengneisses, schists, amphibolites and pegmatites</i>	1925Ma ±330 Ma (Jacob et. al., 1978)

3.1.1 Abbabis Metamorphic Complex (AMC)

The oldest rocks in the region are the pink and grey, commonly reddish weathering quartzo-feldspathic augengneisses, schists, amphibolites and pegmatites of the *Abbabis Metamorphic Complex (AMC)* (Miller, 1983; Brandt, 1987; Steven, 1993). The basement-gneiss lithologies were first recognized on the farm Abbabis 70, approximately 15km SW of Navachab (Gevers, 1931), and have subsequently been described by various authors (Jacob et al., 1978; Brandt, 1985, 1987; Miller, 1983; Kröner, 1991; Steven, 1993). U-Pb zircon ages from gneisses of the AMC yielded minimum ages of $1925\text{Ma} \pm 330\text{ Ma}$ (Jacob et. al., 1978). Subsequent single-grain and conventional zircon dating of basement gneisses in the lower Khan River near the Rössing Uranium Mine demonstrated the widespread presence of Palaeoproterozoic basement as reflected by xenocrystic grains with ages $2014 \pm 39\text{Ma}$ and $2093 \pm 51\text{Ma}$ (Kröner et. al., 1991). At Navachab, the AMC is exposed in an erosional window in the core of the Karibib dome to the SE of the Navachab open pit.

3.1.2 Etusis Formation

Feldspathic quartzites, arkoses, and minor metavolcanics of the *Etusis Formation* form the lowermost formation of the Damara Supergroup. This sequence is commonly interpreted to represent the rift-type succession of the Damara belt (Miller, 1983). In the Karibib dome, the supracrustals unconformably overlie the AMC and represent a sequence of fluvio-deltaic to aeolian sediments derived from pre-existing granitic basement (Miller, 1983). The formation has a diagnostic reddish-pink appearance, with locally well-developed m-scale cross beds and channel-fill conglomerates. The Etusis Formation forms prominent ridges to the southeast of the Navachab open pit, where it attains a thickness of up to 1500m, but is not exposed in the Usakos dome.

3.1.3 Chuos Formation

Overlying the Etusis Formation are the diamictites and dolomitic marker horizons of the *Chuos Formation*. The Chuos Formation consists of a matrix-supported mixtite with a wide variety of clasts ranging from schist, quartzite, granite and pegmatite, set in a matrix of greenish calc-silicate bearing schist (Badenhorst, 1987). Glaciogenic diamictites of the Chuos Formation can be related to the global Sturtian glaciations in the late-Neoproterozoic, with a maximum age constraint of $746 \pm 2\text{ Ma}$ from underlying

volcanics in the Nosib Group (Hoffman et al., 1996). In the Karibib dome, the Chuos Formation reaches a thickness of between 45 and 180m.

3.1.4 Spes Bona Formation

The overlying *Spes Bona Formation* is a mainly metapelitic succession, comprising banded biotite and biotite-cordierite schists and calc-silicate felses with minor amphibolites, metapsammities and marbles. The thicknesses of individual beds are between 0.5cm and 50cm for the calc-silicate felses, and 0.5cm to up to 15m for the schists. Locally, primary sedimentary features such as ripple-marks or cross-beds are well preserved. The mainly metapelitic and metapsammitic nature of the Spes Bona Formation suggests a turbidite-like origin for the sequence. The thickness of the Spes Bona Formation varies dramatically from < 20 m on the SE limb of the Karibib Dome, to ca. 150-200m in the Navachab open pit, to > 600 m in the Usakos Dome. This may suggest structural contacts with the under- and overlying rocks (Kisters et al., 2004).

3.1.5 Okawayo Formation

The Spes Bona Formation is overlain by calcitic and dolomitic marbles and intercalated calc-silicate felses of the *Okawayo Formation*. The formation can be subdivided into an intercalated calc-silicate and calcitic marble in its lower parts, and a calc-silicate free upper dolomitic part. Calcitic marbles are commonly blue-grey to light-grey or white. Dolomitic marbles are creamish on surface but white-grey when fresh. Calc-silicate felses are brownish-red on surface, but greenish to grey when fresh. Individual calc-silicate layers vary from 1 to 10cm in thickness. The marbles may be massive or banded and intercalated sedimentary marble breccias occur locally. The Okawayo Formation ranges in thickness from 80 m in the Karibib dome to up to 150 m in the Usakos dome.

3.1.6 Oberwasser Formation

The overlying *Oberwasser Formation* is up to 160 m thick and consists of a banded siliciclastic sequence of dark grey biotite and biotite-cordierite schists, calc-silicate felses, minor carbonate breccia horizons and, in its upper parts, interbedded amphibolites of the Daheim Member (Badenhorst, 1992) that represent mafic volcanic rocks. It forms the hangingwall sequence to the main orebody at Navachab and is compositionally very similar to the Spes Bona Formation. Hoffmann et al. (2004)

interpreted numerous clasts of dolostone, granite and quartzite in thin-bedded metapelites within the Oberwasser Formation to be glacio-marine in origin. U-Pb zircon dating of thin volcanic ash beds within the same facies constrain the deposition of the sediments to 635.5 ± 1.2 Ma (Hoffmann et al., 2004). This is the first robust age for the Marinoan-type glaciations.

3.1.7 Karibib Formation

The *Karibib Formation* forms the uppermost sequence in the vicinity of the Navachab open pit, and consists of massive and banded, grey and white calcitic and dolomitic marbles. Up to several meter thick marble breccia horizons and finely intercalated calc-silicates are developed throughout the succession. The marble breccias are sedimentary breccias and occur as prominent marker horizons in the field. In the Navachab area, the Karibib Formation attains a thickness of at least 500m, forming most of the high mountains to the west of the open pit.

3.1.8 Kuiseb Formation

The *Kuiseb Formation* represents the uppermost formation of the Damara Supergroup in the Karibib region. It is made up of a basal part consisting of quartz-biotite-muscovite schists with cordierite porphyroblasts, which grade upwards into thick (20-50 m) metapsammites and intercalated biotite schists. Towards the upper stratigraphic levels, a thick unit of biotite schist±cordierite intercalated with thin calc-silicate layers, dominates the Kuiseb Formation. Its upper contacts are eroded so that a total thickness cannot be established. At Navachab, the Kuiseb Formation forms only a small, ca. 15 m thick outlier to the NW of the open pit, but is more prominently developed in the western parts of the mapped area. However, only the lower parts of the > 1000m thick Kuiseb Formation are preserved.

3.2 Intrusive rocks

3.2.1 Syn- to post-tectonic granitoids in the area

To the S and SE of the Navachab open pit, the Damara Supergroup has been intruded by various syn- to post-tectonic granitoids. These include diorites and granodiorites of the Mon Repos diorites, part of the Goas Dioritic Suite, and the Rote Kuppe monzogranite

(Jacob et al. 2000). The nearest contact of these granitoids is within 5 km from the open pit.

The Mon Repos diorites and granodiorites occur as large, zoned plutons 5 km south of the mine. The Mon Repos diorites and granodiorites are medium- to dark-grey in colour, consisting of hornblende, plagioclase, quartz, and microcline as the main constituents, with minor biotite, titanite, apatite and zircon (Jacob et. al., 2000). Magmatic fabrics are widespread in the central parts of the plutons, overprinted by contact-parallel solid state fabrics in the marginal parts of the plutons. The *Rote Kuppe monzogranite* forms a prominent inselberg 4km east of the mine, but numerous whaleback-like granite outcrops in the low-lying alluvial plains indicate the much larger extent of this granite. The main variety of the Rote Kuppe monzogranite is medium grained with anhedral quartz, pinkish microcline and white plagioclase, with minor biotite, and accessory muscovite and Fe-oxide (Jacob et al., 2000).

From crosscutting relationships, it is evident that the Mon Repos diorites are older than the Rote Kuppe monzogranite. Recent SHRIMP U-Pb dating of single zircons by Jacob et al. (2000) are consistent with the field relationships and yield ages of ca. 550Ma for the Mon Repos diorites and ca. 540Ma for the Rote Kuppe monzogranite.

3.2.2 Mafic rocks

Several sills and dyke-like mafic rocks occur in the area and are intrusive into the Damara Supergroup. The Okawayo Formation in the Navachab open pit is intruded by prominent metalamprophyric sills, locally with dyke-like offshoots into the overlying Oberwasser Formation. The lamprophyre intrudes along the contact between a calc-silicate rich unit at the base of the Okawayo Formation (the MC unit, chapter 4) and overlying dolomitic marbles (MDM unit, chapter 4). It also occurs in the schists of the Spes Bona Formation to the north of the open pit.

3.2.3 Pegmatites and aplites

Numerous generations of pegmatites and aplites can be distinguished in the region and around the Navachab open pit. In the open pit, subvertical, mainly NW-trending pegmatite dykes are commonly restricted to the siliciclastic units of the Spes Bona

Formation, while being almost absent in the marble units of the Okawayo Formation. Thicknesses range from 5cm to 5m. Based on cross-cutting relationships and the deformation of the intrusives, early-tectonic dykes (pre-D2) can be distinguished from syn- to late tectonic (D2) dykes. Pre-D2, folded and boudinaged dykes are e.g. found between the Spes Bona and Chuos Formations and also in the Okawayo Formation.

3.3 Structure

The main structural elements in the study area are summarized in Table 3.2. The terminology and conventions used are:

- S: planar penetrative fabrics
- L: linear penetrative fabrics
- F: folding of planar and linear fabrics
- D: deformation phase

Suffixes 1, 2, 3 etc. denote the structural order based on cross-cutting and overprinting relationships. S0 always refers to bedding; S1 to the first recognizable penetrative fabric as a result of a first deformation phase (D1) etc. Structural data displayed on stereographic projections are plotted on the lower hemisphere of an equal-area stereonet (Schmidt projection).

Recent structural studies in the Karibib region have recognized two main deformation phases, D1 and D2 (Kisters et. al., 2004; Johnson, 2005), although D2 related structures and fabrics form part of a progressive deformation event. A bedding parallel and subparallel foliation is correlated with an early deformation phase, D1. Rare recumbent intrafolial folds in marbles are evidence for D1 transposition of the primary bedding. During the second deformation phase (Miller's D3 phase; D2 in this study), the bedding and bedding parallel foliation (S1) were refolded around large NE trending domal structures. Johnson (2005) further subdivided the D2 phase into a D2 earlier and D2 late phase. However, this subdivision is unique to the southwestern lobe of the Usakos dome and was not observed in the study area. In addition to bedding, two penetrative planar fabrics S1 and S2 can be distinguished in the study area. Linear fabric elements include mineral stretching lineations, intersection lineations and the preferred

orientation of the long axis of stretched breccia clasts. Other linear elements include fold hinges, and the necklines and long axes of boudins.

Table 3.2. Summary of main fabric elements in the study area.

DEFORMATION PHASE	STRAIN REGIME	FABRIC ELEMENT	FABRICS
			Field expression, orientation and occurrence
Primary		S0	Primary compositional layering, cross-bedding in siliciclastics
D1	Low angle shearing	S1	Penetrative bedding-subparallel foliation in schistose units and transposition of bedding in marbles
		F1	Intrafolial folds in Okawayo Formation marbles
D2	Top to northwest thrusting and associated northwest-verging folding	S2	Subvertical to steep SE dipping, NE trending axial planar foliation
		F2a	1st order domes: Kilometer scale NW vergent, NE trending double plunging Karibib and Usakos domes
		F2b	Lower order fold structures: Hundreds of meter to centimeter scale NE trending lower order folds
		L2t	Moderately SE plunging lineation on bedding planes of marbles on the SE limb of the Usakos Dome.
		L2m	Shallow NE-SW plunging mineral lineation and mineral stretching lineation, including stretched clasts in marble breccias.
		L2i	Shallow NE-SW plunging intersection lineation between S0/S1 and S2
		L2f	Shallow NE-SW plunging fold axis of lower order parasitic folds

3.3.1 Fabric elements in the study area

(a) *Bedding (S0)*

Bedding is preserved on all scales and most evident between e.g. different formations of the Damara Supergroup, but also within the lithologically heterogeneous formations. On a regional scale, lithological variations are easy to recognize on satellite images and aerial photographs. In the field, the preservation of primary structures varies mainly as a result of the strain intensity as subsequent deformation may, in places, modify or obliterate primary structures due to intense fabric development or fabric transposition. There are systematic variations in strain intensity throughout the area that vary (1) with rock type, i.e. strain is localized and partitioned into less competent, commonly carbonate or micaceous units, whereas competent units such as calc-silicate felses, metapsammites or amphibolites tend to preserve primary structures, and (2) with the location of area with respect to first- and second-order structures.

Compositional variations and primary sedimentary features are well-preserved in schists, metapsammites and calc-silicate felses of the Spes Bona and Oberwasser Formation. Alternating grey and dark grey banding in schists, ripple marks on bedding planes of metapsammites and cross-beds in calc-silicate felses are interpreted as primary structures. In marbles, primary sedimentary features have, in places been obliterated by metamorphic recrystallization and ductile deformation. For the most part, however, compositional contrasts are well displayed by intercalated marbles and calc-silicate bands, alternating grey and dark grey banding in banded marbles, the presence of distinct breccia marble horizons as well as dolomitic and calcitic marbles that all reflect the original compositional layering. Extensive bedding transposition in high-strain areas may have created a pseudostratigraphy.

(b) *Secondary tectonic fabrics (S1 and S2)*

The earliest deformation fabric (S1) in the study area is the result of the preferential alignment of biotite, forming a penetrative bedding-subparallel foliation in the metapelitic units. Where cordierite porphyroblasts are present, the S1 foliation shows a gently undulating geometry, wrapping around the cordierite porphyroblasts. Centimeter- to several m-scale, tight- to isoclinal, intrafolial folds in schists provide evidence for the transposition of bedding into the S1 fabric. Drillcore intersections show

a considerable amount of strain localization into the strongly foliated schistose units during the D1 deformation, while e.g. metapsammites and calc-silicate felses preserve intricate sedimentary details that indicate much lower internal strain intensities in the more competent units. Marble units lack micas and, in general, minerals that may define the S1 foliation. In addition, evidence of the early S1 foliation is likely to have been obliterated as a result of the pervasive recrystallization that has affected the marble units. However, evidence for the early D1 event can be found in rare intrafolial folds in marbles of the Okawayo Formation, and this may account for the often discontinuous extent of some marble horizons. On a regional scale, the development of S1 is heterogeneous and mainly confined to the lower units of the Damara Supergroup and up to the Okawayo Formation. Rocks of the Oberwasser and Karibib Formations are largely devoid of D1-related fabrics. Kisters et al. (2004) related S1 development, associated truncation of marker layers in e.g. the Etusis and Chuos Formations and dramatic along-strike thickness variations of units to the presence of low-angle D1 shear zones.

A steep SE dipping, NE-SW trending penetrative foliation (S2) in the study area is related to a second deformation event (D2). The S2 foliation is axial planar to the first-order, northwest-verging dome structures of the Karibib and Usakos domes (F2, chapter 3.3.2) and associated lower-order F2 folds, and dips steeply to the SE. Good examples of crosscutting relationships between S2 and S0/S1 are found in the hinge of the 1st order fold of the Usakos dome and also in tight 2nd order folds. The S2 fabric is more subtle on the limbs of folds, and may be difficult to distinguish from S0/S1 where the latter is steep. In marbles, the S2 foliation is manifested as dark-grey pressure solution seams and S2-parallel flattened breccia clasts in intraformational marble breccias. In addition, this study has identified NE trending and up to 100 m wide high-strain zones preferentially developed in marbles of the thick Karibib Formation on the NW limbs of the Karibib and Usakos domes. These mylonitic zones are interpreted as being D2 related (chapter 3.3.2).

(c) Linear fabrics (L2)

In the study area, four different types of lineations occur (Table 3.2), including mineral stretching lineations and the preferred orientation of marble breccias clasts,

intersection lineations, orientation of the long (y-) axis of boudins and plunges of folds. Almost all of the linear elements in the study area are associated with the regionally developed D2 phase of deformation and are referred to as L2 (Table 3.2).

The structural grain in the study area is dominated by a shallow NE and SW plunging lineation, L2. In the siliciclastics the L2m lineation is manifested by the preferred alignment of stretched biotite flakes and the stretching and preferred orientation of strain shadows around cordierite porphyroblasts. Recrystallization of the marbles has made the recognition of mineral stretching lineations difficult, and most of the L2 lineations that were documented in the study area are intersection lineations (L2i) between S0/S1 and S2. However, an L2m stretching lineation is defined by the preferred orientation of stretched marble clasts in the intraformational marble breccias. The plunge of most of the folds observed in the study area was categorized under L2f.

A second moderately northwest-southeast plunging lineation (L2t) occurs in the study area. The lineation is rare and only weakly developed on the weathered surfaces of S0/S1 planes of marbles. However, the intersection of steeply dipping quartz gashes and S0/S1 planes in calc-silicates and schist, forms a visible intersection lineation with similar L2 plunge as the lineation in the marbles. A prominent northwest-southeast lineation also occurs on the vein surfaces of shallow dipping quartz veins in metapsammities.

3.3.2 Folding and transposition

Folding, on all scales, is probably the most prominent structural feature that characterizes the geology of the Karibib area. Based on their orientation and relationships to planar and linear fabrics, two main fold generations, F1 and F2, can be distinguished.

(a) F1 folding

Intrafolial folds in the hinge zone of the Usakos Dome with subhorizontal fold axis are interpreted as F1 folds related to an earlier D1 deformation event (chapter 3.3.1b). Typically, F1 folds occur as small (cm- to m-scale) isoclinal, intrafolial folds that refold the compositional bedding (S0), but folds with half-wavelengths of up to 10m have been

recognized in this study. F1 folds are most easily recognized in marbles of the Okawayo Formation around the hinge of the Karibib and Usakos Dome, defined by the folding of calc-silicate felses in the grey, banded marble units. The F1 folds are refolded by later upright to NW-verging F2 folds.

(b) F2 folding

The study area is dominated by NE-trending, NW-verging folds that refold the bedding and the S0/S1 foliation. This NE-trending fold pattern (F2) is characteristic for the CZ of the Damara belt and is related to the D2 deformation event (Jacob, 1974; Kisters et. al., 2004; but D3 after Miller, 1983).

In the study area, the F2 folding can be subdivided according to scale:

- (a) The first-order folds in the region are the doubly-plunging NE trending Karibib and Usakos domes that have half-wavelengths of ca. 5km. The domes are asymmetric and verge to the NW, consisting of a shallower SE limb and a steep-to overturned NW limb.

- (b) The NW limb of the Usakos dome is made up of tight, upright- to NW verging 2nd-order folds with half-wavelengths of between 400m and 600m.

- (c) Parasitic lower order folds have the same geometry as the 1st order structures. Typically, the parasitic folds are tighter and more pronounced in the banded marbles and on the hinge zones of 1st and 2nd order fold structures. Spectacular examples of F2 folding are preserved in the banded marbles of the Karibib Formation.

Evidence for major transposition of bedding was recorded in the upper parts of the marbles of the Okawayo Formation, and in the basal Karibib Formation. Transposition folds show shallow northeasterly plunges similar to the first- and lower-order F2 folds. In the field, the pseudostratigraphy can easily be mistaken for bedding. The largely symmetrical folding and chocolate-tablet type boudinage of competent horizons contained within the transposed fabric indicate that the high-strain zones record a largely coaxial flattening strain normal to the transposition fabric and the NE strike.

The layer-normal flattening strains together with the NE strike and steep- to subvertical dips suggest that the up to 100m wide corridors of fabric transposition are related to the D2 formation. They have the orientation of regional scale crenulation foliations, being axial planar to the first-order F2 folds in the intervening areas.

3.3.3 Mon Repos Thrust Zone - MRTZ

The presence of a regional-scale thrust zone straddling the SE limbs of the Karibib and Usakos domes is indicated by the juxtaposition of basement gneisses of the AMC and rocks of the Etusis Formation against marbles of the Karibib Formation along a steep SE dipping sharp contact (Kisters et al., 2004). This suggests a thrust contact along which basement gneisses and the lowermost parts of the Damara Supergroup were thrust over the upper formations of the Damara sequence. The thrust trends NE-SW and can be traced for at least 40 km along strike, overriding the shallowly-dipping SE limbs of the Usakos and Karibib Domes that, in fact, represent the footwall of the thrust. The presence of a thrust is furthermore suggested by up to km-scale allochthonous rocks of e.g. the Chuos Formation that occur as high-strained, elongated blocks within the pervasively recrystallized and bleached marbles of the Karibib Formation. Kinematic indicators, lineations and also the NW vergence of regional fold structures suggest a top-to-the-NW transport along the MRTZ.

3.4. Metamorphism

The sCZ is characterised by a high temperature, low pressure metamorphism at granulite-facies grades in the southwest (T estimates between 700°C and 800°C at 4-5 kbar e.g. Masberg et. al. 1992; Masberg, 2000; Nex et. al., 2001; Jung and Mezger, 2003) to lower amphibolites-facies grades in the east (T estimates between 550°C and 650°C at 3 ± 1 kbar e.g. Puhon, 1983; Steven, 1993; Wulff, 2008). In the Navachab area, lower amphibolite-facies metamorphism resulted in biotite-cordierite mineral assemblages in metapelites and clinopyroxene-actinolite-plagioclase assemblages in calc-silicate felses. Garnet is conspicuous by its regional absence in unaltered rocks, and only occurs as an alteration around hydrothermal quartz veins and pegmatites. In the marbles, the high-temperature metamorphism resulted in the pervasive recrystallization and annealing of calcite-dolomite assemblages.

4. Geology of the Navachab open pit

The Navachab open pit (Fig. 4.1) exposes a near-complete cross-section through the central formations of the Damara Supergroup, from the Spes Bona Formation in the east to the Oberwasser and Karibib Formations in the west. Figure 4.2 shows a detailed lithostratigraphic column of the lithologies in and beyond the open pit as they are exposed on the NW limb of the Karibib Dome. This succession broadly corresponds to the general stratigraphy of the Damara Supergroup outlined in chapter 3, but lithological variations within the sequence exert significant controls on the quartz veining, so that a detailed breakdown of the lithological sequence is given here.

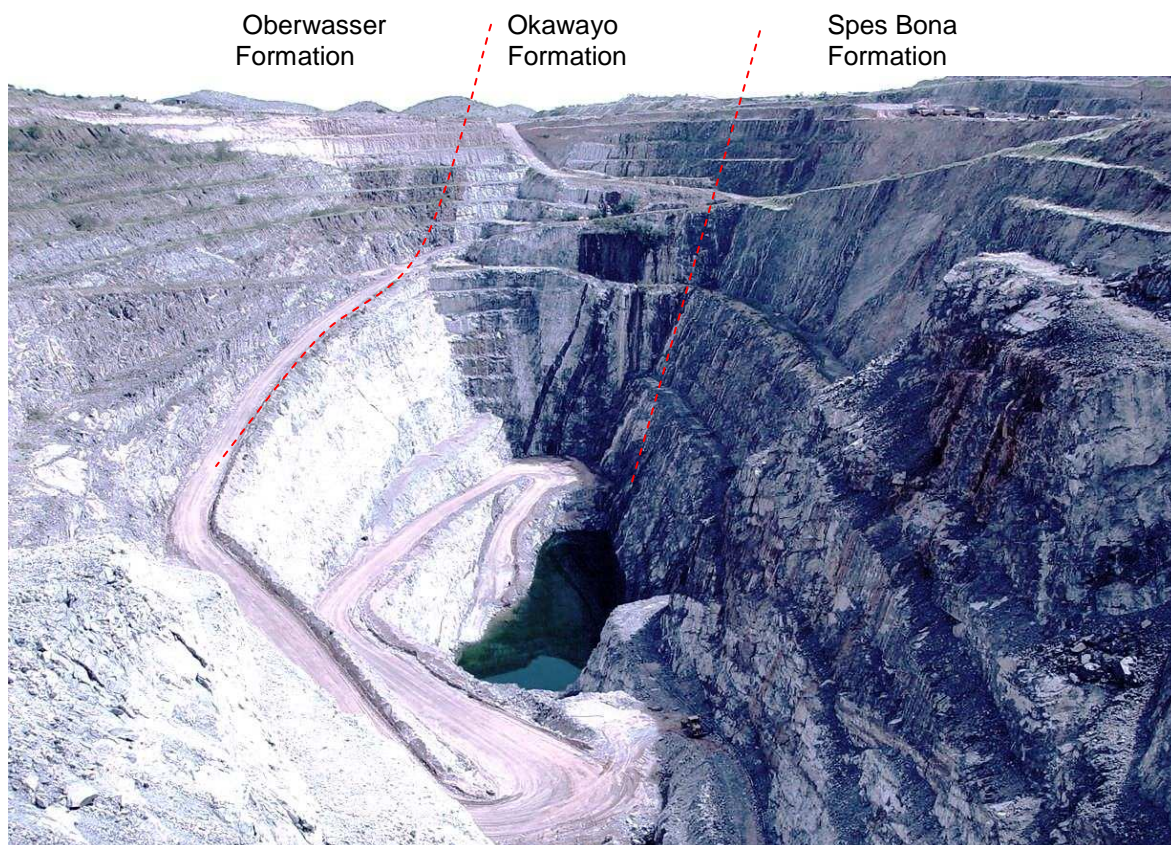


Fig. 4.1 View to the NNE of the Navachab Open Pit Mine (February 2006). The strata dips to the WNW (left-hand side of the photo) and the central metalamprophyre sill is clearly visible in the central portion of the marbles of the Okawayo Formation (light).

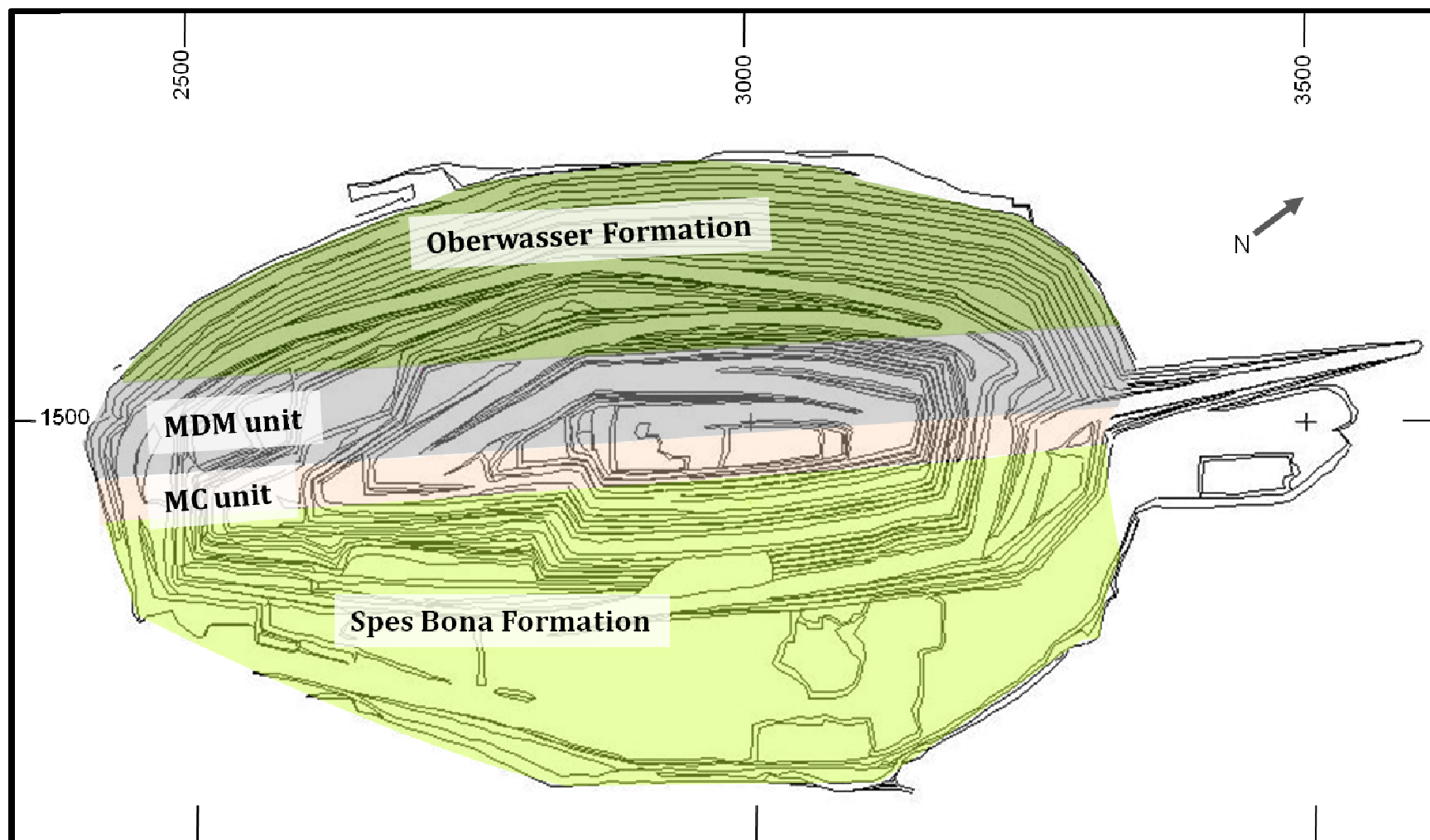


Fig. 4.2 Plan map of the Navachab Open Pit showing the main lithological units exposed in the pit.

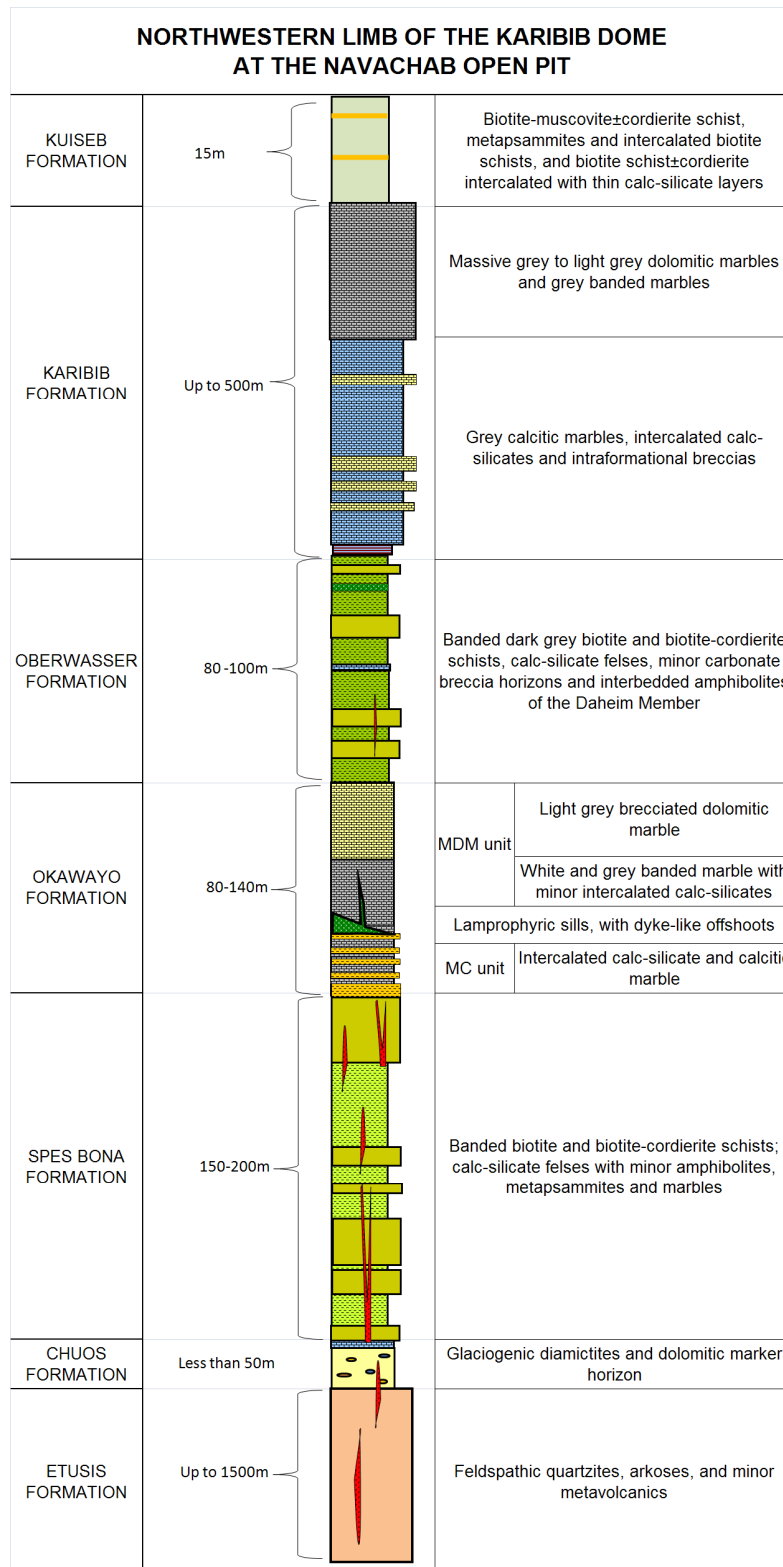


Fig.4.3 Detailed lithostratigraphic column through the lithologies in and around the Navachab open pit.

Rocks of the ***Spes Bona Formation*** (Fig 4.4a-c) form the footwall sequence to the Navachab open pit orebody, attaining a thickness of up to 200m. The Spes Bona Formation is developed as a sequence of intercalated biotite schists, biotite-cordierite schists, calc-silicate felses and metapsammities. The lower part of the Spes Bona Formation consists predominantly of biotite schists, while the upper part is dominated by intercalated quartz-biotite schists and calc-silicate felses. The thickness of individual layers may vary from only a few millimeters to up to several meters.

The biotite schists are commonly very fine grained, consisting of fine-grained (max. up to 0.5mm) biotite (40-60%), plagioclase and K-feldspar (30-50%), and less than 10% quartz (Fig. 4.5a) The biotite schists display a well-defined foliation due to the preferred alignment of biotite, but, because of the fine-grained nature of the biotite, they appear mainly massive and well jointed in outcrop along the eastern sidewall of the open pit (Fig. 4.4b). The calc-silicate felses consist of coarser (up to 2mm) diopside (50-60%), plagioclase and K-feldspar (30-50%), biotite and minor sphene and quartz (Fig. 4.5b). They are typically massive and weather positively on surface. Garnet is abundant in schists immediately below the massive sulfide mineralization at and close to the contact between the Spes Bona and overlying Okawayo Formation. This garnet growth is likely to be related to the alteration associated with the hydrothermal mineralization (Wulff, 2008).

The overlying ***Okawayo Formation*** has a thickness of between 80m and 150m in the open pit and can be subdivided into two main parts. The basal part of the Okawayo Formation is made up of a between 30m and 60m thick sequence of intercalated calc-silicates felses and calcitic marbles, locally known as the MC unit (MC: Marble and Calcitic Marble), which forms the host rocks to a significant part of the gold mineralization. The thickness of the individual calc-silicate and calcitic layers varies from less than 1cm to up to 10cm (Fig. 4.4d-f). The calc-silicate felses consist of large (up to 2mm) anhedral and poikiloblastic diopside (50-80%) set in a fine-grained matrix of plagioclase and K-feldspar (20-40%) and minor quartz (Fig. 4.5c). The marbles consist of fine-grained (0.05-0.5mm) recrystallized calcite, with minor quartz and feldspar. Large poikiloblastic diopside may occur as porphyroblasts in some calcitic marble layers (Fig. 4.5c). Sphene is, locally, intergrown with calcite.

The MC unit is overlain by a marble unit, locally termed the MDM unit (MDM: Marble and Dolomitic Marble)(Fig. 4.4g-j). The term MDM unit is retained in this study, despite the fact that the MDM is made up of mainly calcitic marbles and only very minor intercalations of dolomitic marble. The contact between the MDM and MC units is marked by a mafic lamprophyre sill (Fig. 4.4d and chapter 4.2.1). The MDM unit is between 60m and 120m thick and can be subdivided into a basal white and grey banded calcitic marble with minor intercalated calc-silicates, and an upper brecciated dolomitic marble (Fig. 4.4g). The basal banded marble is between 30m and 70m thick and typically has a darker appearance than the upper unit due to the presence of 1cm to 50 cm thick, dark grey marble bands (Fig. 4.4h). The upper brecciated marble is between 10m and 50m thick and consists of grey to light brown dolomitic marble clasts in a grey calcitic marble matrix. Individual clasts in the breccia are, on average, 10-30cm in size (Fig. 4.4i). The clast population in the breccia marble and its concordant relationship with the footwall marble and hangingwall schists indicates that this is not a tectonic, but an intraformational, sedimentary breccia, as they are common in marble units of the Okawayo and Karibib Formations (Badenhorst, 1992).

Petrographically, the banded marble is made up thin layers of fine- to-large (0.1 to 2 mm), recrystallized calcite and fine-grained biotite and/or muscovite (0.1- 0.5 mm) (Fig 4.5d). Biotite forms thin, up to 5 mm wide bands between white and grey layers and typically shows a preferred orientation. The darker colouration of the grey marble layers is due to small amounts of disseminated fine-grained biotite and muscovite and very fine-grained graphite.

The overlying ***Oberwasser Formation*** is approximately 80-100m thick and forms the hangingwall of the Navachab Open Pit. It is very similar to the Spes Bona Formation and consists of biotite schists, calc-silicates felses, minor marble bands and amphibolites. The biotite schists consist predominantly of fine-grained biotite with, in places, large cordierite porphyroblast, plagioclase, K-feldspar, and quartz. The calc-silicate felses consist of coarse-grained diopside, and finer-grained plagioclase and K-feldspar, with minor quartz and biotite.

SUMMARY OF THE MAIN ROCK TYPES IN THE NAVACHAB OPEN PIT

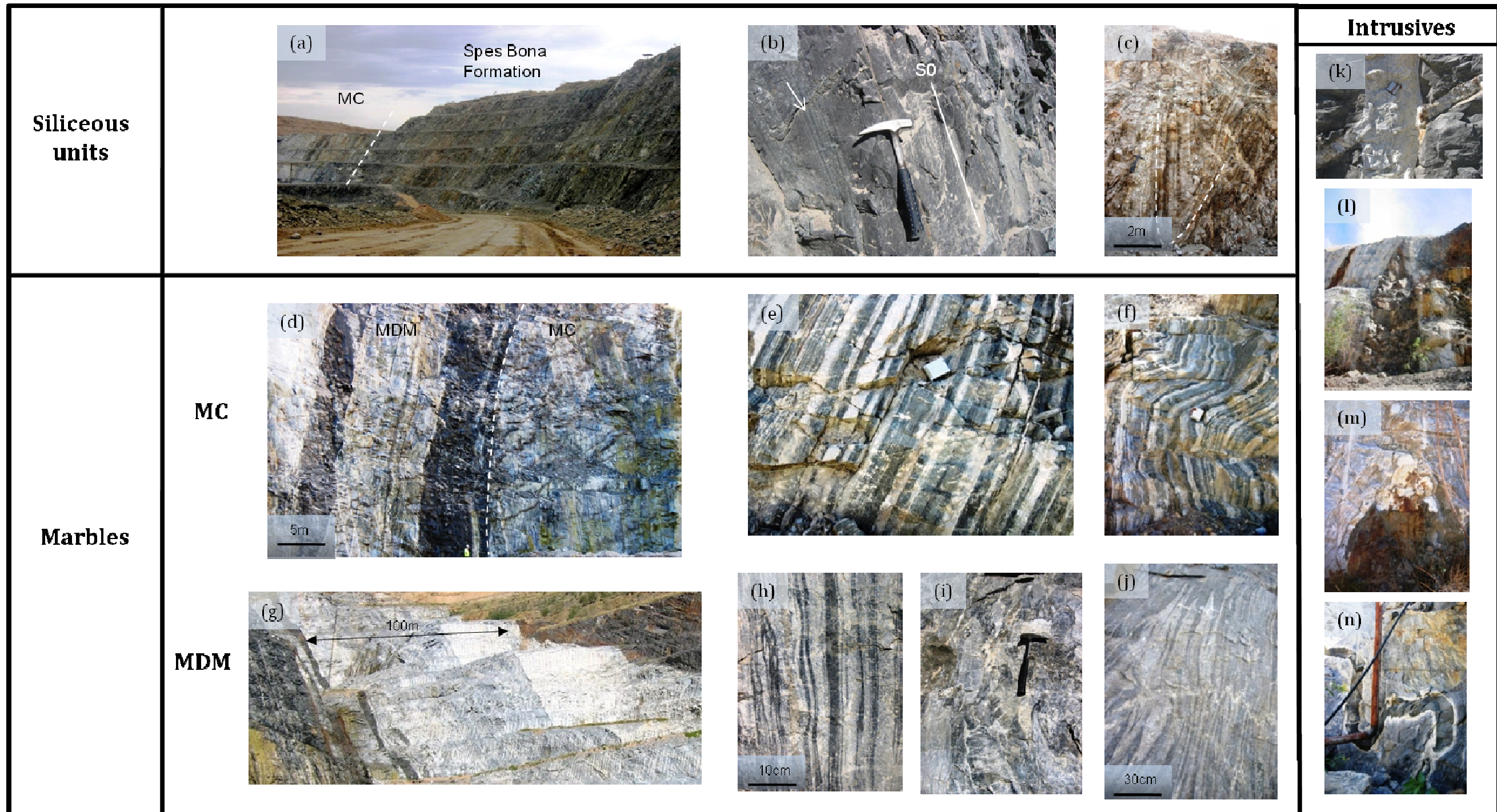


Fig 4.4 Characteristics of the main rock types in the Navachab open pit. (a) View to the north of the Spes Bona Formation schist. (b) Intercalated dark grey biotite schist and greenish calc-silicate felses (arrow) typical for the siliceous units in the open pit (c) Rare parasitic folds in the Spes Bona Formation schist to the NE of the open pit. (d) View of northern wall of the open pit showing the MC and MDM units of the Okawayo Formation, intruded by metalamprophyric sills. (e) MC unit showing the intercalated marbles (white) and greenish calc-silicates (compass for scale). (f) Parasitic F2b fold in the MC unit (compass for scale). (g) View to the SW of the MDM unit showing the darker coloured basal grey banded calcitic marbles and light coloured upper brecciated dolomitic marble. (h) Grey banded marble of the MDM unit showing the centimeter scale white and dark grey calcitic marble banding. (i) Brecciated marble of the MDM unit with grey and light brown dolomitic marble clasts in a grey calcitic marble matrix (hammer for scale). (j) Tight intrafolial F1 folds refolding the bedding in banded marbles of the MDM unit. (k) Subvertical pegmatite dyke crosscutting shallow north dipping quartz vein in Spes Bona Formation schist (compass for scale). (l) Metalamprophyre sill with primary horn-and-bridge structure between adjacent sills (field of view is roughly 10m). (m) Boudinaged metalamprophyre sill with pegmatite in boudin neck (field of view is 5m). (n) Folded metalamprophyre dyke with bleached margins (field of view is 3m).

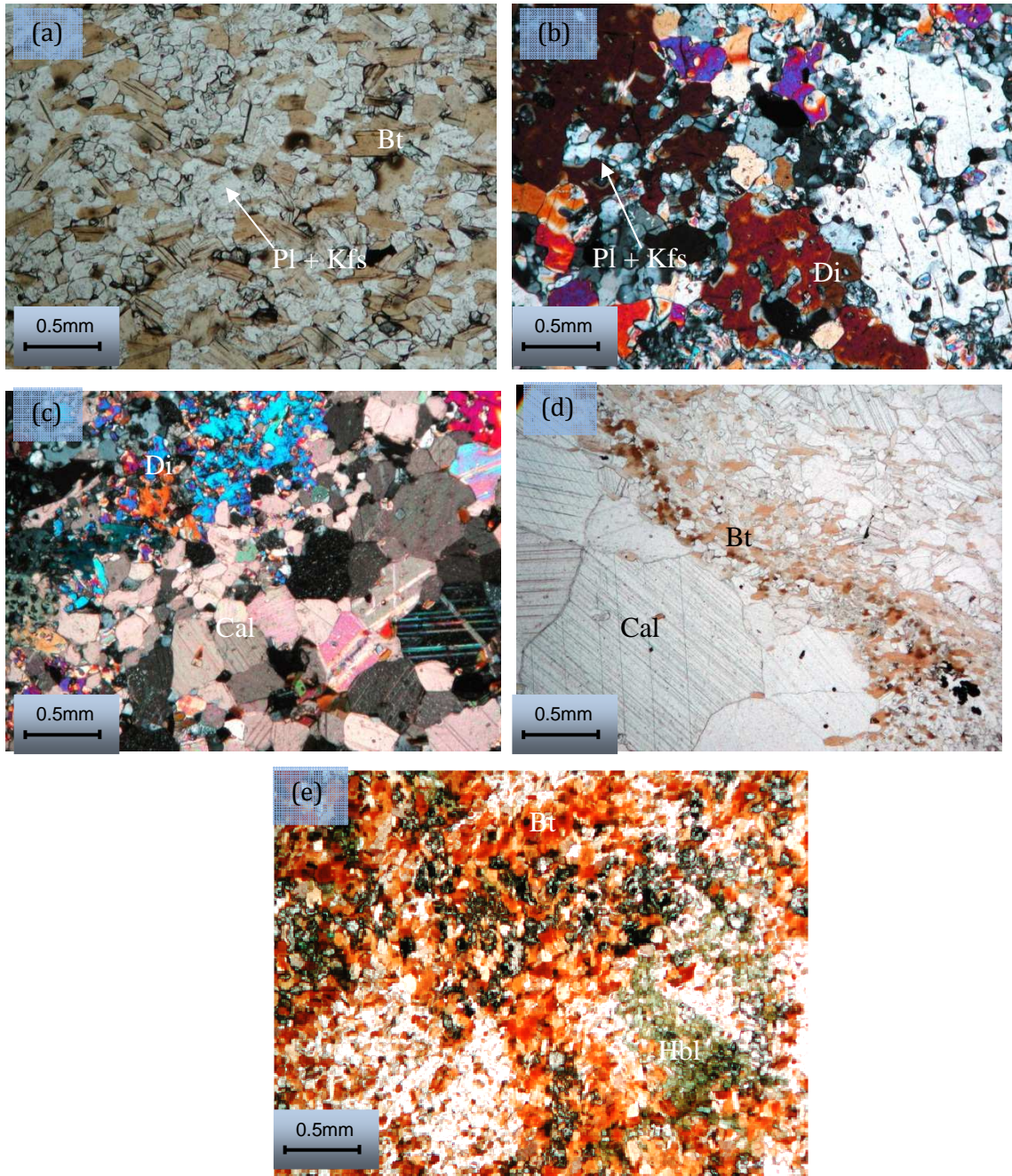


Fig. 4.5 (a) Photomicrograph of biotite schists of the Spes Bona Formation in the open pit with abundant preferably aligned biotite. Plagioclase, K-feldspar and minor quartz make up the rest of the matrix minerals (plane polarized light, PPL). (b) Photomicrograph of a calc-silicate fels from the Spes Bona Formation in the open pit, with large anhedronal diopside in a matrix of plagioclase, K-feldspar and minor quartz (crossed nicols). (c) Photomicrograph of a contact between calc-silicate and calcite from intercalated marble and calc-silicates from the MC unit, showing large anhedronal diopside in the upper left corner and large recrystallized calcite in the lower left corner (crossed nicols). (d) Photomicrograph of banded marble from the MDM unit in the open pit, with large recrystallized calcite, bordered by a thin fine-grained biotite rich layer (PPL). (e) Photomicrograph of the metalamphiphyre with large anhedronal porphyroblasts of hornblende in a fine grained matrix of biotite, plagioclase and K-feldspar (crossed nicols). All mineral abbreviations after Kretz (1983).

4.1 Structural geology of the Navachab open pit

The Navachab gold mine is situated on the steep NW limb of the Karibib Dome. The Karibib dome is a 12km long, 4km wide doubly-plunging anticline, and forms part of a series of NE trending dome structures developed in the sCZ. It has a pronounced NW vergence, consisting of a shallow-dipping SE limb and a steep NW limb. In the open pit, the lithologies dip steeply (70° to 80°) to the WNW and trend, on average, NNE-SSW (210°).

Although the area has been affected by at least two deformation phases (chapter 3.3), sedimentary features such as ripple marks are still well preserved in the siliceous units. Marble units of the Okawayo Formation, in turn, are highly strained. This underlines the rheologically heterogeneous nature of the wall-rock succession. Fabric elements that can be ascribed to the main deformation phases, D1 and D2 are summarized in Table 3.2.

In the open pit, *D1* is expressed as a bedding sub-parallel foliation (S1), but is only observed in the schistose units (Fig. 4.4b). The marbles are pervasively recrystallized and lack S1. However, in banded marbles of the Okawayo Formation in the MDM unit, tight- to-isoclinal intrafolial folds (F1) typically refold the bedding, indicating that the S1 fabric is developed as a transposition fabric (S0/S1) in marbles (Fig. 4.4j).

During *D2*, bedding (S0) and D1 related fabrics (S1) were refolded around the Karibib Dome. The Karibib Dome is a doubly-plunging anticline (F2a), plunging shallowly (ca. $15-20^{\circ}$) to the SW in the SW hinge, showing shallow NNE plunges of 15° in its NE hinge. In the open pit, lower order (F2b) folds with wavelengths and amplitudes ranging from a few centimeters to several meters, are developed in both the schistose and marble units (Fig. 4.4c and Fig. 4.4f). F2b folds typically plunge shallowly (15°) to the NE and are parallel to the first-order F2a dome structure. A penetrative, sub-vertical foliation (S2) is axial planar to the F2b folds and also accounts for local transposition of bedding in marbles. On the steep NW limb of the Karibib Dome, the S1 and S2 foliations are parallel to each other and, consequently, indistinguishable. Subvertical calc-silicate felsens and dolomitic marbles are often boudinaged. Boudinage is of a symmetrical, chocolate-tablet type implying a large component of subhorizontal shortening normal to

S2 and bedding. A shallow NE and SW plunging lineation (L2) is associated with S2. In the open pit, this lineation is defined by stretched clasts in syn-sedimentary marble breccias and stretched mineral aggregates (L2m) in siliciclastic units as well as the plunge of the fold axes of lower order parasitic folds (L2f).

4.2 Intrusive rocks in the Navachab open pit

4.2.1 Metalamprophyres

The Navachab open pit is intruded by several metalamprophyre sills and associated dyke-like offshoots (Fig. 4.4d). Two main lamprophyre sills are developed over the length of the open pit and attain a maximum thickness of up to 8 meters. The sills intrude along the contact of the MC with the overlying MDM unit and are generally used as a marker horizon between the two marble packages. Up to 0.5m wide dyke-like offshoots of the lamprophyre are transgressive and also intrude into the Oberwasser Formation along the western sidewall of the open pit as well as into the Spes Bona Formation north of the main open pit. The lamprophyre sills preserve primary intrusive structures such as horn-and bridge structures between adjacent sill segments (Fig. 4.4l). Cross-cutting, dyke-like offshoots are often folded and boudinaged (Fig. 4.4n). Boudin necks are filled by pegmatites, indicating the presence of granitic melts during deformation (Fig. 4.4m). Recent U-Pb dating of single titanite grains yielded an age of 496 ± 12 Ma, which is interpreted to reflect a high-temperature metamorphic overprint rather than the crystallization age of the lamprophyres (Jacob et. al., 2000).

In thin section, the lamprophyre consists of anhedral porphyroblasts of hornblende and poikilitic clinopyroxene in a fine-grained matrix of mostly biotite and minor plagioclase and K-feldspar (Fig. 4.5e). Sphene is a common accessory mineral.

The timing of emplacement of the lamprophyres is somewhat enigmatic. Geochemically, they resemble the high-Ti alkali basalts of the Daheim Member at the top of the Oberwasser Formation (Fig. 4.3), and Badenhorst (1992) suggested the sills and dykes to possibly represent the feeders to the volcanics of the Daheim Member. In the open pit, the sills and dykes are boudinaged and gently folded. However, they have not been affected by the pervasive isoclinal intrafolial folding and bedding transposition shown by the host MDM (Fig. 4.4j), showing well-preserved primary intrusive relationships

with the marbles. Moreover, the lamprophyre-marble contacts are commonly coarsely recrystallized and bleached (Fig. 4.4n). Both features would suggest a late-tectonic (D2) emplacement of the lamprophyres, rather than having formed part of the original stratigraphy.

4.2.2 Pegmatites and aplites

The Navachab open pit is intruded by several generations of subvertical NW trending pegmatites and aplites (Fig. 4.6a, b). They range in size from less than 1cm to up to 5m in width and are almost exclusively restricted to the siliciclastic units of the Spes Bona Formation. Pegmatites terminate abruptly against Okawayo Formation and are also rare in the Karibib Formation, suggesting that pegmatite dyke emplacement is controlled by the competence of wall rocks. The majority of pegmatites are late-(D2) tectonic and cross-cut the main sheeted vein set (chapter 5.2). However, there are also rare cases where pegmatite and aplite dykes can be seen to have undergone folding and boudinage and some auriferous quartz veins cross-cut the aplite dykes (Fig. 4.5a). This suggests that plutonic activity was contemporaneous with, at least, the later stages of mineralization.

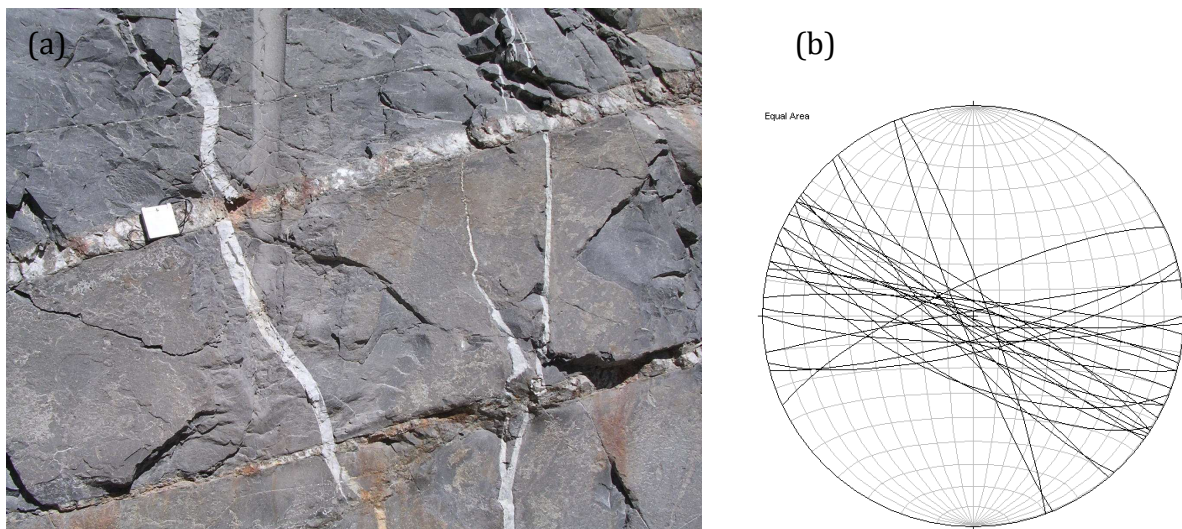


Fig. 4.6 (a) View to the east of an aplite dyke in the Spes Bona Formation of the Navachab open pit, cross-cut by a shallowly dipping sheeted quartz vein (top half of photo), but cross-cutting a shallowly dipping vein (bottom half of photo). This suggests that quartz veining and the intrusion of felsic dyke swarms were contemporaneous. Compass for scale. (b) Lower hemisphere, equal area projection of pegmatite and aplite dykes in the Navachab open pit, showing the subvertical NW trend of most of the dykes (n=27).

5. Quartz veins in the Navachab Open Pit

5.1 Data collection and analytical techniques

The open pit (Fig 5.1) provides good 3D sections of the composite quartz vein sets that host the gold mineralization. Quartz veins extend from the Etusis Formation in the E, into the Karibib Formation in the W and the mineralized system is roughly 900m wide, in a WNW-ESE direction, and at least 2, and possibly up to 5 km long, parallel to the NNE strike of the strata (Steven, 2002). The down-dip extent of the veins can be followed for more than 300m along the eastern and western sidewalls of the open pit, but borehole data suggests that quartz veining continues well beyond this (Steven, 2002).

Spatial (orientation, spacing, size, geometry) and textural data from quartz veins was collected mainly from the accessible eastern, northern and western sidewalls of the open pit (Fig. 5.1). The sidewalls dip at 70° and offer well exposed sections through the quartz veins. Figure 5.2 shows the sampling technique that was used to collect vein data in the open pit. The location at which individual veins first intersect the sampling line and the vein thickness parallel to the sampling line (T) were recorded. The spacing between veins were calculated from the position and thickness data and the relative orientation of the sampling line and vein were used to convert apparent thickness to true thickness.

Mapping was limited to three levels (1050, 1010, and 970) on the eastern wall, two levels (980 and 970) on the northern wall, and the haul road on the western wall of the open pit, which also covers approximately three levels between 1150 and 970. The size of the area mapped was approximately 900 m long, parallel to the long axis of the open pit, and ca 350 m wide, straddling different lithologies from the Spes Bona Formation in the E to the Karibib Formation in the W. The vertical extent covered between levels 1160 and 970 is 190 m. Panels were mapped on a 1:200 scale and the results were then combined into composite panels presented throughout the text. Additional vein data was collected from several core holes drilled in the open pit, the locations of which are presented in Figure 5.1.

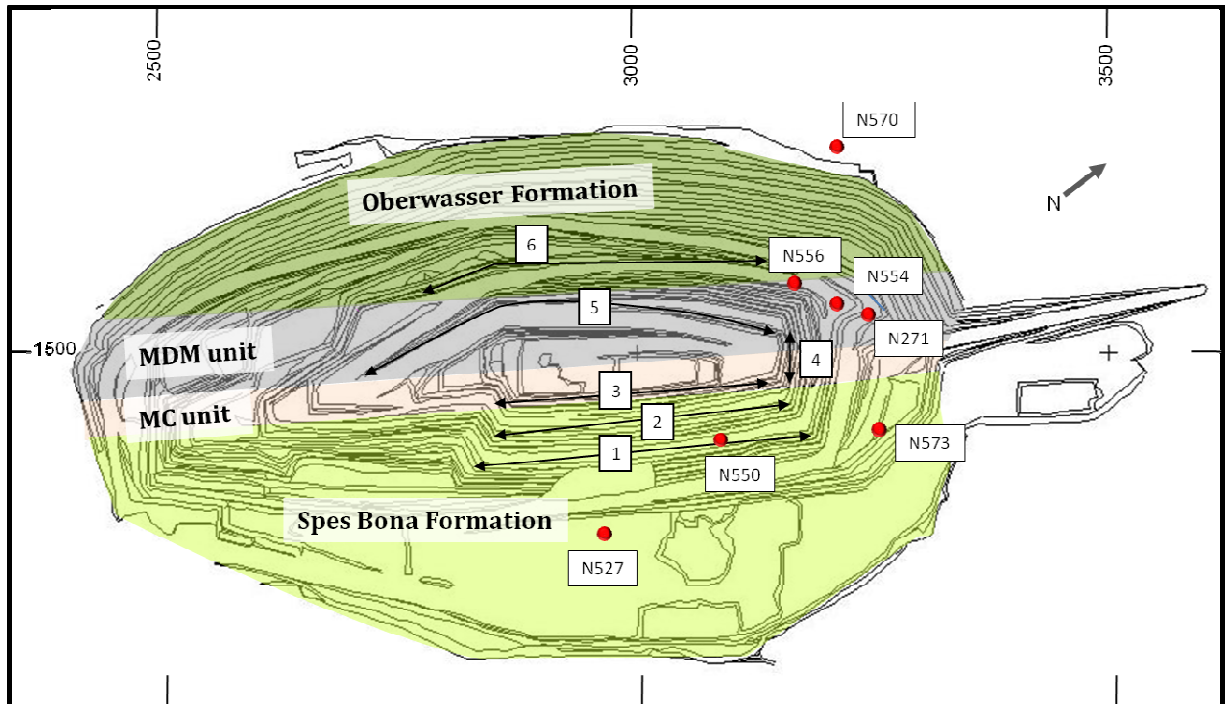


Fig. 5.1 Plan map of the Navachab Open Pit, showing localities of mapped panels (1 to 6) indicated by black lines and logged boreholes (N570 etc.) used in the study. Details of borehole data presented in Appendix III.

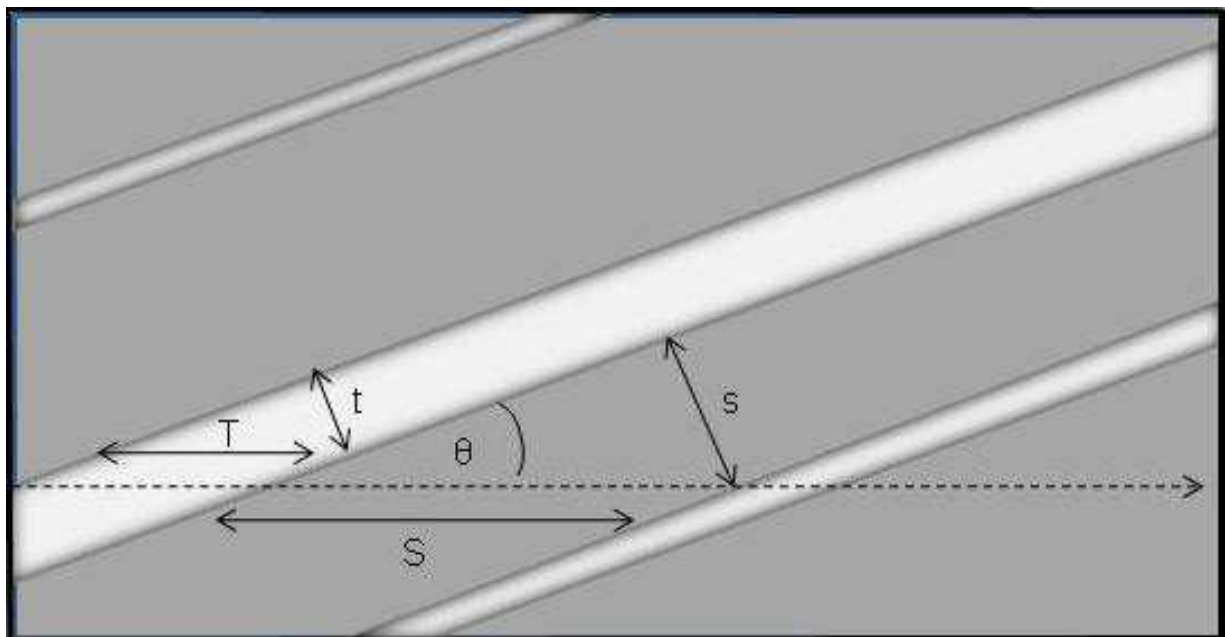


Fig. 5.2 Diagram of a typical line sample through shallow dipping sheeted quartz veins in the open pit, showing apparent spacing (S), true spacing (s), apparent thickness (T), true thickness (t) and the vein orientation relative to the sampling line (θ). $s = S \sin(\theta)$.

Despite the good exposure, the analysis of veins sets is hampered by the fact that the main set of shallowly dipping quartz veins shows very large down-dip extents of several hundred meters (Figs 5.3 and 5.4), so that the full length of veins is not exposed along the sidewalls of the open pit. Veins < 1 cm in thickness were not considered, so that e.g. strain values are minimum estimates (chapter 5.2). Moreover, post-emplacement deformation of veins (folding, boudinage) has modified the geometry and orientation of veins, particularly in marble units, so that the geometric analysis of original vein geometries is largely restricted to siliciclastic units.

In this study, the orientations of quartz veins form the basis for distinguishing different sets of veins, following a similar approach by previous workers (Steven and Badenhorst, 2002; Kisters, 2005).

- (a) The main set of shallow-dipping quartz veins, also referred to as *sheeted quartz veins* by Moore et al. (1998), Steven and Badenhorst (2002) and Kisters (2005) make up the bulk of auriferous quartz veins in the pit. They typically form discordant veins that cross-cut the steeply dipping host-rock lithologies at high angles (Fig. 5.3, 5.4, 5.5 and 5.6).
- (b) Massive sulphide lenses have been the main mineralization mined until recently and are confined to the MC unit (Moore et al., 1998; Steven and Badenhorst, 2002; Kisters, 2005; Wulff, 2008). Previously, they have been described as meter scale massive, bedding sub-parallel sulphide lenses with shallow NNE plunges parallel to the fold hinge of the Karibib dome. Grade envelopes around this mineralization define two, to possibly three main shoots that can be traced for up to 1800 m in a down-plunge direction (Steven and Badenhorst, 2002).
- (c) Several *subordinate vein sets* exist, but with a considerable scatter of orientations. These veins are by far more dominant in the siliciclastics, where they are generally confined to distinct lithological units. The most common types are (i) bedding parallel veins, (ii) subvertical N-S trending veins, (iii) steep southerly dipping veins, and (iv) several types of quartz filled gashes with variable orientations.

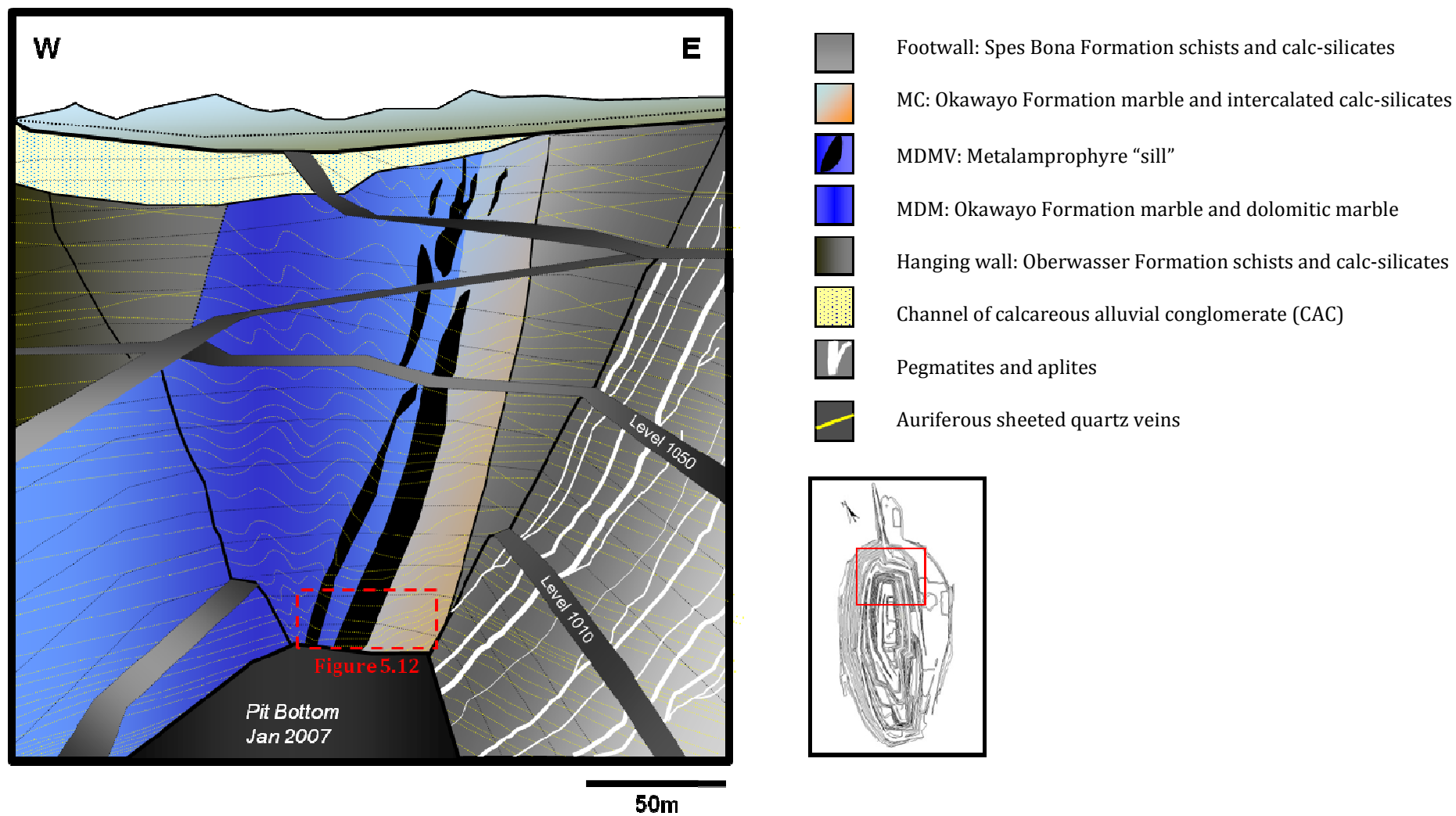


Fig. 5.3 Simplified 3D panels of the northern, and parts of the eastern and western sidewalls of the Navachab open pit (viewed to the north), illustrating the occurrence of sheeted quartz veins (yellow) in the open pit. The insert shows the location of the area depicted in Fig. 5.12.

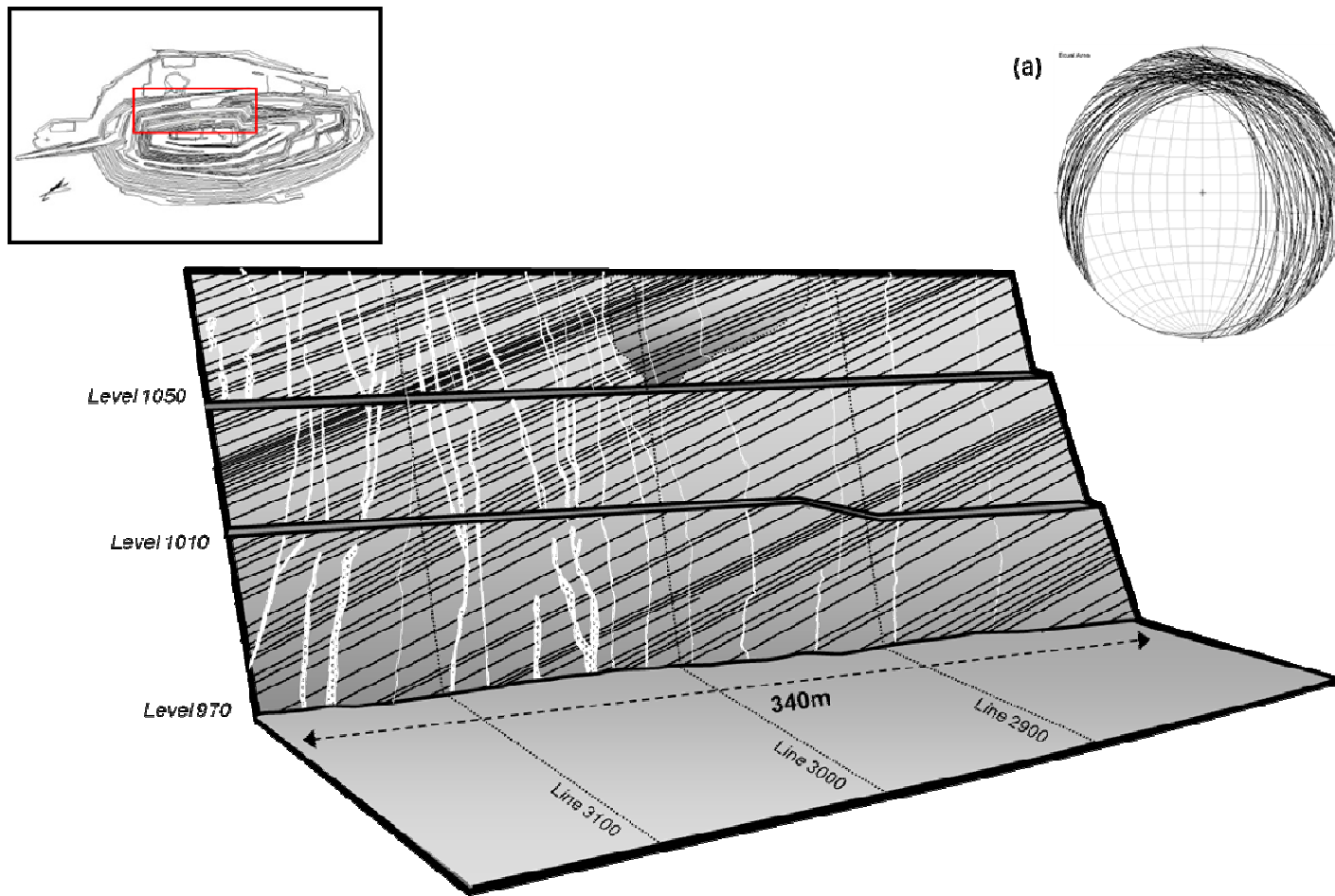


Fig. 5.4 Synoptic profile of the footwall schist in the open pit depicting the shallow N and NE dipping sheeted quartz veins, crosscut by subvertical pegmatite dykes (white), compiled from detailed mapping of panels. The section illustrates the continued down-dip extent of quartz veins, that can be traced for over 300m, as well as a clustering of quartz veins separated by up to 8m wide zones of less dense quartz veining. The overall thickness of the quartz vein swarm is more than 150m. (a) Lower hemisphere equal area projection of conjugate vein sets in the footwall schist (n = 72).

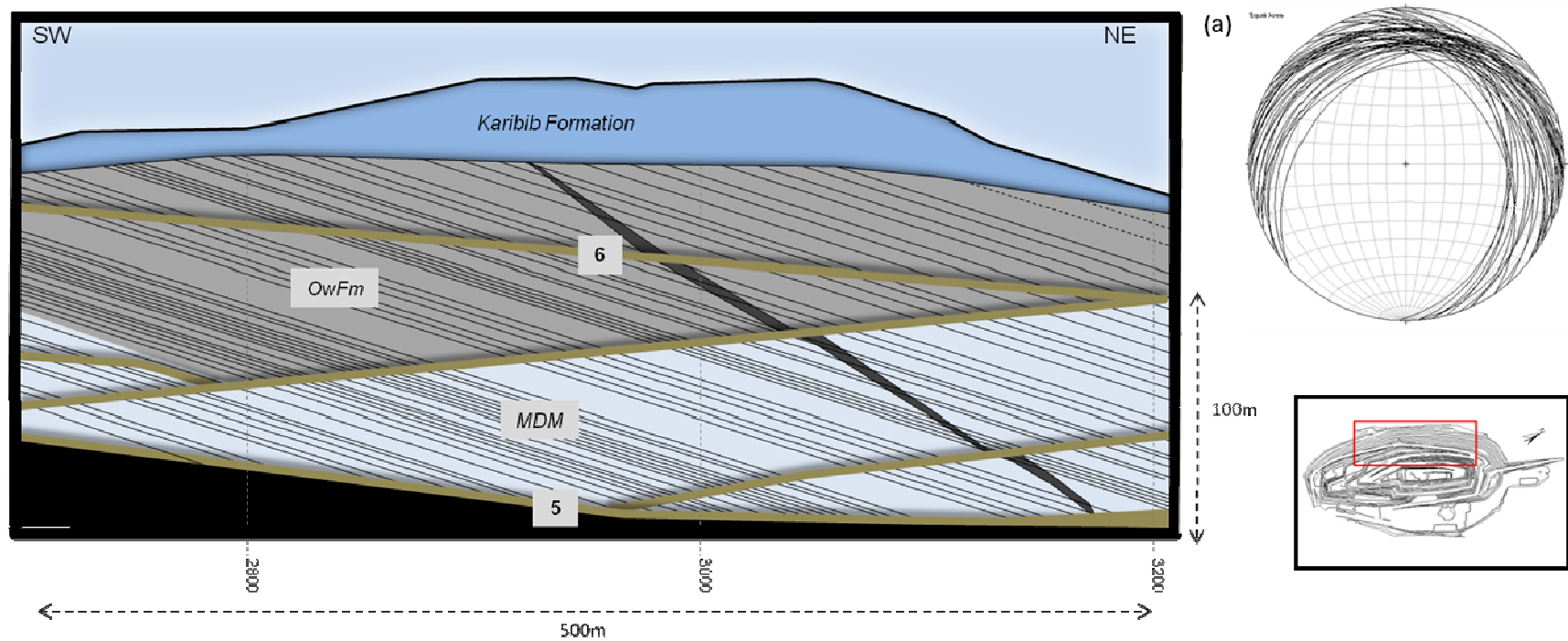


Fig. 5.5 Synoptic profile of the hangingwall schist and marbles in the open pit depicting the shallow N and NE dipping sheeted quartz veins, compiled from detailed mapping of panels (numbers 5 and 6 indicate location of panels, indicated in Fig. 5.1). The section illustrates the continuous down-dip extent of quartz veins, that can be traced for over 300m, as well as a clustering of quartz veins separated by ca. 20-30 m wide zones of less dense quartz veining. View to the NW. (a) Lower hemisphere equal area projection of conjugate vein sets in the hangingwall schist (n = 44).

SHEETED QUARTZ VEINS IN THE NAVACHAB OPEN PIT

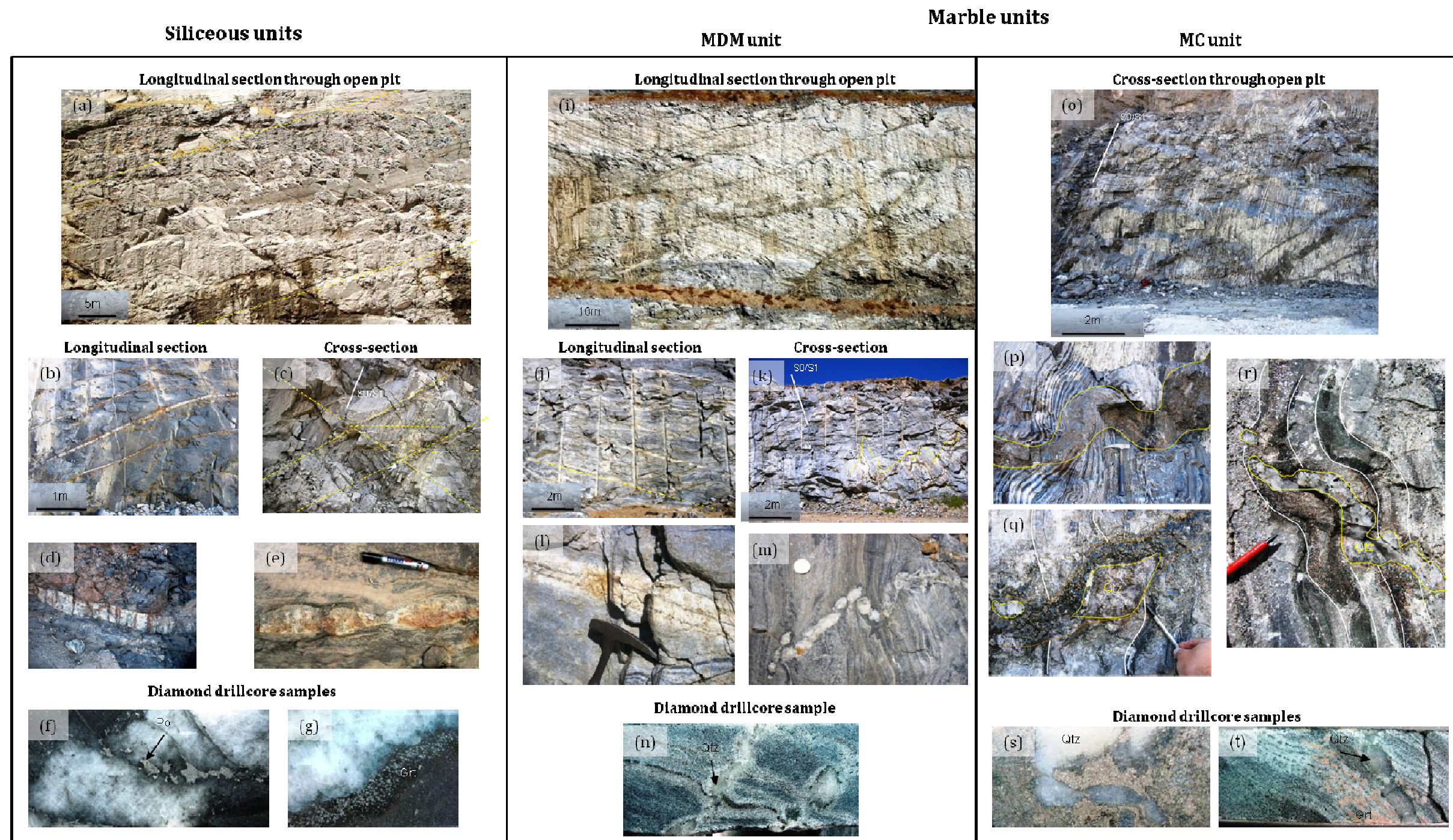


Fig. 5.6 Characteristics of sheeted quartz veins in the Navachab open pit. (a-b) Longitudinal (down-dip) section through open pit showing shallow dipping sheeted quartz veins in the Spes Bona Formation (view to the SE). (c) Cross-section (view to the NE) through open pit showing shallow dipping sheeted veins in Spes Bona Formation schists, consisting of a NW and NE dipping conjugate vein set, intersected by subhorizontal extensional veins. (d-e) Thick (10-15cm) boudinaged sheeted vein in Oberwasser Formation schists. (f-g) Diamond drillcore sample of veins in Spes Bona Formation schists with pyrrhotite in boudin necks and garnet in vein selvages. (i-j) Longitudinal (down-dip) section through open pit showing shallow dipping sheeted quartz veins in the MDM unit (view to the NW). (k) Cross-section through open pit showing buckled quartz veins (view to the SW). (l) Typical bleached halo around sheeted quartz veins in the MDM unit. (m) Buckled and segmentation of quartz veins due to pressure solution in grey banded marbles. (n) Diamond drillcore sample of typical quartz vein in MDM unit with slight bleaching around vein. (o) Cross-section through open pit showing shallow NE dipping veins in MC unit with large (dark) alteration halos around veins. (p) Buckled massive sulphide vein cross-cutting steeply dipping MC. The vein consist of thin (2-5cm thick) bead-like quartz with an up to 20cm thick alteration. (q) Boudinaged quartz vein with garnet-pyrrhotite alteration (dark). (r) Quartz vein in MC layering. Note gentle folding of quartz vein with the parasitic F2b fold. (s) Diamond drillcore sample of folded and boudinaged vein in MC unit with massive sulphide (mainly pyrrhotite) alteration around vein. (t) Diamond drillcore of boudinaged vein in MC unit with garnet alteration.

5.2. Sheeted quartz veins

5.2.1 Geometry and morphology

Sheeted quartz veins are parallel-sided, planar veins in siliciclastic units (Fig. 5.6a-g). In marble units, they are irregularly shaped, with highly varying thicknesses showing pronounced pinch-and-swell and boudinage-type structures (Fig 5.6l-t). In places, quartz veins in the marble units are only expressed by very thin quartz stringers and associated sulphides, surrounded by cm-wide alteration halos of bleached, coarsely recrystallized carbonates (Fig. 5.6l).

Vein walls are sharp and the veins incorporate no wall-rock slivers. In longitudinal (down-dip) sections along the eastern and western sidewalls of the open pit, the veins appear straight and can be followed for at least 300m, i.e. along the entire sidewalls. As a consequence, vein terminations are rare, but where exposed, are often characterized by a gradual thinning of the vein over several meters. The down-dip thinning and termination of a vein is associated with the formation and thickening of an adjacent vein, indicating some degree of hydraulic connectivity within the larger vein set (Fig. 5.7c). Rare examples of vein terminations show that adjacent veins typically overlap at termination zones. These overlaps are up to 10 m long. In most cases, the vein fracture, and alteration halo (chapter 5.2.5) continues well beyond the termination of the quartz vein itself.

5.2.2 Orientation of veins

Geometrically, a number of different veins and vein sets can be described that have previously been grouped together under the term 'sheeted quartz veins' (Moore et al., 1998; Steven and Badenhorst, 2002; Kisters, 2005). All of these veins are highly discordant and sharply truncate the steeply dipping bedding and S1/S2 fabrics of the wall rocks. There is no evidence that the veins exploited pre-existing anisotropies during their growth and propagation. As stated in chapter 5.1, the original geometries and orientation of the veins are mainly preserved in siliciclastic units of the Spes Bona and Oberwasser Formation. In marbles of the Okawayo and Karibib Formation, the subsequent deformation (folding, boudinage) of veins has largely obliterated original orientations (chapter 5.4). Hence, most of the orientation data are taken from the Spes Bona and Oberwasser Formation, as well as the central lamprophyre sills.

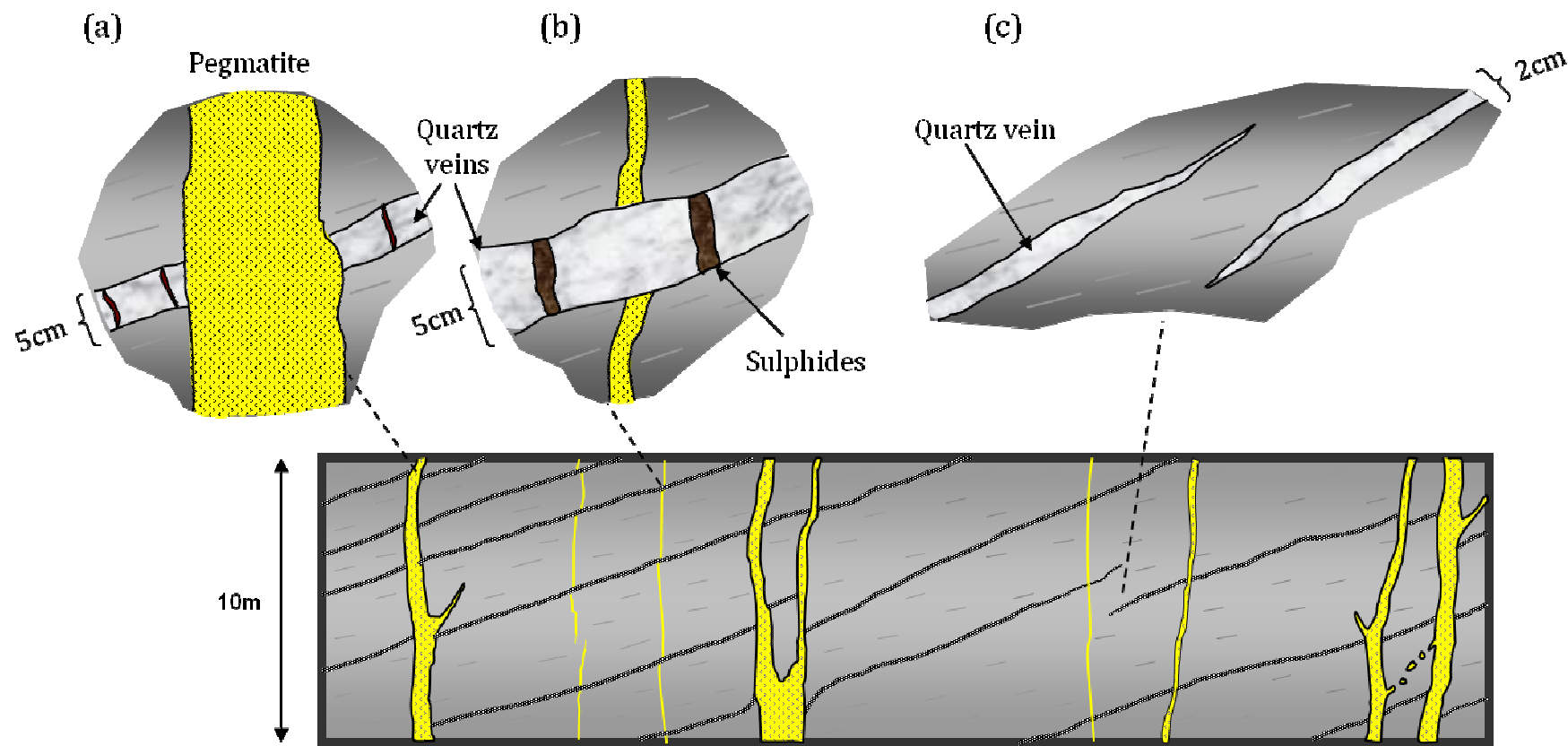


Fig 5.7 Profile of quartz veins and pegmatites (yellow) in the Spes Bona Formation along the eastern sidewall at Level 970. (a) Sheeted quartz vein (grey), crosscut by a pegmatite dyke (yellow). (b) Rare example of an early thin pegmatite cut by a quartz vein. Note sulphides (dark grey) in neck of boudinaged vein. (c) Typical termination of a vein, characterized by the formation and thickening of another vein, with some degree of overlap.

Conjugate vein sets: At least two subsets can be distinguished, consisting of an array of (1) shallow north (14° - 34°) and (2) northeast (14° - 50°) dipping quartz veins that are particularly well developed in the siliceous units in the footwall and hanging wall of the open pit (Fig. 5.6c and Fig. 5.8). The two main vein sets are approximately equally developed and can be mapped throughout the open pit. The two vein sets show relatively constant angular relationships enclosing an acute angle of 55° and an obtuse angle of 125° . Where crosscutting relations occur between the two conjugate sets of veins, these are not consistent, which suggests that they have formed contemporaneously, so that the vein sets are truly conjugate. Importantly, conjugate sets are not observed in marbles of the Okawayo Formation, where only one set of parallel veins is developed. The fact that veins are conjugate indicates that they represent extensional veins with a vein-parallel shear component. This is confirmed by the locally observed offset of layering in finely laminated wall rocks across vein walls.

If co-axial strain can be demonstrated during vein formation, then conjugate sets allow to determine the orientation of the principal strain and also stress axes. The bisetrix of the acute dihedral angle between conjugate vein sets show that the principal compressive stress (σ_1) during veins formation acted subhorizontally to the WNW (Fig. 5.8).

Extensional veins: Extensional veins occur in addition to conjugate veins sets and are often developed in the same outcrop, facilitating their identification. The veins dip shallowly to the north-northeast at angles of 10° - 20° , showing very little offset of host rock bedding or fabrics or any indications of vein-parallel slip, confirming that they represent extensional (mode 1) fractures. Extensional veins form the most common vein set in marbles of the Okawayo Formation, but are also developed in the Oberwasser and Spes Bona Formations (Fig 5.6o).

5.2.3 Size of veins

Veins were analyzed for their thickness and spacing along the three main wall rock panels in the pit. In addition, borehole data from 7 selected cores was analyzed, the location of which are shown in Fig 5.2. The raw data for the panels and boreholes are given in Appendix II and III, and are summarized in Table 5.1.

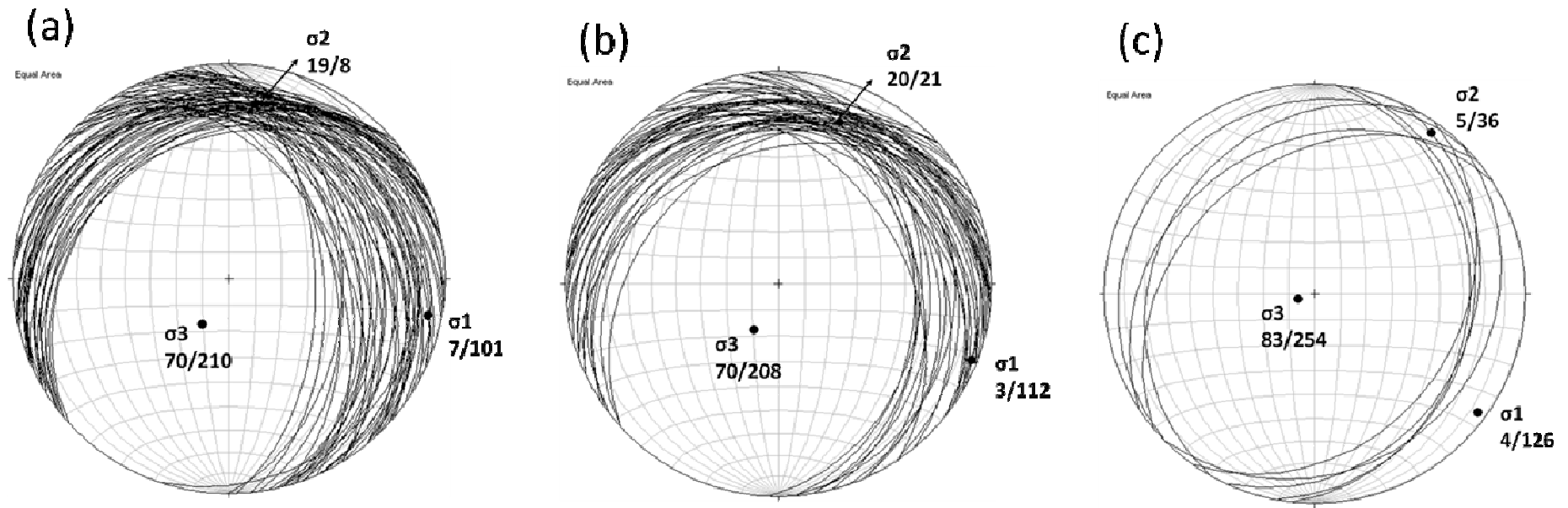


Fig. 5.8 Lower hemisphere, equal-area projection of conjugate quartz vein sets measured in (A) Spes Bona Formation in the open pit (n=72), (B) Oberwasser Formation in the open pit (n=44), (C) Metalamprophyre in open pit (n=9). The intersection of the conjugate vein sets indicates the σ_2 direction during quartz vein emplacement. The principal compressive stress is indicated by σ_1 , and is roughly ESE which corresponds to the regional D2 shortening direction during the main phase of collisional tectonics in the Damaran belt. The least compressive stress (σ_3) is subvertical.

Table 5.1 Summary of vein data from sampling lines and drillcores from the open pit. The sampling line and borehole numbers refer to Fig. 5.2. Cv refers to coefficient of variance, and ΔL the percentage vertical extensional strain. ΔL was not calculated for the MC unit and the marble units in boreholes N554 and 556, because only a small part of the vein swarm was intersected. Full data set is presented in Appendix II and III.

Area	Sampling line / borehole	Host lithology	Line length (m)	Total veins (N)	Vein Thickness (cm)				Vein Density (N/m)	Cv Vein Spacing	ΔL (%)
					Min	Max	Average	Cummulative			
Eastern wall (level 1050)	1	Spes Bona Formation biotite schists and calc-silicates	77.65	46	1	20	3.17	146	0.59	0.85	1.88
Eastern wall (level 1010)	2	Spes Bona Formation biotite schists and calc-silicates	67.55	39	3	15	5.69	222	0.58	0.73	3.29
Eastern wall (level 970)	3	Spes Bona Formation biotite schists and calc-silicates	64.45	35	3	12	6.53	227	0.54	0.79	3.52
Northern wall (level 980)	4	MC unit: Intercalated calcitic marbles and calc-silicates	12	7	3	12	4.4	45	0.58	0.41	
Western wall (west ramp)	5	MDM unit: Dolomitic and calcitic marbles	73.25	41	<1	7	2.51	103	0.56	1.49	1.40
Western wall (west ramp)	6	Oberwasser Formation biotite schists and calc-silicates	87.22	48	1	20	5.4	260	0.55	0.77	2.98
Eastern Pushback	N573	Spes Bona Formation biotite schists and calc-silicates	155.07	75	1	20	4.48	365	0.48	0.98	2.35
Western Pushback	N554	MDM unit: Dolomitic and calcitic marbles	133.71	36	<1	4	1.39	50	0.27	0.85	
Western Pushback	N554	MC unit: Intercalated calcitic marbles and calc-silicates	19.71	11	1	20	4.82	44	0.56	1.27	
Western Pushback	N570	Oberwasser Formation biotite schists and calc-silicates	254.93	73	1	10	3.19	239	0.29	0.96	0.91
Western Pushback	N556	MDM unit: Dolomitic and calcitic marbles	143.55	72	<1	15	2.1	151	0.50	1.12	
Western Pushback	N556	MC unit: Intercalated calcitic marbles and calc-silicates	34.26	16	1	5	2.75	44	0.47	0.64	
Western Pushback	N271	MDM unit: Dolomitic and calcitic marbles	333.58	112	<1	22	2.34	262	0.34	1.16	0.77
Eastern Pushback	N527	Spes Bona Formation biotite schists and calc-silicates	220.89	131	<1	21	4.92	645	0.59	0.67	3.01
Eastern Pushback	N550	Spes Bona Formation biotite schists and calc-silicates	151.19	75	<1	25	5.1	382	0.50	0.96	2.60

(a) Vein thickness

The veins mapped in this study range in thickness from less than 1cm to up to 20cm (Table 5.1). There are consistent variations in quartz-vein thickness that relate to wall-rock lithology, and sheeted quartz veins in marble units appear thinner than those in the siliceous units (Table 5.1). Veins in the siliceous units have an average thickness of 4.81cm, and veins in the Spes Bona Formation (4.98cm, n = 120) are only slightly thicker than in the Oberwasser Formation (4.30cm, n = 48). Systematic thickness variations with respect to wall-rock lithology are most pronounced for the MDM unit, where sheeted quartz veins are seldom more than 2cm thick. Although veins in the MDM unit have an average thickness of 2.09cm (n = 41), 75% of veins measured have a thickness \leq 2cm. In contrast, detailed mapping of a well-exposed section in the northern side of the open pit across the MC unit shows that more than half of the veins measured have very little change in thickness between the two units. Here, like in the siliceous units, most shallow dipping veins vary in thickness from 1cm to 10cm, with an average thickness of 3.91cm (n = 7).

In the Spes Bona and Oberwasser Formations, individual veins can be followed for up to 300 m along the western and eastern sidewalls of the pit (Fig.5.4 and Fig. 5.5). As a result, veins show remarkably high length-to-thickness aspect ratios of \gg 1000:1, although the full down-dip extent of the veins can, in most cases, not be established, so that this value must be taken as a minimum and conservative estimate. Individual veins show very little thickness variations along their down-dip extent. In cross section (WNW-ESE), individual quartz veins are more difficult to trace due to the post-emplacement deformation of veins (folding and refraction of veins along lithological contacts) and the often discontinuous outcrop conditions along the northern panel of the pit. However, thicker (> 5-10cm) veins can be traced for, at least, several tens of meters.

The staircase plots for cumulative vein thicknesses of veins in the Navachab open pit show irregular curves for all the lithologies in the open pit (Fig 5.10). The irregularity of these types of plots is a measure of the heterogeneity of the strain in the rocks. Typically irregular curves would be expected for non-stratabound veins such as at the Navachab system, because of the heterogeneity of the strain in the different layers.

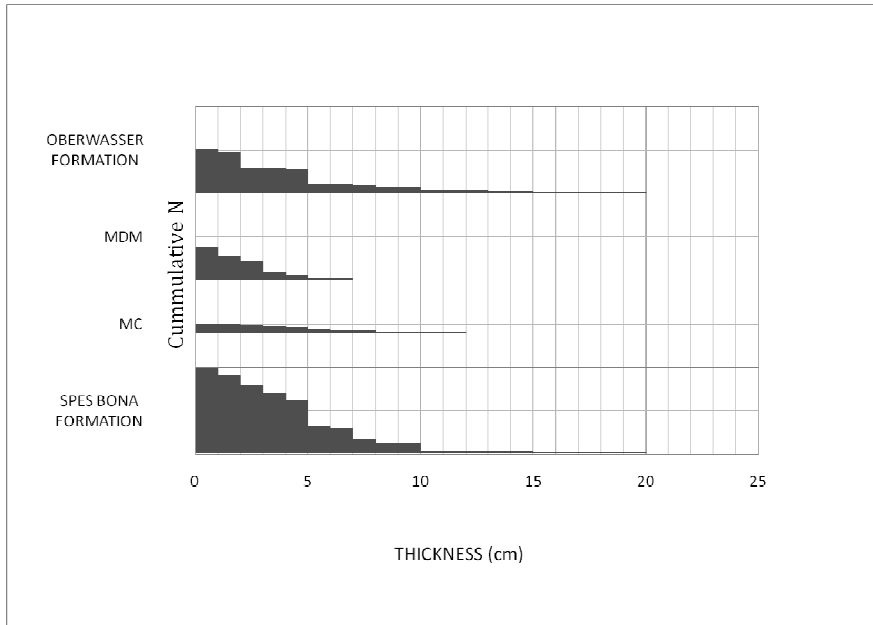
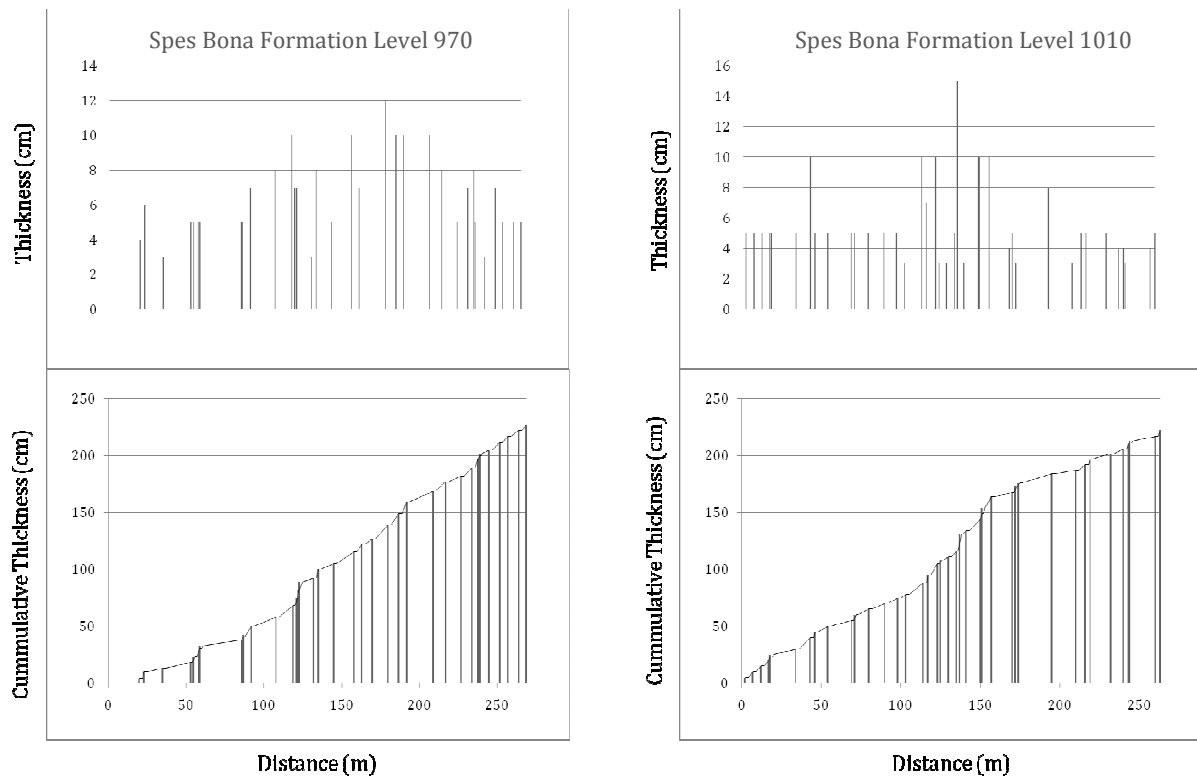


Fig.5.9 Histogram of the thickness of veins in the different lithologies in the open pit, derived from the panels mapped. Veins in the siliciclastic Spes Bona and Oberwasser Formations are typically thicker than veins in the MDM unit. Veins in the MC unit show similar thicknesses to the siliciclastics (n = 216; refer to Appendix II for original data).



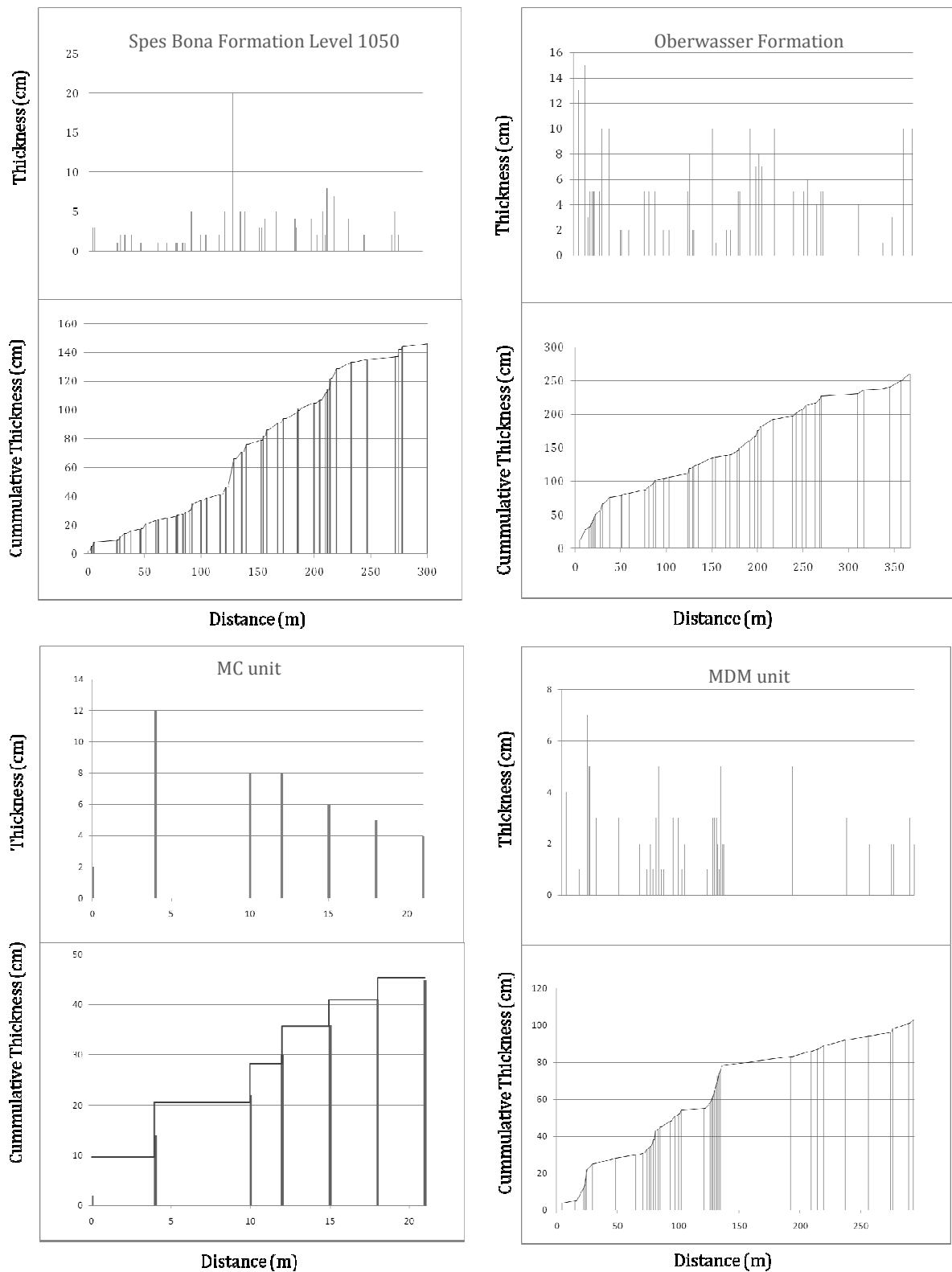


Fig. 5.10 Stick diagrams and staircase plots from 6 panels through sheeted quartz veins in the different lithological units of the open pit. The gradient of the staircase plot is a measure of the extensional strain, and the irregularity of the curve is a measure of the heterogeneity of the strain (Gillespie et. al., 1999). Note that the apparent lack of veining from 140m to 180m in the diagrams and plots for the MDM unit, is due to the limited sampling because of bad outcrop conditions.

(b) Vein spacing

The variability of spacing of veins along a sampling line, is given by the coefficient of variation (C_v), and is defined as the ratio of the standard deviation ($SD_{(s)}$) to the mean value of the spacing (s) (Gillespie et. al., 1999):

$$C_v = SD_{(s)} / s$$

This factor is used to determine the degree of clustering of points along a sampling line. Typically, clustered veins will have spacings that show larger variations compared to equally spaced veins, and therefore will have a $C_v > 1$. Regularly spaced veins (anticlustered) have a $C_v < 1$, whilst veins with a $C_v = 0$ are equally spaced.

At Navachab, vein spacing estimates are complicated due to the presence of conjugate sets in the siliceous units of the open pit. Although the distribution of veins along the siliceous units of the open pit appear regular, zones of closely spaced veins (herein referred to as clusters) with distributions of up to 8 veins over 10m have been identified. Vein clusters are typically bounded by less populated zones, but even here, the spacing does not exceed 8m (Fig. 5.4 and Fig 5.5). Clustering is much more pronounced in the MDM unit, where up to 10 veins can occur over 3m. Here, like in the siliceous units, clusters are often separated by less populated zones (Fig 5.4 and 5.5). The lack of veining surrounding vein clusters may suggest that the veins are separated by strain shadows, i.e. repeated fracturing and veining is confined to existing veins, rather than initiating in intact wall rock. Vein spacing data from the MC unit are limited to one sampling line and short intersections by two boreholes, but show distributions of up to 10 veins over less than 15m, similar to clusters in the silicious units.

Quartz vein data from sampling lines and drillcore from the open pit have a C_v for the spacing of veins ranging from 0.67 to 0.98 for the siliciclastic units and from 0.41 to 1.49 for the marbles (Table 5.1). Although clustering is observed in outcrop, the overall spacing of veins in the siliciclastics is generally regular, whilst veins in the marbles can be regular or clustered. In the MDM unit, one sampling line and two boreholes show veins with power law distributions ($C_v > 1$), whilst only one borehole has a $C_v < 1$.

5.2.4 Vertical extensional strain

Vein opening directions in the shallowly-dipping sheeted quartz veins are subvertical, so that aggregated vein thicknesses (V_t) measured parallel to vein opening directions and perpendicular to vein walls provide an estimate of vertical extensional strain during veining. The extensional strain is calculated here as a percentage

$\Delta L = e \times 100$, where:

$$e = L_f - L_i / L_i = V_t / L_i$$

and where L_f is the thickness of the vein swarm, measured from the base of the lowermost-vein to the top of the uppermost-vein, and L_i the pre-failure thickness of the host rock given by $L_i = L_f - V_t$, assuming ideal elastic behaviour of the host rock during fracturing.

The extensional strain for the different lithologies in the Navachab open pit were derived from vein data from the eastern and western walls of the open pit and 5 boreholes that intersect the vein swarm (Fig 5.2). The data indicate that extensional strains are, on average, 2.25 %. On average, higher values are reached in the siliceous units (0.91% - 3.52%), while marbles yield consistently lower values (0.77% - 1.4%). From Table 5.1 it is also evident that veining and, as such, the computed extensional strains are higher towards the base of the open pit in rocks of the Spes Bona and Oberwasser Formations.

5.2.5 Vein mineralogy and hydrothermal alteration

The vein mineralogy and alteration associated with quartz veins is briefly presented in the following, since massive sulphide veins form an important component of the economic intersections in the open pit. The quartz veins and associated wall-rock alteration provide evidence for fluid flow, representing the vestiges of fluid pathways. The actual vein mineralogy and associated hydrothermal alteration that can be used to describe the composition of the fluid and P-T conditions of the mineralization and alteration have been studied in detail by Wulff (2008). In this chapter, the focus is on alteration geometries that may be used to describe fluid pathways and the salient mineralogical features of the alteration are only briefly summarized. The veins themselves consist of quartz with minor amounts of K-feldspar and carbonates.

Sulphides are locally abundant and contain mainly pyrrhotite with minor amounts of chalcopyrite, pyrite, arsenopyrite, maldonite and bismuthinite. Gold is typically very fine grained, rarely exceeding several tens of microns in size, and occurs mainly as free gold.

Alteration selvages around veins differ in thickness and mineralogy, depending on host rock type, as well as vein type. In the siliceous footwall and hangingwall units, quartz veins are typically surrounded by up to 2cm thick zoned alteration selvages (Fig. 5.6g). Wulff (2008) recognized two types of alteration around veins in the biotite schists of the Oberwasser and Spes Bona Formations:

1. actinolite-alteration typically consists of large porphyroblasts of actinolite (up to 20% of the alteration zone), relicts of biotite and feldspar, minor calcite, titanite and rare garnet (Fig 5.11b), and
2. garnet-biotite-alteration constitutes massive garnet replacement of the host rock, with associated biotite and minor K-feldspar.

In this study, veins with alteration mineralogy consisting mainly of chlorite, with minor calcite, biotite and sphene were also observed (Fig. 5.11a). Chlorite is overgrown by large (up to 4mm diameter) subhedral garnet porphyroblasts. At the same time, chlorite is slightly deflected around garnet porphyroblasts indicating the contemporaneous growth of garnet and chlorite and their late-kinematic growth in vein selvages. The outer zone of the selvedge is composed of mostly biotite overgrown by garnet porphyroblasts, with minor quartz, K-feldspar, sphene and plagioclase. In addition to the hydrothermal mineral assemblages, vein selvages are often associated with sulphides such as pyrrhotite, chalcopyrite, and minor pyrite.

Wulff (2008) recognized two types of alterations related to veins in the MC unit:

1. garnet-clinopyroxene-K-feldspar-quartz alteration, generally only restricted to the calcitic layers of the MC unit, and consisting of large irregular clinopyroxenes and garnets with a gradual increase of small recrystallised quartz and K-feldspar distally, and
2. garnet-biotite alteration of calc-silicate and calcitic layers, with large amounts of actinolite and relict K-feldspar and clinopyroxene in the altered calc-silicate rock.

The main shallow dipping sheeted quartz vein set in the *MDM unit* is characterized by an up to 4cm thick bleaching of the host rock around the veins (Fig. 5.6l). The bleached halos make the otherwise thin veins (often less than 1cm) easier to recognize in the open pit. Sulphides (pyrrhotite and chalcopyrite) occur as either disseminated inclusions in the alteration halo of veins, or associated with garnet and green clinopyroxene in necks and rims of boudinaged veins.

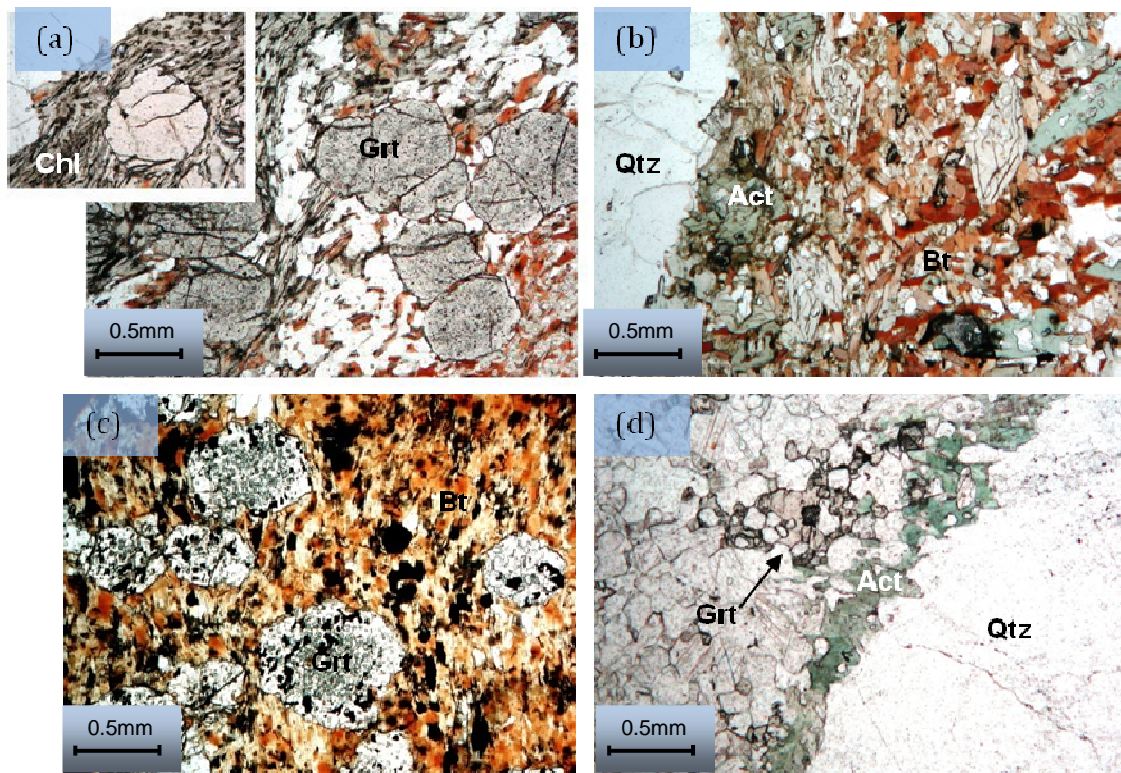


Fig. 5.11 Photomicrographs of (a) garnet-biotite-chlorite alteration around quartz vein in schist (PPL). (b) actinolite alteration around quartz vein in schist (PPL). (c) garnet-biotite alteration related to massive skarn-type replacement around a quartz vein (PPL). (d) garnet-actinolite alteration around a vein in calcitic layers of MC-unit (PPL). All mineral abbreviations after Kretz (1983).

5.2.6 Vein textures

Quartz veins in the open pit are predominantly massive and made up of milky or slightly smokey grey to clear quartz. Microcracks in veins are common and occur as thin sulphide-filled (mostly pyrrhotite and chalcopyrite) cracks perpendicular to the vein walls (Fig. 5.6f). In thin section, veins consist dominantly of coarsely recrystallized quartz (up to 5mm diameter), with subordinate fine-grained K-feldspar and carbonates. Apart from the thin microcracks, quartz in the veins shows undulose extinction and, in places, subgrain boundaries that indicate the ductile recrystallization of veins. For the most part, however, quartz is statically recrystallized displaying well-developed equilibrium textures with straight grain boundaries and 120 degree triple junctions between adjacent grains. Primary quartz-vein growth microstructures such as crack-seal textures or open-space filling are conspicuous by their absence. These textures testify to the post-emplacement deformation of veins and the fact that veins were emplaced at high temperatures that allowed for the post-tectonic recrystallization of the textures.

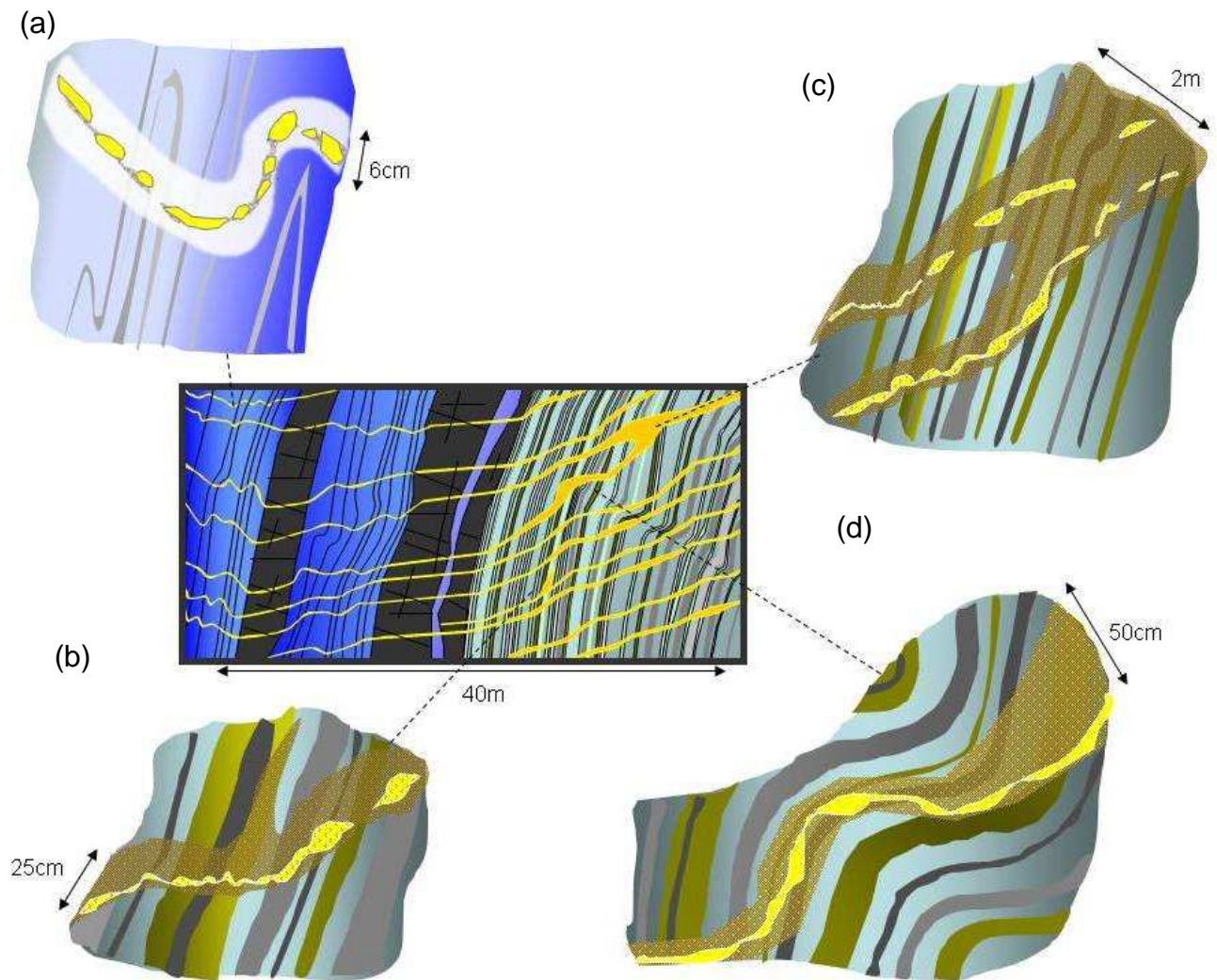


Fig.5.12 The central panel represents a structural profile of the northern open pit wall (view to the north) showing quartz veining in the Okawayo Formation in the Navachab open pit (See Fig 5.2). Blue: banded marbles of the MDM unit; dark grey: metalamprophyre; banding denotes interlayered marble and calcisilicate bands of the MC unit (light blue: marbles; green/grey: calcisilicate felses). Outcrop sketches a-d represents detailed observations of deformation and alteration features associated with quartz veins. (a) Irregularly-shaped and buckled quartz vein in the MDM unit with bleached halo around vein. (b) Irregular and buckled quartz vein in the MC unit with massive alteration halo around vein. Note (1) how alteration halo branches off parallel to the bedding of the MC unit, and (2) that the alteration halo is significantly wider along the top margin of the vein. It is characteristic for the MC, not so well developed in the MDM. (c) Discontinuous, irregular and buckled quartz veins in MC unit. Note how alteration halo significantly widens where veins are closely spaced. (d) Irregular and folded vein in MC unit. Note that the quartz vein cross-cuts the layering, but is folded together with the layering, displaying more open fold shapes, suggesting that veining occurred during folding.

5.2.7 Massive sulphide veins

Massive sulphide veins, also referred to as massive sulphide lenses, are restricted to the MC unit and are particularly pronounced at the contact with the Spes Bona Formation schist (Fig 5.12a-d). Macroscopically, massive sulphide lenses consist predominantly of pyrrhotite, with minor amounts of specks of chalcopyrite. Quartz commonly occurs as short stubby lenses. A relic banding parallel to the banding in the MC unit is, locally, defined by alternating garnet, garnet-diopside and biotite-rich bands. The preservation of this banding was previously interpreted as a stratiform replacement skarn (e.g. Moore et al., 1998).

The mineralogy of the massive sulphide alteration lenses has been studied in detail by Wulff (2008) who recognized two main alteration assemblages:

1. garnet-biotite alteration
2. garnet-clinopyroxene-K-feldspar-quartz alteration

Typically, massive sulphide lenses are associated with an increase in garnet toward the lens, followed by a garnet-biotite alteration at the contact with the massive sulphide lens. In the massive sulphide lens, alteration assemblages are typically zoned, defined by the pre-existing compositional variations of the host rock. Ore minerals make up >50% of the altered rock and consist of pyrrhotite (more than 70% of ore minerals), chalcopyrite, sphalerite, arsenopyrite, as well as minor native bismuth, bismuthinite, and bismuth-tellurides. Small grains (0.1 mm) of free gold are associated with native bismuth, bismuthinite, bismuth-tellurides, and arsenopyrite.

Detailed mapping of a well exposed section along the northern panel through the MC unit in the open pit shows that massive sulphide veins are alteration products of the main sheeted quartz veins as they cross-cut the intercalated marbles and calc-silicates of the MC unit (Fig. 5.12a-d). Massive sulphide alteration around shallowly dipping veins in the MC unit can be up to 50cm wide, but may form several meter wide lenses where veins are closely spaced. The massive sulphide lenses that characterize the mineralization in the Navachab open pit form due to the coalescence of alteration halos around closely spaced (< 0.5-1m) sheeted quartz veins that intersect the MC unit (Fig.

5.13a). In general, alteration halos around shallow-dipping veins in the MC unit show a distinctly asymmetric development around the central vein (Fig. 5.12c and Fig. 5.13b). The alteration halos at the bottom margins of the veins are commonly less than 5 cm wide, planar to slightly undulating and parallel to the vein, sharply truncating the compositional layering in the MC unit. In contrast, alteration halos in the immediate hanging-wall of the veins are highly irregular and characterized by bedding-parallel offshoots giving the otherwise vein-parallel alteration a very ragged and sawtooth-like geometry. These flame-like alteration offshoots can reach widths of up to 50 cm and cross-sectional lengths of up to 2m. Bedding-parallel massive sulphide veins develop when these vertical offshoots of two or more closely-spaced horizontal veins combine and overlap (Fig 5.13a.). In these cases, quartz veins remain only as small relics and, in many cases, a clear connection between sheeted quartz veins and massive sulphide lenses is easily overlooked when mapping these lenses. The massive sulphide lenses have highly irregular shapes, and characteristically assume a subvertical orientation, often making use of the pre-existing anisotropy of the host rock, by branching off into the compositional banding (Fig. 5.12b) The original layering of the MC unit is, locally, preserved, but the mineralogy of the calc-silicate bands consists mainly of garnet, diopside and biotite. Massive sulphide veins range from < 1 to > 3m in width and up to > 5 m in height. The pyrrhotite-dominated massive sulphide lenses weather quite easily and typically have a rusty brown colour when exposed on fresh surfaces. The massive sulphide lenses plunge shallowly (10° - 25°) to the NNE, parallel to the intersection lineation between the shallowly-dipping veins and the steep layering of the MC unit (Fig. 5.13c). This corresponds to the plunge of the main mineralized shoot in the MC unit as described by previous authors (Moore et al., 1998; Steven and Badenhorst, 2002; Kisters, 2005).

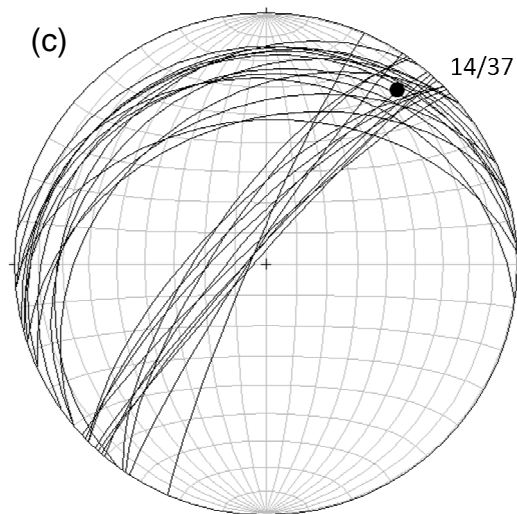


Fig. 5.13 (a) Quartz veins in the MC unit, with massive sulphide alteration halos around veins (annotated), showing the significant widening of the alteration halo where 2 or more veins are closely spaced. Note how the cross-cutting quartz vein and alteration halo is folded with the MC layering (blue). Field of view is 10m. (b) Irregular quartz vein with massive sulphide alteration, localized almost exclusively on the surface side of the vein. (c) Lower hemisphere equal area projection of shallow northerly dipping sheeted quartz veins and the steeply NW dipping layering in the MC unit. The intersection of the veins and the layering in the MC unit plunges shallowly to the NNE (14/37), parallel to the plunge of the mineralized shoot in the MC unit, and defined by the grade envelope around the massive sulphide lenses.

5.3 Subordinate veins:

Subordinate quartz veins are only developed as thin, less than 1cm thick veinlets, not more than 8 to 10 meters in strike. They are largely confined to the siliceous units of the open pit. The only exception are short and stubby “penny shaped veins”, often exceeding thicknesses of more than 10cm.

Similar to the sheeted veins, the geometry and morphology of subordinate veins in the open pit is strongly influenced by the host rock type. They all have sharp vein boundaries, with only thin biotite-amphibole alteration halos around some veins. Subordinate quartz veins are generally near planar, and incorporate no wall-rock slivers. Vein terminations are usually abrupt (e.g. penny-shaped veins), often only characterized by a sudden thinning of the vein over a couple of centimeters.

Four types of subordinate veins occur (Fig. 5.14):

Bedding parallel veins are generally more common in well-bedded schistose units, where they occur along bedding planes or parallel to the penetrative bedding sub-parallel schistosity of the host rock. In places, quartz veining is very subordinate and fluid flow is only evidenced by thin biotite-actinolite alteration halos and associated sulphide mineralization. Bedding-parallel veins are relatively inconspicuous in the marble units, occurring only as, rare thin quartz stringers, not more than 1cm thick.

Similarly, *sub-vertical N-S trending veins* are predominantly confined to schistose units of the siliciclastics, where they cross-cut the host rock fabric at low angles. Rare examples of E-W trending veins in siliciclastics occur as thick (up to 10cm wide), short (not more than 5m in strike length) gashes.

Steep southerly dipping veins, also referred to as “penny-shaped veins” (Kisters, 2005), are strictly confined to the metapsammitic and calc-silicate layers of the siliciclastic formations. These veins show a strong lithological control being confined to relatively competent beds such as metapsammites and terminating sharply against for example schistose lithologies and the hanging- and footwall. The veins are typically short (0.5 to 1.5 m), determined by the thickness of the competent bed. The maximum thickness of

up to 20 cm is commonly reached in the central parts of the veins, tapering towards vein terminations, which results in their penny- or disc-shaped geometry. They occur at high angles to the host layer and the spacing between veins is between 2-5 meters.

5.4 Vein deformation

The competency contrast between different host rock types in the open pit exerts a profound control on the progressive deformation of quartz veins. Syn-emplacment deformation effects can be distinguished from those that have affected veins after their emplacement.

Refraction of veins:

Veins show a clear refraction across lithological contacts, best observed across contacts between for example rocks of the Oberwasser Formation with marbles of the Okawayo Formation. As veins cross-cut the contact between siliciclastics and marble units, the veins are refracted to steeper dips, by angles between 10-20 degrees. The refraction of veins is likely to be related to the actual fracture propagation during veining rather than reflecting post-emplacment deformation. It illustrates strain refraction in rocks of different competencies, which is also evidenced by the development of conjugate shear veins versus extensional veins in siliciclastic and marble units.

The refraction of veins is also evident on a smaller scale and veins in marble units are typically refracted between centimeter scale intercalated calc-silicate felses and marble bands. Here, the orientations of veins are less consistent due to post-emplacment deformation of the veins and host lithologies, but measurements of the enveloping surface of buckled veins show that the veins dip shallowly (14° - 37°) to the north and northwest. Similar relationships are recorded along the contact of the MDM and MC units with the central lamprophyre sills. Quartz veins are refracted to steeper dips in the marbles along the contact and only one vein set is developed in the marbles, whereas shallower dips and conjugate vein sets dominate in the metalamprophyre sills.

Folding and boudinage of veins:

The folding and boudinage of veins illustrates the deformation of the vein sets after their formation. Folding and boudinage of shallowly-dipping quartz veins is most pronounced in marble units, but rather subtle in siliceous rocks, including the central metalamprophyre. The intensity of deformation varies even between different marble units. For example, shallow veins in the MDM unit are often tightly folded compared to only slightly buckled veins in the MC unit (Fig. 5.15). Analysis of the fold shapes suggests a minimum amount of shortening of 35% for the MC unit, and up to 50% for the MDM unit. The axial planes of folds are mainly upright and folds are symmetrical. Fold limbs may undergo boudinage as they assume an upright orientation during fold amplification and tightening. Although shallow veins cross-cut the main lithotypes at high angles, clear examples exist in the MC unit where veins and the intercalated calc-silicates were folded together (Fig. 5.6r and 5.13a). The folds defined by quartz veins have been referred to by Kisters (2005) as F2b folds. They show similar shallow NE plunges compared to parasitic folds, but are rather symmetrical folds, whereas F2a folds are asymmetric vergence folds, related to the first-order Karibib dome. The upright NE trending axial planes and symmetrical fold shapes of F2b folds record a largely co-axial shortening strain at high angles to the steep bedding on NW limb of the Karibib dome.

Shallowly dipping quartz veins in siliceous units are only gently folded and appear considerably less deformed compared to veins in the marbles. This probably reflects the similar competence of quartz veins in schists as opposed to the large competence contrast between veins and marbles that promotes folding.

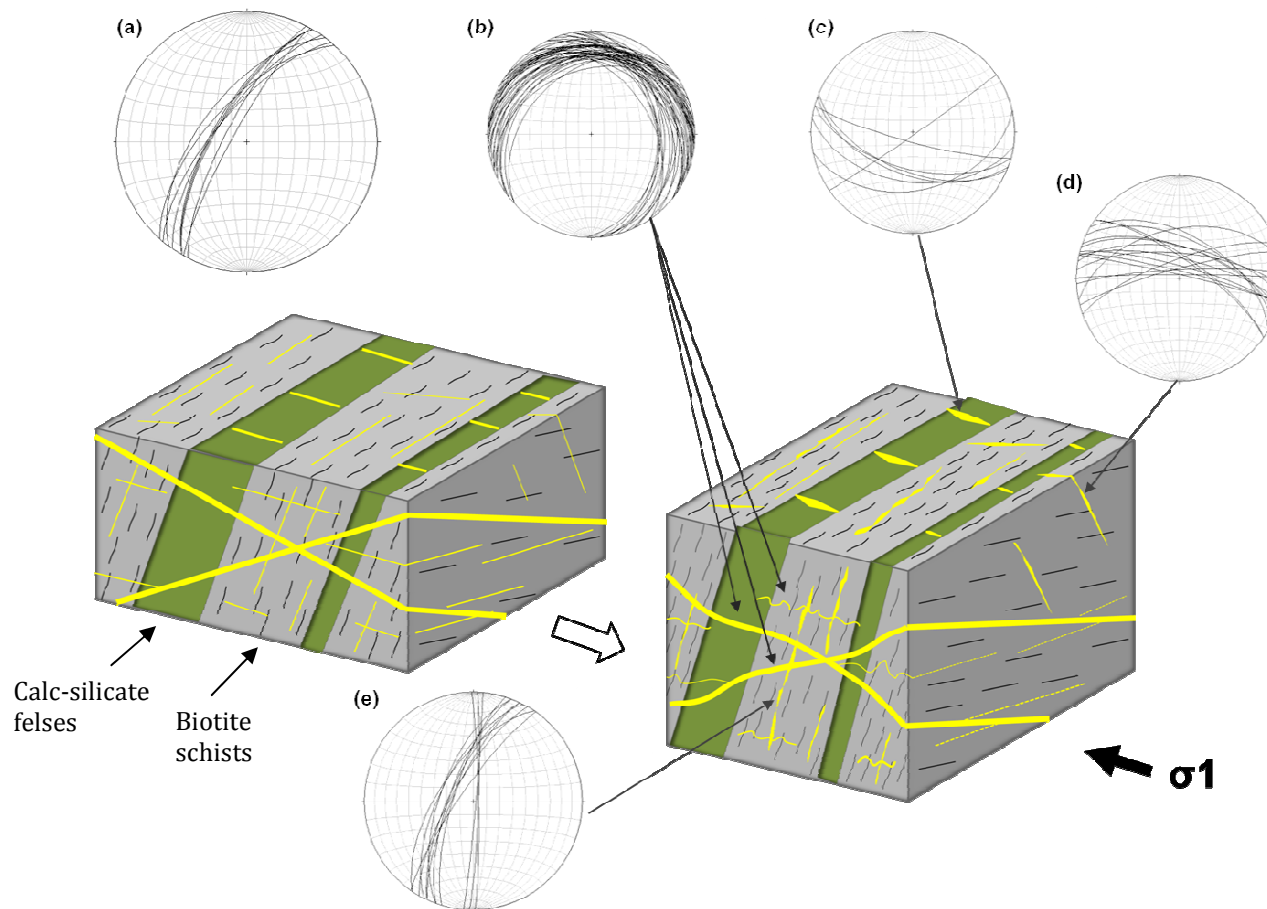


Fig. 5.14 Isometric block diagram illustrating the orientation and deformational behaviour of quartz veins (yellow) in siliceous units of the open pit during coaxial deformation (left-hand diagram: undeformed; right-hand diagram: deformed). The stereonets show the orientation of veins sets in siliceous units (lower hemisphere equal area projection). (a) Shallow northerly dipping sheeted quartz veins consists of a conjugate veins set as well as sub-horizontal extensional veins that show varying degrees of buckling (b) Short and stubby “penny shaped” veins are typically confined to metapsammitic and calc-silicate layers and have a scatter of orientations, but with predominantly steep southerly dips. (c) Steep E-W trending, N-dipping veins. (d) N-S trending and bedding parallel veins are typically boudinaged during coaxial deformation.

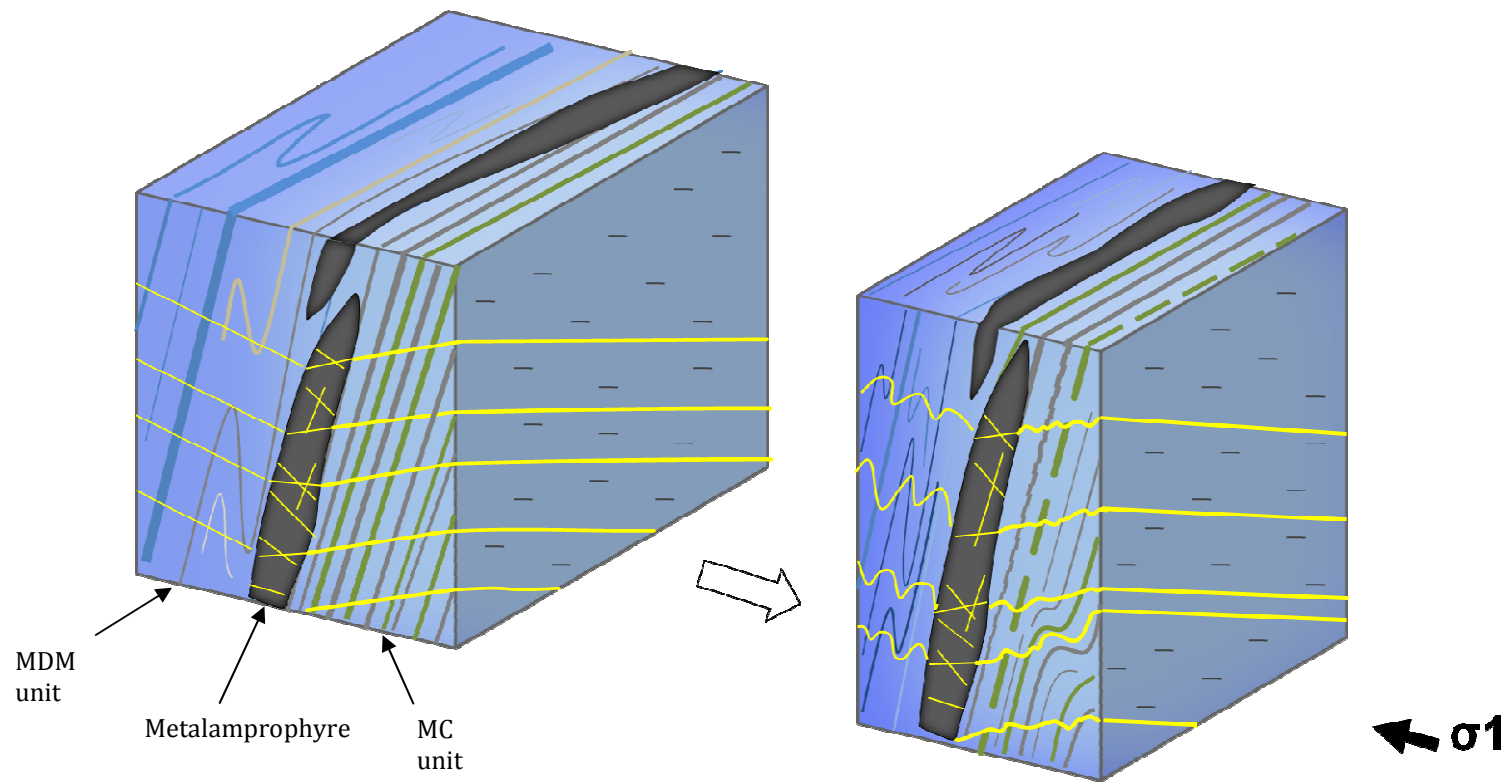


Fig. 5.15 Isometric block diagram illustrating the deformational behaviour of shallow dipping sheeted quartz veins (yellow) in marble units of the open pit during coaxial deformation (left-hand diagram: undeformed; right-hand diagram: deformed). Veins crosscut earlier folds (F1 and early F2), but clear examples exist in the MC unit where veins and the intercalated calc-silicates were folded together. Note the tight folding of veins in the MDM unit compared to only a slight buckling in the MC unit.

Shallowly-dipping quartz veins in siliceous units are commonly boudinaged in the plane of the veins (Fig 5.16). Quartz boudins are either rectangular shaped or veins may show “pinch and swell” structures, but are rarely separated by more than 1cm. Coarsely recrystallized pyrrhotite commonly occupies the necks of boudinaged quartz veins, indicating the post-emplacment remobilization of sulphides (Fig. 5.6f). Necklines between boudins show relatively consistent plunges of 20°-30° to the SE and 25°-45° to the NE. Importantly, the boudinage of the shallowly-dipping quartz veins suggests subvertical shortening, at high angle to the NW-directed subhorizontal shortening strain recorded on a regional scale and by the folding of for example quartz veins in marbles.



Fig. 5.16 Shallow northerly dipping and boudinaged quartz vein, showing well-developed necklines on the surface of the vein. Note the pyrrhotite in the necks of the boudinaged vein, indicating post-emplacment remobilization of sulphides.

6. Geology of the NE part of the Usakos dome

The northeastern hinge of the Usakos dome was mapped on a 1:10 000 scale, covering an area of 35km² (Fig 6.2). In the Usakos Dome and around Anomaly 16, basement rocks of the *Abbabis Metamorphic Complex* together with the *Etusis* and *Chuosi Formations* are not exposed. Instead, rocks of the *Spes Bona Formation* form the lowermost stratigraphic unit of the Damara Supergroup exposed in the area.

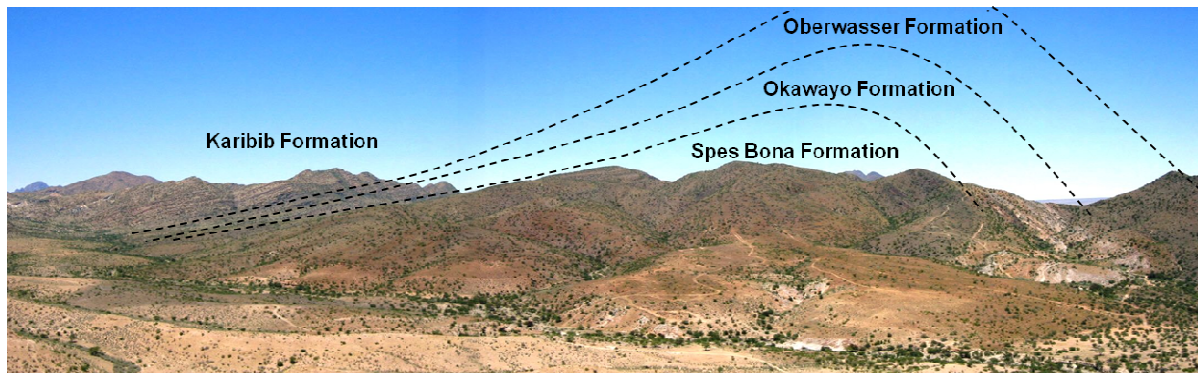


Fig. 6.1 View of the NE hinge of the Usakos dome to the SW, subparallel (up plunge) to the foldaxis of the fold, showing the regional NW vergence of the dome, defined by a shallow dipping SE limb and a steep NW limb. Note also the thickening of the lithologies on the NW limb.

The *Spes Bona Formation* makes up the core of the Usakos dome (Figs 6.1 and 6.2). It consists of well-developed, stratigraphically correlateable units and reaches a minimum thickness of 600m (Fig. 6.3 and Fig. 6.4). This indicates an, at least, fourfold increase in thickness compared to the *Spes Bona Formation* in the adjacent Karibib dome. The basal parts of the *Spes Bona Formation* consist of a ca. 200m thick succession of biotite-cordierite schists that grades upward into a sequence of thick, interbedded metapsammities (20-50m) and biotite schists. Alternating grey and dark grey banding and grain-size variations indicate the bedding in the schists. In contrast, the metapsammities are typically light grey to greenish in colour, but reddish brown when weathered (Fig. 6.5a). The preservation of sedimentary features like cross-bedding in metapsammities points to the competence of metapsammities during deformation, contrasting with the pervasive schistosity developed in biotite-rich rocks (chapter 6.1). Most of the topographic highs in the core of the Usakos dome are made up of metapsammities. Several massive milky quartz veins and pegmatite dykes and sills intrude the *Spes Bona Formation* in the core of the Usakos Dome.

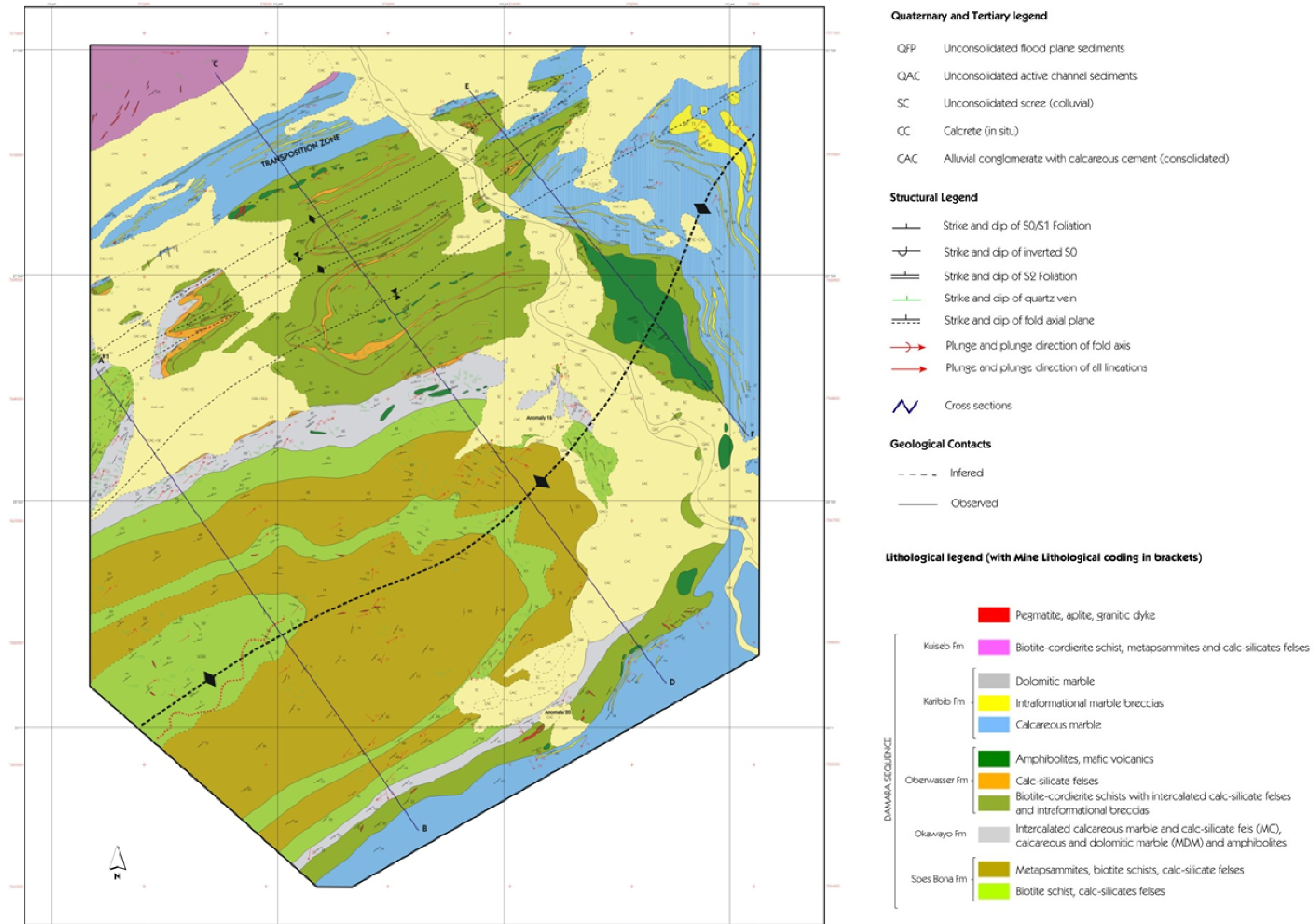


Fig 6.2. Geological map of the northeastern part of the Usakos dome, showing the axial traces of the first-order Usakos dome and secondary folds. Original map (scale 1:10 000) is included in Appendix 10.3

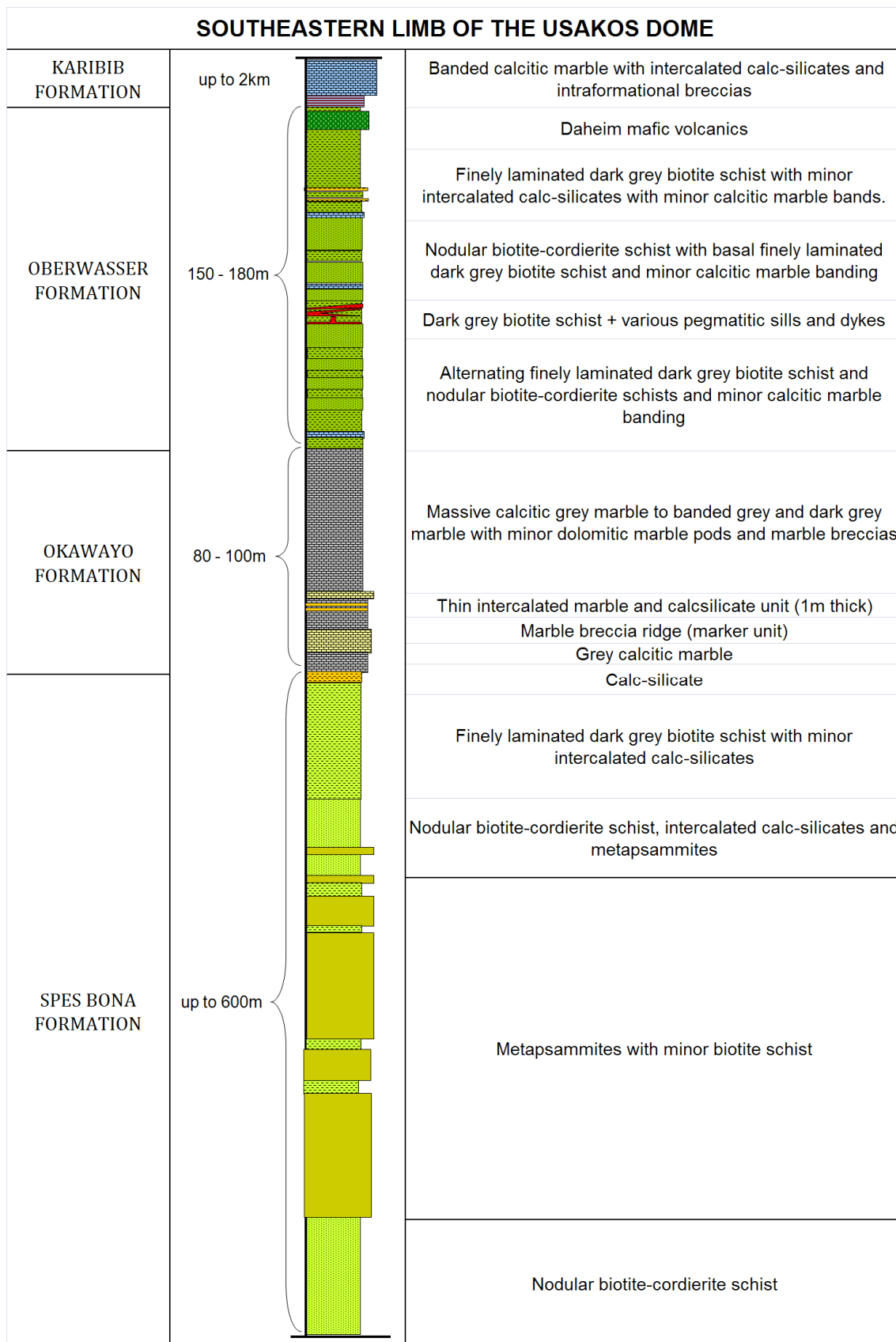


Fig 6.3 Lithostratigraphic column of the southeastern limb of the Usakos Dome; the lower contact of the Spes Bona Formation is not exposed.

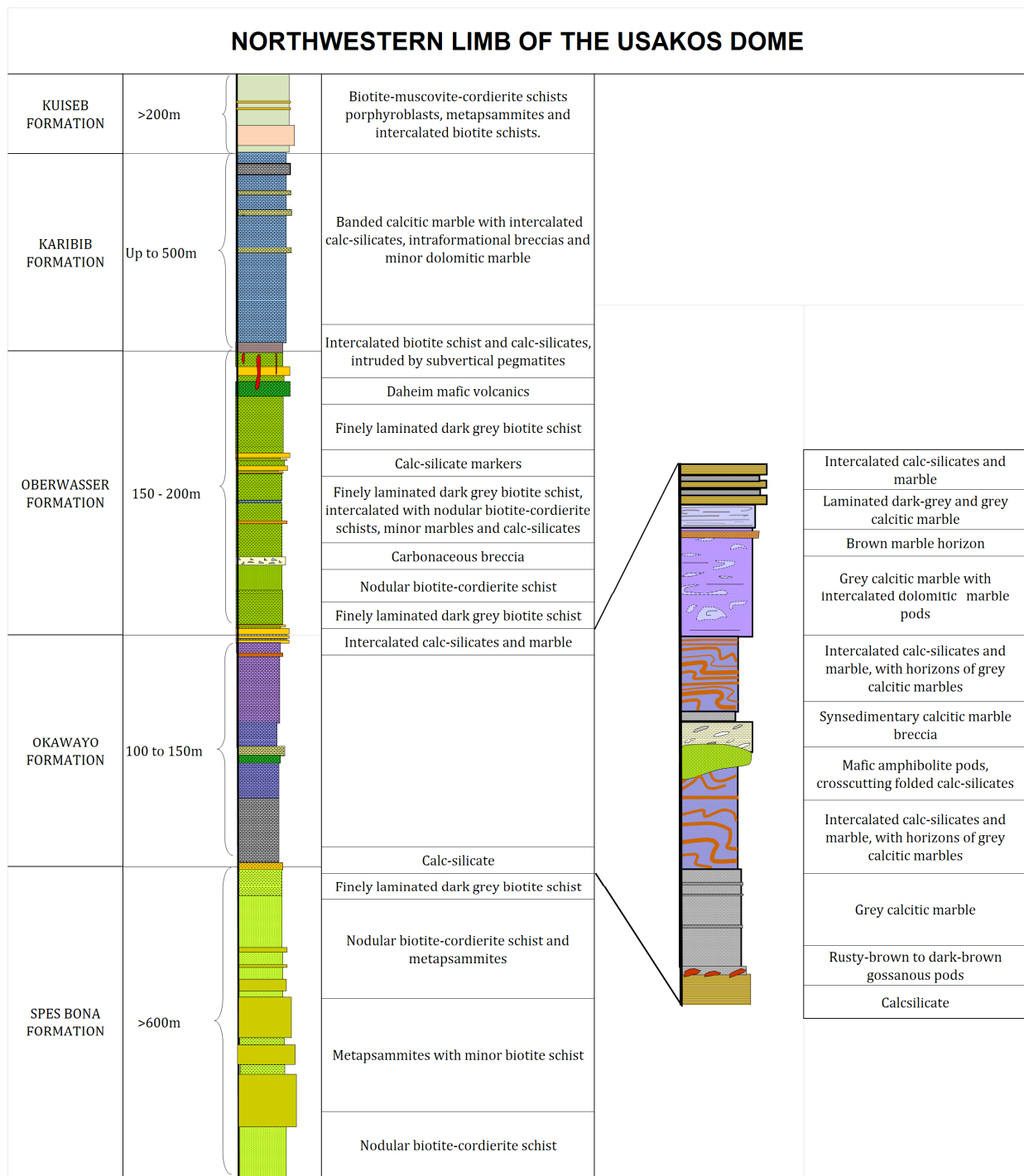


Fig 6.4 Lithostratigraphic column of the northwestern limb of the Usakos dome. The inset shows details of the lithologically and structurally heterogeneous Okawayo Formation at Anomaly 16.

The Spes Bona Formation is overlain by the *Okawayo Formation* (Fig. 6.3 and Fig. 6.4). The contact is marked by a 2m to 10m wide calc-silicate unit with minor intercalations of marbles and biotite schists. The Okawayo Formation is a heterogeneous unit with highly variable thicknesses, ranging from 80m on the SE limb to 150m on the NW limb. It consists of various marble-dominated subunits that vary in thickness from 1m to 100m. These subunits cannot be readily correlated throughout the hinge of the dome, suggesting that the Okawayo Formation preserves, at least in parts, a tectonostratigraphic succession (chapter 6.1). The following subunits could be distinguished in the Okawayo Formation, from bottom to top (Fig. 6.4, inset):

- A fairly homogenous recrystallized *grey marble*, with minor interbedded breccias is located at the base of the Okawayo Formation and ranges in thickness from 10m to 40m (Fig. 6.5b). At Anomaly 16, rusty brown gossanous pods occur along the contact between the *grey marble* unit and calc-silicate felses of the Spes Bona Formation.
- An *intercalated marble and calc-silicate* unit occurs in the lower to middle parts of the Okawayo Formation (Fig. 6.5c-d). The calc-silicates felses range in thickness from less than 1cm to more than 10cm, showing a regular spacing. In the field, it is a highly recognizable unit that is often characterized by the tight folding and boudinage of the calc-silicate layers (chapter 6.1). The marbles are commonly recrystallized, light-grey to brownish-grey in colour, but may appear reddish-brown due to staining from the weathering of calc-silicate felses. The overall thickness of the unit ranges from less than 1m on the SE limb of the Usakos dome to up to 80m on the NW limb.
- *Marble breccias* are recognized by highly stretched, white to light-grey marble clasts in a recrystallized darker-grey matrix. The breccia horizons commonly form prominent ridges that can be used as markers in the field. In high-strain zones, the clasts in the marble breccias may be drawn out to such an extent that the stretched fragments mimic a compositional banding (chapter 6.1).
- A *marble and dolomitic marble* unit occurs toward the top of the Okawayo Formation, and is distinguished from the other units by intensively deformed cream-coloured dolomitic boudins set in a grey to dark-grey marble matrix (Fig. 6.5e). The dolomitic marbles boudins are often associated with quartz veining and the growth of tremolite.

Large amphibolite bodies occur in the Okawayo Formation on the northwestern limb and in the hinge of the Usakos Dome. The amphibolites cross-cut the layering in the marbles and can be up to 500m in length and 50m wide. In thin section, they consist of radiating clusters of actinolite and irregular hornblende prophyroblasts in a fine-grained matrix of mostly biotite, minor plagioclase and K-feldspar and opaques. Sphene is a common accessory mineral.

The contact of the Okawayo Formation with the overlying *Oberwasser Formation* is marked by the occurrence of several intercalated bands of prominent calc-silicate felsels in the marble units. The *Oberwasser Formation* is a thick sequence of biotite schists, biotite-cordierite schists, calc-silicate felsels, metapsammities, marble horizons, amphibolites and minor marble breccias. The unit varies in thickness from 150m on the SE limb to more than 200m on the NW limb (Figs 6.2 to 6.4). The subunits range from 5m to up to 50m in thickness. The biotite schists are the dominant rock type. They are dark-grey to brownish in colour (when oxidized) and display a penetrative schistosity (Fig. 6.5f). Bedding is recognized by changes in colour, texture and compositional variations, but is usually obscured by the penetrative schistosity. The schists often contain up to 1cm large cordierite porphyroblasts, which result in a spotted appearance. In the field, cordierite is confined to certain horizons, reflecting different compositions of the sedimentary protolith and, thus, outlining bedding. A 2m to 5m thick marble breccia horizon is confined to the lower parts of the Oberwasser Formation. Several layers of calc-silicate felsels toward the upper parts of the sequence provide good marker horizons in the field. They are between 1 and 5m thick and fairly continuous, especially along the NW limb of the Usakos dome. In the field, the calc-silicates felsels have a light-brown to reddish appearance, but are grey-green on fresh surfaces (Fig. 6.5g).

The upper parts of the Oberwasser Formation are characterized by black amphibolites of the *Daheim Member* that occur as massive lenses. The most prominent of these lenses includes a large amphibolite body in the northeastern hinge of the Usakos dome (Fig 6.2), where primary volcanic textures such as lapillis testify to the volcanic origin of the amphibolites (Badenhorst, 1992). On the southeastern limb the amphibolites tend to thin out, and eventually disappear along strike to the southwest. Rare, centimeter-scale

carbonates lenses in the biotite schists occur in the upper parts of the Oberwasser Formation. Hoffmann et al. (2004) correlated these, together with thin marble horizons, to the Ghaub glacial diamictite and associated volcanics, which yielded a U-Pb zircon age of 635.5 ± 1.2 Ma.

The overlying *Karibib Formation* is a thick sequence of dolomitic and calcitic marbles forming the uppermost formation exposed in the hinge of the Usakos dome (Fig 6.5h-j). It varies in thickness from 500m on the NW limb to up to 2km on the SE limb. In the mapping area it is made up of predominantly calcitic marbles with minor (less than 1m thick) dolomitic layers, and several intraformational marble breccias that can be used as marker units in the field. The breccias occur mainly in the lower parts of the Karibib Formation, are between 0.5m and 5m thick, and are made up of white to light-grey marble clasts in grey to dark-grey marble matrix (Fig. 6.5i). The calcitic marbles are fairly heterogeneous and consist of grey marble, grey banded marble and intercalated calc-silicates felses. The grey banded marble units are made up of alternating, 0.5 to 10cm thick, white and dark-grey marble bands with associated reddish-brown calc-silicates felses. On the northwestern limb, a thin (5 - 20m thick) cream-colored dolomitic marble unit occurs at the top of the Karibib Formation, easily recognized in the field by the growth of tremolite and its positive weathering relief.

The *Kuiseb Formation* forms the topmost unit of the Damara Sequence in the area and is only exposed on the NW limb of the Usakos dome. It consists of biotite schists, biotite-cordierite schists, metapsammites and calc-silicate felses, and is intruded by several pegmatitic dykes. The base of the Kuiseb Formation is made up of more than 250m of biotite schists, which grade upwards into interbedded metapsammites, biotite schists, biotite-cordierite schists and calc-silicate felses. The upper part of the Kuiseb Formation is dominated by a thick sequence of biotite schists that are, however, only poorly exposed and largely covered by thick calcrete terraces. The grey to dark-grey biotite schists show a penetrative schistosity defined by the preferred orientation of biotite flakes. The schistosity obliterates most of the primary sedimentary features in the schists. In general, the schists are fine grained, but spotty when cordierites are present.



Fig. 6.5 Summary of the main rock types and styles of deformation on the NE part of the Usakos dome: (a) Metapsammites with well-preserved ripple marks in the core of the dome. (b) Grey marbles of the Okawayo Formation with intrafolial folds. (c) Folded intercalated marbles and calc-silicates in the Okawayo Formation. (d) Folded calc-silicates in the Okawayo Formation marbles, showing bedding (S0) overprinted by S2. (e) Folded and boudinaged dolomitic marble layers in the upper parts of the Okawayo Formation. (f) Oberwasser Formation biotite schists with large (up to 0.5cm) cordierite porphyroblasts. (g) Calc-silicates in the Oberwasser Formation on the NW limb of the Usakos dome, showing bedding (S0) overprinted by S1. (h) Grey marble of the Karibib Formation with moderate dipping lineation (L2t). (i) Typical monomict marble breccia of the Karibib Formation, with flattened grey marble clasts in a darker grey marble matrix. (j) Folded, boudinaged and transposed breccia and dolomitic marble layers of the Karibib Formation on the NW limb of the Usakos dome.

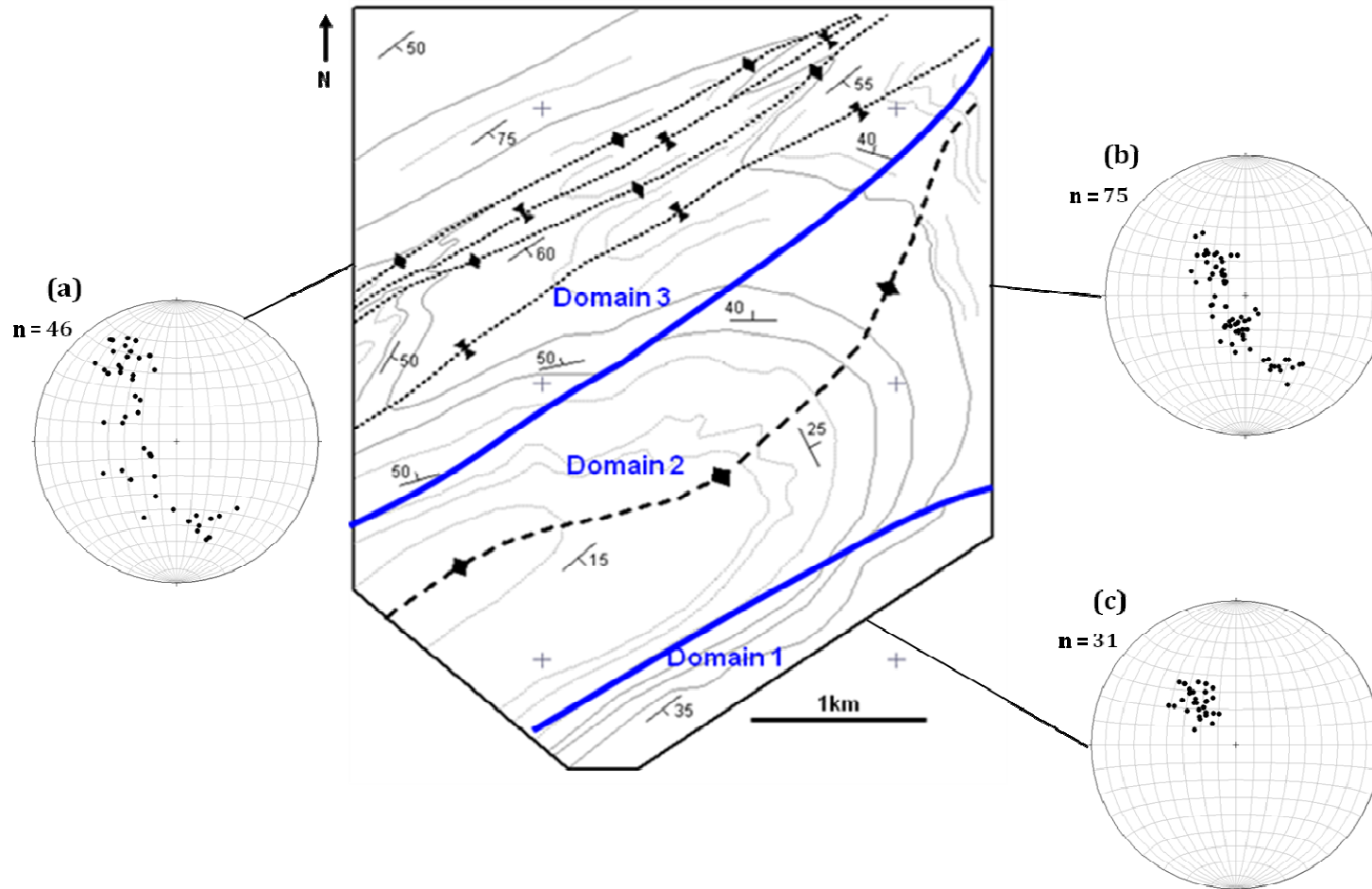


Fig 6.6. Simplified structural formline map of the NE part of the Usakos Dome showing the axial traces of the main first- and second-order folds, as well as the selected domains in the study area. All stereographic projections are equal-area, lower-hemisphere projections. (a) Poles to bedding of the lithologies that make up Domain 3, consisting of the tightly folded NW limb of the Usakos dome; (b) poles to bedding of the lithologies that make up Domain 2, consisting of the hinge of the Usakos dome. (c) poles to bedding of the lithologies that make up the Domain 1, consisting of the SE limb of the Usakos Dome.

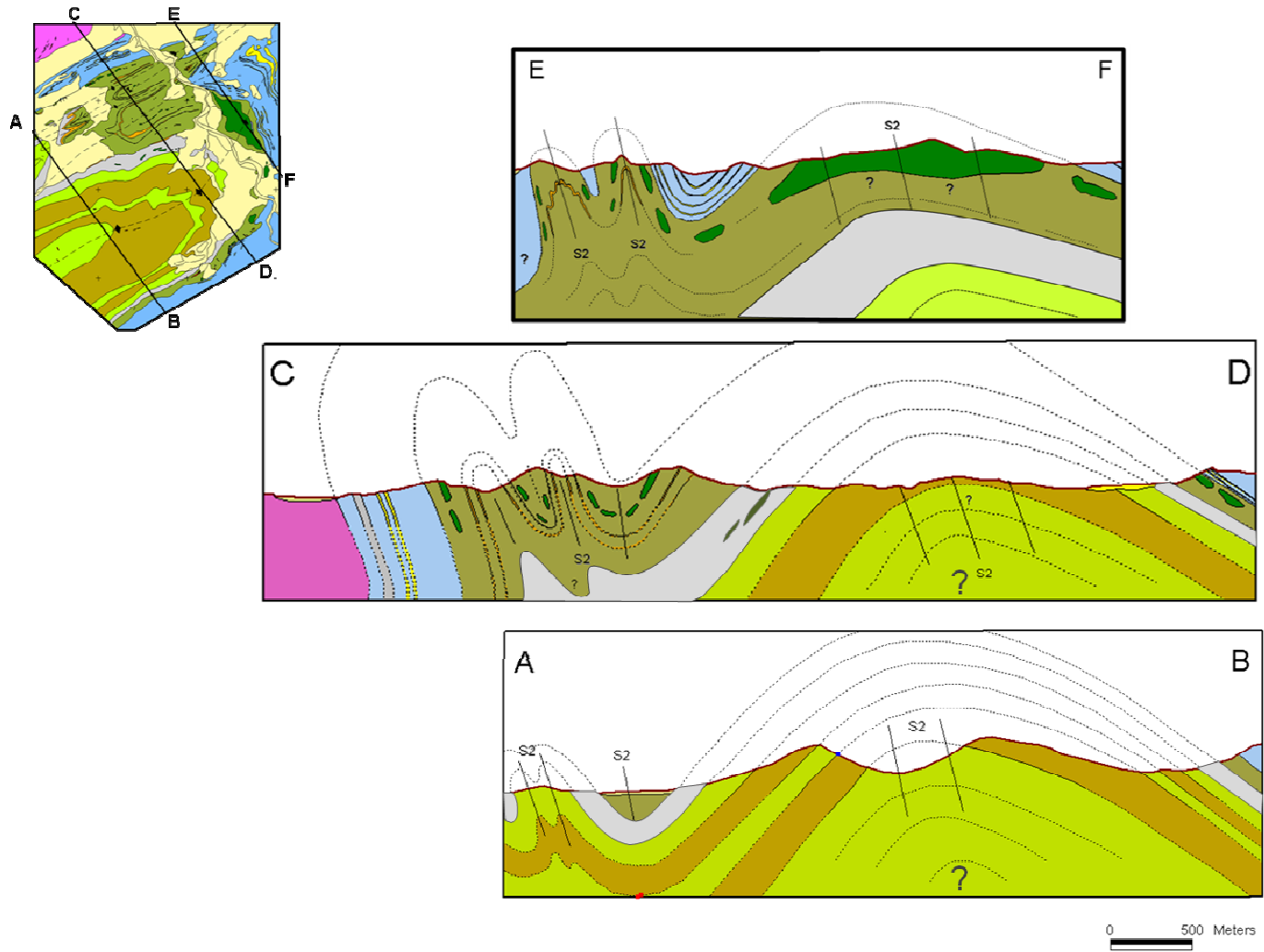


Fig 6.7. Geological cross-sections (view to the NE) through the NE lobe of the Usakos dome, showing the characteristic (1) NW vergence of the main lithologies, (2) thickening of the Okawayo and Oberwasser Formations on the NW limb, and (3) 2nd order, overturned tight folds on the NW limb of the Usakos Dome. Legend as in Fig. 6.2.

6.1 Structural geology of the NE part of the Usakos Dome

The study area is situated in the northeastern closure of the Usakos dome. The Usakos dome is a NW verging, doubly-plunging antiform that forms part of a series of NE trending dome structures in the sCZ (Neumaier, 2002; Kisters, 2004; Johnson, 2005). It consists of a shallow-dipping SE limb and a steep to overturned NW limb (Fig. 6.6 and Fig. 6.7). The axial trace of the anticline can be followed for over 25km along strike from the SW of Navachab to the E and SE of the town of Usakos (Smith, 1965). The Usakos Dome has a half-wavelength of, on average, 5km. The SW closure of the Usakos dome differs significantly from the NE hinge, the former representing a SW-ward closing sheath fold exposing largely overturned strata of the Damara Sequence that represent the lower limb of the km-scale sheath fold (Johnson, 2005). In contrast, the NE hinge shows, for the most part, gentle NE plunges and normal stratigraphic relationships. The fabric elements in the Usakos Dome are similar to those of the Karibib Dome, related to the two main deformation phases, D1 and D2 (Table 3.2). In the following, the broad hinge of the Usakos dome was subdivided into 3 domains, covering the NE and SW limbs as well as the core and hinge zone of the Usakos dome (Fig 6.6).

6.1.1 Domain 1: The SE limb of the dome

Domain 1 encompasses, from top to bottom, rocks of the Karibib, Oberwasser, Okawayo and Spes Bona Formations. This sequence dips at moderate to shallow angles to the SE and forms the SE limb of the Usakos dome (Fig. 6.6a and Fig. 6.7). Primary sedimentary features are well preserved, but strain intensities increase to the SE, where second- and third- order folds are abundant and where the marbles of the Karibib Formation are pervasively recrystallized and bleached. The marbles attain an apparent thickness of > 1500m in this zone, which indicates considerable structural thickening. Further to the SE the marbles are overlain by basement gneisses. This contact is obviously tectonic in nature and marks the trace of the regional-scale Mon Repos Thrust Zone (Kisters et al., 2004), along which rocks of the AMC were thrust over the Karibib Formation.

The S1 and S2 foliations are subparallel to each other, showing moderate SE dips (Fig. 6.6a). Lineations (L2m) in the schists are defined by either elongated aggregates of quartz or biotite, or trains of aligned cordierite porphyroblasts. Two orthogonal lineation populations can be distinguished; one plunging shallowly to the SW or NE,

parallel to the trend of the first-order Usakos dome, one plunging moderately to the SE. The latter (L2t) has a down-dip orientation and corresponds to the top-to-the-NW kinematics recorded in the Mon Repos Thrust Zone to the immediate SE (Fig. 6.5h). Toward the upper parts of the unit and close to the contact with the Karibib Formation marbles, occur massive, elongated (up 25 meters wide and tens of meters long) black amphibolite lenses of the Daheim member.

Several NE-SW and NW striking pegmatite dykes intrude into the schists of the Oberwasser Formation, terminating abruptly against the carbonate units of the Karibib and Okawayo Formations. The pegmatites show an internal layering and are, in places, gently folded into upright folds.

6.1.2 Domain 2: The hinge of the dome

Domain 2 includes the broad hinge of the Usakos dome, including lithologies from the Spes Bona Formation in the core of the dome, to the Karibib Formation. The ca. 2 km wide hinge of the Usakos dome is defined by the folding of lithologies and the earlier S1 fabric, bounded by steeply dipping NW and shallowly dipping SE limbs, resulting in the overall NW vergence of the dome (Fig. 6.7). The folding of bedding and S1 defines a shallow NE plunging hinge (Fig. 6.6b). S1 occurs as a well-developed penetrative bedding subparallel foliation in the schists of the Spes Bona Formations. Rare, tight, recumbent intrafolial folds occur in the schists, and are interpreted as F1 folds. Cordierite porphyroblasts are flattened in the S1 foliation. Compared to the pervasively foliated schists, the competent metapsammities and calc-silicate felses in the core of the dome show very little internal strain and primary sedimentary features such as ripple marks are well preserved (Fig. 6.5a). The S2 foliation is less prominent, occurring as a variably developed, steep (50°-70°) SE dipping foliation (Fig. 6.7). A weak mineral stretching lineation (L2m), defined by the alignment of mica and cordierites in the schist, plunges shallowly to the NE.

One of the most distinctive features of the hinge zone is the thickening and internal structural complexity of the Okawayo Formation that contrasts with the well-preserved stratigraphy of the under- and overlying formations. Compared to its development on the SE limb of the dome, the Okawayo Formation is highly heterogeneous and it can be

subdivided into several subunits (Fig. 6.4, inset) that show considerable thickness variations along strike.

Two fold generations can be distinguished in the marbles that lead to the duplication of units:

- (a) An earlier fold generation of intrafolial F1 folds that refolds bedding around shallowly-dipping axial planes contained within the composite banding (S0/S1) (Fig. 6.5f). F1 folds plunge shallowly toward the east (14/82) and range in size from a few centimeters to several meters in half-wavelength and amplitude.
- (b) A subsequent generation of F2b folds that refolds earlier folds. F2b folds have axial planes that dip between 40 and 65° to the SE, plunging shallowly to the NE and SW and parallel to the first-order Usakos dome.

Several large elongated (up to tens of meters wide, and hundreds of meter long) mafic bodies, intrude along the contact of the grey and the calc-silicate marble, as well as toward the middle of the latter. They are boudinaged, and cross-cut the primary layering in the marbles, indicating a pre or syn-tectonic origin.

Mineral lineations (L2m and L2i) are best developed in siliceous units and show shallow NE and SW plunges. In marble units, stretching lineations (L2m) are defined by highly stretched light grey marble clasts in marble breccias units, showing shallow plunges to the NE. Lower order parasitic folds in marble units have fold axes (L2f) that plunge shallowly to the NE. In calc-silicate felses, a prominent NE plunging lineation is developed, representing an intersection lineation (L2i) between S0 and S1. In addition, a moderately NNW plunging (45/340) lineation was also observed on the bedding planes of marbles

Rocks of the overlying Oberwasser and Karibib Formation record a marked decrease in D1-related strains, i.e. there is only little evidence of the bedding-parallel S1 foliation and primary features are well preserved. The S2 foliation and associated L2 lineation are, however, well developed in both formations.

6.1.3 Domain 3: The NW limb of the dome

Domain 4 represents the NW limb of the Usakos Dome, and encompasses lithologies of the Okawayo, Oberwasser, Karibib, and Kuiseb Formations. The NW limb is characterized by four upright to NW verging, shallow NE-plunging F2b folds that are second-order folds of the Usakos dome (Fig. 6.7). The folds are tight with half-wavelengths of less than 500m. The lithologies dip steeply (50° to 75°) to the SE and define the regional NW vergence of the domes in the area. S1 is well developed in the schistose units, and defined as a bedding-parallel penetrative fabric. The S1 fabric is overprinted by a subvertical to steeply SE dipping S2 fabric (Fig. 6.5g). The axial planar S2 foliation is particularly well-developed in the hinges of lower order F2 fold structures, where it cross-cuts bedding and S1 at high angles (Fig. 6.5d). An intersection lineation (L2i) is associated with the intersection of S0 and S2 and a stretching lineation (L2m) is defined by stretched biotite, cordierite and quartz-feldspar aggregates in schists, as well as the stretching and realignment of marble fragments in sedimentary marble breccias (Fig. 6.5i).

A prominent NE-trending high-strain zone is developed in the lower part of the Karibib Formation on the NW limb (Fig. 6.5j). The high-strain zone is ca. 50m wide and comprises banded marbles that are isoclinally folded (F2b) and transposed. Fold axial planes are overturned and dip steeply to the SE, parallel to S2. Competent lithologies such as intercalated calc-silicate and dolomitic marble bands are commonly boudinaged. Boudinage is of a chocolate-tablet type indicating that the high-strain zone records are largely layer-normal shortening strain, underlining its relationship with the S2 foliation.

7. Quartz veins in the NE part of the Usakos Dome

7.1 Data collection and analytical techniques

For this study, spatial (orientation, spacing, size and geometry) and textural data from quartz veins was collected from all lithologies around the NE part of the Usakos dome by mapping the area on a 1:10 000 scale. Quartz veins are best observed in several small mountain streams that cut through the competent metapsammite ridges formed by the Spes Bona Formation and, therefore, most of the vein data was collected around these localities. In addition, detailed structural mapping on a 1:2000 scale at Anomaly 16 recorded spatial and textural data of veins. Vein data was also collected from 4 boreholes drilled through the main mineralized part of Anomaly 16.

Similar to the approach in the Navachab open pit, the orientation of veins formed the basis for distinguishing between different sets of quartz veins. Post-emplacement deformation of veins has locally overprinted original geometries, particularly in the marble units of the Okawayo Formation, so that the geometric analysis of original vein geometries is largely restricted to siliciclastic units. In the field, no distinction was made between mineralized and unmineralized veins, but a biotite-garnet-amphibole alteration around quartz veins is interpreted to be diagnostic for the auriferous quartz veins. Based on the orientation of veins in the siliciclastic units, different sets of quartz veins could be distinguished:

- (a) A main set of shallow-dipping quartz veins, henceforth referred to as *sheeted quartz veins*, make up the bulk of auriferous quartz veins in the Usakos Dome. They are similar to the sheeted veins at Navachab, but in the shallowly plunging hinge of the Usakos dome, they form discordant veins that cross-cut the host-rock lithologies at both high and low angles (Fig. 7.1 and Fig. 7.2a-d).
- (b) Several *subordinate vein sets* also occur (Fig. 7.2e-h). These veins are generally confined to distinct lithological units. The most common types are (1) sub-horizontal extensional veins, spatially associated with conjugate sets in metapsammites, (2) steep S-dipping veins, (3) steep NE-dipping veins and (4) several types of short, stubby quartz-filled gashes with variable orientations.

7.2. Sheeted quartz veins

7.2.1 Geometry and morphology

The geometry and morphology of sheeted quartz veins in the Usakos Dome are very similar to the sheeted veins described in the Navachab open pit. The veins sharply truncate the host-rock fabric with parallel and planar walls in metapsammities and calc-silicate felses. In the schistose units of the Spes Bona and Oberwasser Formations, as well as marbles of the Okawayo Formation, veins have irregular outlines, with highly varying thicknesses due to the pronounced pinch-and-swell and boudinage-type geometry of veins (Fig. 7.2c-d and Fig. 7.2i-j). The barrel-shaped, 1-5cm long quartz-vein blocks are commonly connected by thin, bead-like quartz- and quartz-sulphide stringers. The vein walls are sharp and the veins do not contain any wall-rock scepta. Veins could be followed for several meters along outcrops in river sections, but the full down-dip extents are not exposed.

7.2.2 Orientation of veins

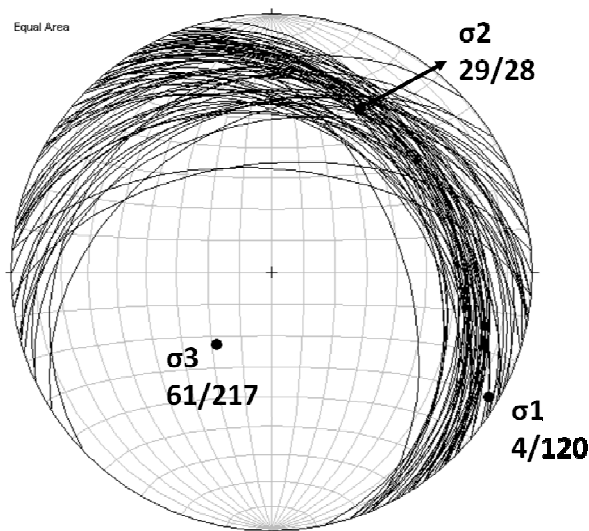


Fig. 7.1 Lower hemisphere, equal-area projection of conjugate quartz vein sets measured in metapsammities of the Spes Bona Formation in the NE part of the Usakos Dome ($n = 84$). The intersection of the conjugate vein sets indicates the σ_2 direction during quartz vein emplacement. The principal compressive stress (σ_1), is roughly ESE which corresponds to the regional D2 shortening direction during the main phase of collisional tectonics in the Damara belt. The least compressive stress (σ_3) is steep.

Vein orientation data was collected from all units in the Usakos Dome, but only data from the siliceous units was used to distinguish between different vein sets. In marble units, the original geometry and orientation of veins has been extensively modified during the post-emplacement deformation of the veins (Fig. 7.2j).

Sheeted quartz veins consist of a conjugate vein set, shown by the bimodal distribution of veins when plotted on stereographic projections (Fig. 7.1). The conjugate vein set is made up of shallow- to moderate ($30\text{-}35^\circ$) NE- and NW-dipping veins that show constant angular relationships including an acute angle of 60° and an obtuse angle of 120° . Veins within the conjugate sets show no consistent crosscutting relationships, which indicates that they formed contemporaneously. In the biotite schists, the conjugate set is not well developed, and only one set of shallow (25°) E- to NE-dipping veins dominate. Importantly, the orientation of sheeted veins is relatively consistent throughout the hinge of the Usakos dome, recording very little changes between different lithologies and is consistent in orientation irrespective of their position with respect to the the first order dome, i.e. whether veins are located in the hinge or on the limbs of the dome (Fig. 7.3a-d). Sheeted veins also occur in marbles of the Okawayo and Karibib Formation. In the marbles, veins are refracted and their orientation is distinct from that in the siliceous units. Refraction also occurs between different marble subunits, indicating the role of relative competency between adjacent units. Sheeted veins are best developed in the lower intercalated marble and calc-silicates in the hinge and NE segment of the NW limb of the Okawayo Formation. Conjugate sets are less well developed in marbles, but do occur in intercalated marbles and calc-silicate units, as well as dolomitic lenses and pods in the Okawayo and Karibib Formations. Conjugate vein sets in the Karibib Formation are best developed in the competent dolomitic marble ridges (7.2l).

SUMMARY OF QUARTZ VEINS ON THE NE LOBE OF THE USAKOS DOME



Fig. 7.2 Characteristics of quartz veins in the NE lobe of the Usakos Dome. (a) Conjugate quartz vein set in Spes Bona Formation metapsammities consisting of shallow (30°) NE dipping and shallow (35°) NW dipping veins that cut the shallow dipping bedding at shallow and steep angles. Note small extensional veinlet. (b) Sheeted quartz veins in the Spes Bona Formation metapsammities. (c)-(d) Sheeted and boudinaged quartz veins in Spes Bona Formation schists. (e)-(h) Subordinate veins and extensional gashes in metapsammities and schists. (i) Necklines on surface of chocolate tablet type boudinaged sheeted quartz vein in metapsammities. (j) Veins in intercalated marbles and calc-silicates, showing the control of the heterogeneity of the host rock on the orientation, thickness and deformation of the quartz vein. (k) Sheeted quartz veins, consisting of zones of closely spaced veins in Okawayo Formation marbles. Malachite is commonly associated with veins in the Okawayo Formation in the Usakos Dome. (l) Conjugate quartz vein gashes in dolomitic marble ridges in Karibib Formation. (m) Folded and boudinaged quartz vein cross-cutting tightly folded marbles and calc-silicates. (n) Boudinaged quartz veins with malachite, garnet and sulphides in boudin necks. (o) Gossanous vein with malachite forming characteristic rusty brown pods at the contact between the Spes Bona and Okawayo Formations.

7.2.3 Size of veins

Quantitative vein data was collected through detailed mapping in the field and logging of 4 boreholes drilled in the schistose units at Anomaly 16. The raw data from boreholes are given in Appendix IV, and are summarized in Table 7.1.

Table 7.1 Summary of vein data from drillcores from Anomaly 16. Cv refers to coefficient of variance, and ΔL the percentage vertical extensional strain. Full data set is presented in Appendix IV.

Borehole number	Host lithology	Line length (m)	Total veins (N)	Vein Thickness (cm)				Vein Density (N/m)	Cv Vein Spacing	Cv Vein Thickness	LA (%)
				Min	Max	Average	Cummulative				
ND10	Spes Bona Formation biotite schists and calc-silicates	31	32	1	7	1.78	57.00	1.03	0.68	0.73	1.84
ND16	Spes Bona Formation biotite schists and calc-silicates	24.65	14	1	5	1.89	26.5	0.57	0.92	0.74	1.02
ND17	Spes Bona Formation biotite schists and calc-silicates	28.68	22	1	4	1.43	31.5	0.77	0.79	0.73	1.24
ND18	Spes Bona Formation biotite schists and calc-silicates	37.72	34	0.5	10	1.9	64.5	0.9	1.14	1.01	1.73

(a) Vein thickness

Sheeted quartz veins in the Usakos Dome range in thickness from less than 1cm to up to 15cm. There is a good correlation between vein thickness and the host lithology and, as a general rule, veins in siliceous units are thicker than veins in marble units. In the Spes Bona Formation, conjugate vein sets in the metapsammities have consistent thicknesses of 1 to 2cm. In schistose units, vein thicknesses are more variable, ranging from less than 1cm to up to 15cm. The average vein thickness calculated from 4 coreholes drilled through sheeted veins in schistose units at Anomaly 16 was between 1.40 and 1.90cm. Again, vein thicknesses are more variable in the marble units than in the siliciclastic rocks, and clear thickness variations occur in the different marble subunits. Veins in homogeneous grey marble units at Anomaly 16 are rarely more than 1cm thick. This is in contrast to veins in the intercalated marble and calc-silicate felses, where veins are between 1 and 5cm thick. In marbles of the Karibib Formation, sheeted veins are consistently between 1 and 2cm in thickness.

(b) Vein spacing

In the field, vein spacing data was collected from well-exposed pavements and river sections. Data depends on the extent and condition of the outcrop and therefore, vein spacing data from field mapping is only seen as first-order estimates, since the observed veins represent, in most cases, only portions of a larger swarm of veins. In the siliceous units, sections with sheeted veins of approximately 6 to 8 veins over a thickness of 10 m are commonly followed by zones of several tens of meters with no veining. Vein spacing data from intercalated marble and calc-silicate pavements show similar vein spacing compared to the siliceous unit. Again, the spacing of veins in marble units are highly dependent on the type of host lithotype, being closer in intercalated marbles and calc-silicates, and wider in grey marble and dolomitic marble units.

Vein spacing data from 4 boreholes drilled through a mineralized vein swarm at Anomaly 16 had a vein density of between 0.5 and 1 veins/meter. The coefficient of variation (Cv) was used to characterize vein spatial distributions for each borehole following the method described by Gillespie et. al. (1999) (chapter 5.2.3b). At Anomaly 16, the average Cv values are 0.88, with only 1 of the 4 boreholes returning a Cv of more than 1 (ND10: Cv = 1.14), indicating that, for the most part, veins are regularly spaced.

Despite the lithological controls on vein spacing, the regional mapping allows to delineate zones with closer and more abundant veins from areas where veining is only very sporadic (Fig. 7.3) The threshold values chosen to distinguish areas of high (>10 veins per 50m, minimum vein thickness of 1cm), intermediate (5-10 veins per 50m) and low (1-5 veins per 50m) vein abundance are arbitrarily chosen, but are taken to be good representations of relative vein abundance on a regional scale. Zones of high vein abundance are found on the SE limb of the UD around coordinates 22°00'45"; 15°42'55", the hinge of the UD between coordinates 22°00'20"; 15°42'30" and 21°59'20"; 15°43'40" and in domain 3 around coordinates 22°00; 15°41'05". These are surrounded by zones of distinctly lower vein abundance, including large parts of the SE limb of Domain 1 and the steeper NW limb of the UD around Domain 3. Importantly, zones of higher vein abundance define a N trending, ca. 2.5km long and 1km wide corridor that not only crosscuts lithologies, but also the first-order hinge of the UD.

This illustrates that despite the control of veining by wall rock lithology on a local scale, veining on a regional scale appears to be determined by additional controls that are not necessarily the first- or second-order structures of the regional geology.

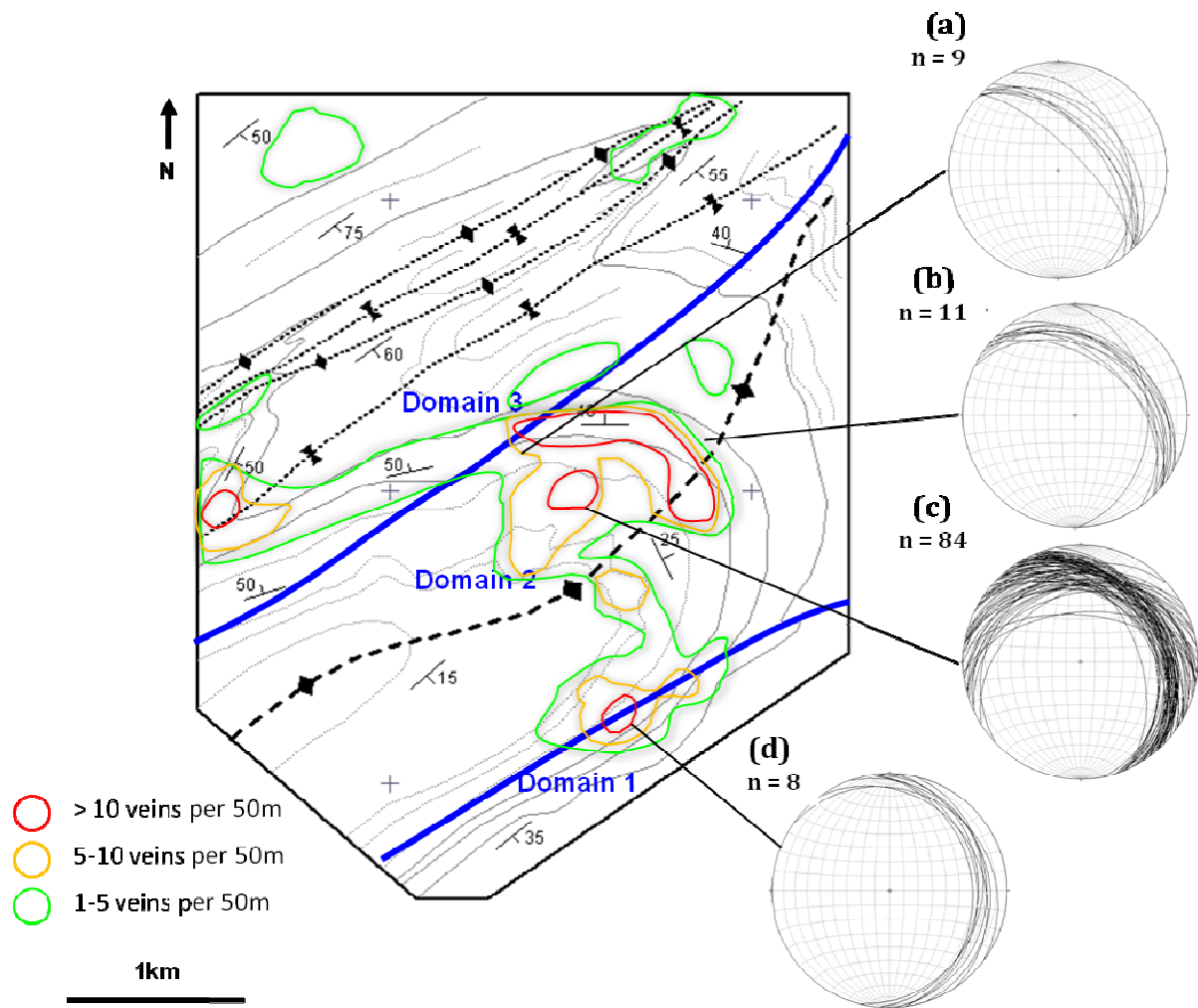


Fig 7.3 Structural formline map of the Usakos dome with the relative abundance of quartz veins in the Usakos Dome plotted. (a) - (d) Lower hemisphere equal area projections of sheeted quartz veins on the NE part of the Usakos dome, showing that the orientation of veins is consistent, irrespective of their position relative to the Usakos dome.

7.2.4 Vein textures, mineralogy and hydrothermal alteration

Quartz veins in the Usakos dome are typically massive, consisting of coarsely recrystallized milky or smokey-grey to clear quartz, with subordinate K-feldspar and carbonates. Quartz is commonly statically recrystallized, displaying straight grain boundaries, 120° triple junctions and largely strain-free grains and the lack of primary crack-seal textures or open-space filling, testify to the post-emplacement, high-temperature recrystallization of the veins.

The mineralogy and hydrothermal alteration of quartz veins in the Usakos dome is similar to that of veins described for the Navachab open pit. The mineralogy of alteration assemblages around quartz veins depends on the composition of the host lithologies. In metapsammities of the Spes Bona Formation, alteration halos around quartz veins are very inconspicuous, varying from being completely absent, to a slight bleaching of the host rock, to a few millimeter wide halo consisting of large euhedral grains of clinopyroxene (1mm-2mm), green actinolite (~1mm), biotite and garnet. Actinolite is, together with sulphides, also recorded in the necks of boudinaged quartz-vein sets, indicating the high-temperature formation and deformation of veins in metapsammities (Fig. 7.4a).

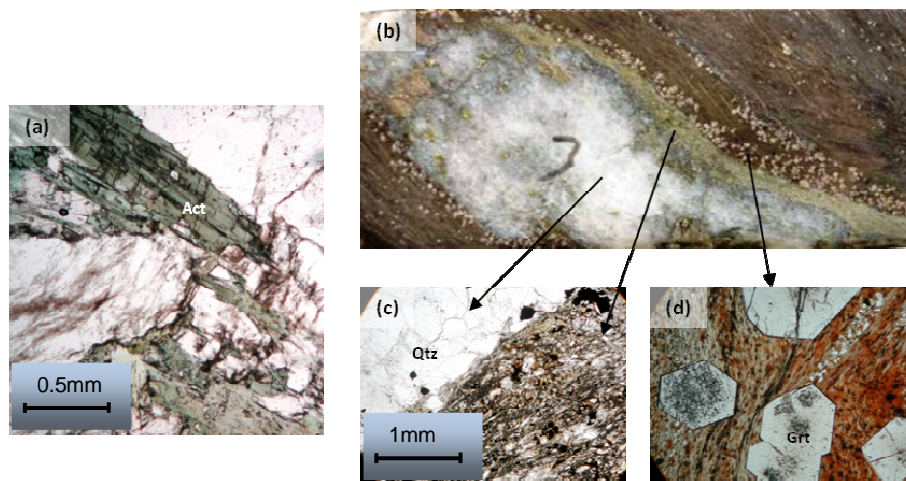


Fig 7.4(a) Actinolite in the neck of boudinaged quartz vein in metapsammities in the Usakos Dome. (b) Typical zoned alteration around vein in Spes Bona Formation schists consisting of (c) proximal fine grained biotite (retrograde to chlorite) and greenish amphibole with relicts of feldspar and quartz and (d) distal large euhedral poikiloblastic garnet in a fine grained matrix, with a strong fabric defined by the orientation of biotite, feldspar and minor quartz. Note how the biotite rich fabric is typically cut by the garnet porphyroblast, but deflected around the garnets.

Quartz veins in the schistose units of the Usakos dome vary from having no alteration to zoned alteration halos that are up to 2cm wide (Fig. 7.4b). Zoned alteration assemblages consist of proximal fine-grained biotite (retrogressed to chlorite) and greenish amphibole, with relics of feldspar and quartz (Fig. 7.4c), surrounded by a more distal assemblage consisting of large (1mm - 4mm), euhedral, poikiloblastic garnet in a fine-grained matrix of biotite, in which biotite, together with K-feldspar and quartz defines a vein-parallel fabric (Fig. 7.4d). The biotite fabric is typically overgrown by, but also deflected against the garnet porphyroblast, indicating their contemporaneous growth. In places, biotite is replaced by chlorite. In the schistose units, pyrrhotite, chalcopyrite and native bismuth are the most common ore mineral assemblages. The ore minerals commonly occur as large grains in (1) micro-fractures in quartz veins, (2) necks of boudinaged veins, or as (3) part of the alteration assemblage around veins.

In the marbles, most quartz veins have bleached and recrystallized alteration halos that can vary from a few millimeters to up to 2cm in width around the veins. Veins in the intercalated marble and calc-silicate unit have associated biotite, clinopyroxene, fine grained amphibole and garnet. Although rare, garnet usually occurs in necks of boudinaged veins, together with mostly chalcopyrite and pyrrhotite. Green malachite is a secondary oxidation product, but is a characteristic mineral associated with veins in the Okawayo Formation marbles at Anomaly 16 (Fig. 7.2k). It commonly occurs in the necks of boudinaged quartz veins (Fig. 7.2n). In the marble and dolomitic marble unit of the Okawayo Formation, quartz veins crosscutting dolomitic boudins have associated massive alteration halos of radiating tremolite needles.

7.2 Subordinate veins

Subordinate veins occur mainly in competent layers and are more commonly observed in the siliciclastics than in the marbles. In the siliciclastics, subordinate veins are short (up to 15cm long), subvertical (80/190), planar to sigmoidal quartz filled gashes. They form at high angles to the walls of competent layers (Fig. 7.2e,f) and typically show an en echelon arrangement (Fig. 7.2h). Short and stubby, steep veins are also frequently associated with shallow dipping sheeted quartz veins in the metapsammities where they clearly cross-cut the shallow veins (Fig. 7.2g). Thin (less than 1cm thick) veins, occur as

subhorizontal gashes in the metapsammites, and are commonly associated with the conjugate vein set.

7.3 Vein deformation

In the Usakos dome, the deformation of quartz veins depends on the relative competence of the vein with respect to the host rock, and the orientation of the vein with respect to the regional strain field.

In siliciclastic units, where there is only little competency contrast between veins and their hosts, veins deform homogeneously with the host rock. Conjugate vein sets in metapsammites of the Spes Bona Formation appear undeformed or only very gently folded in cross section, retaining their original orientations. In plan view, however, the veins have undergone chocolate-tablet boudinage. Two near-perpendicular necklines can be defined, plunging shallowly to the NE and SE respectively (Fig. 7.2i). The separation between quartz boudins rarely exceeds 5 mm and necks are filled with hornblende and sulphides, now largely weathered to iron hydroxides. The boudinage indicates a subvertical shortening strain at high angles to the shallowly dipping veins. In biotite schists, thin quartz veins appear only gently folded when viewed to the NE and in cross section. When viewed in a down-dip direction, the shallowly dipping veins are boudinaged into isolated quartz pods, again indicating a significant component of subvertical flattening strains (Fig. 7.2d). Similar to the metapsammites, original vein orientations seem to have been more or less preserved.

Quartz veins in marbles of the Okawayo Formation are invariably folded and/or boudinaged to the extent that the original orientation of veins is no longer recognizable (Fig 7.2j). This not only illustrates the competence contrasts between veins and enveloping marbles, but also markedly higher-strain intensities in the Okawayo Formation compared to the Spes Bona and Oberwasser Formations, as well as the stratigraphically higher marbles of the Karibib Formation. The type and intensity of deformation vary between different marble subunits, reflecting that host-rock competency has a major control on vein deformation. Quartz veins in homogeneous grey marble units are typically straight, but with highly irregular walls and segment into often blocky quartz-vein studs, separated by wall rock, giving it a boudin-type

appearance (Fig. 7k,n). Individual quartz segments can be separated by several cm, and veins are often only recognizable by the bleached alteration halos around the vein. In contrast, quartz veins in the heterogeneous intercalated marbles and calc-silicate units are tightly folded, boudinaged and clearly refracted between layers (Fig. 7.2j,m). In calc-silicate layers veins are generally less deformed than marble layers, and the lithological heterogeneity of the Okawayo Formation evidently contributed to the serrated form of veins in these units.

The orientation of veins with respect to the main stress field and regional strain during quartz-vein formation and the progressive post-emplacement deformation is an important aspect for the understanding of the controls of veining. Previous studies in the Karibib-Usakos area have indicated that the principal shortening direction during veining was subhorizontal and orientated in a WNW-ESE direction, corresponding to the regional D2 fold-and-thrust event (Kisters, 2004). Regional deformation outlasted vein formation, as is clearly evidenced by the progressive deformation of veins, resulting in the folding and boudinage of differently orientated veins.

In intercalated marbles and calc-silicate felses, veins crosscut tight F2 folds, but are, at the same time, folded and boudinaged (Fig 7.2m). Buckled veins show axial planes subparallel to the main penetrative S2 foliation, whereas boudinaged veins occur parallel to the axial planes of folded calc-silicate felses. This deformation pattern is also recorded for rare conjugate veins in the intercalated marbles, showing boudinage of veins that are parallel or have been rotated into parallelism with the main S2 fabric, whereas veins emplaced at high angles to the main foliation are buckled.

Folded quartz veins in schistose units of the Spes Bona Formation are rare and have only been observed in the hinge of the Usakos Dome. The folded veins are commonly thin (ca. 1 cm wide) and have axial planes subparallel to the S0/S1 foliation. These veins are, therefore, interpreted as early veins. Shallow veins cross-cut the shallowly-dipping S0/S1 fabric at low angles and are commonly boudinaged. Both the folding of steep veins and boudinage of shallowly-dipping veins indicate a vertical flattening strain that deviates from the subhorizontal flattening strain recorded elsewhere.

8. Discussion

Vein-fracture networks at outcrop represent evidence for hydraulic failure and the flow of large volumes of near-lithostatic pressured fluids in deeper crustal levels (Cox et al. 1991). Any fluid flow in the crust is determined by two main factors, namely (1) hydraulic gradients that drive fluid flow, generally from areas of higher to lower mean rock stress, and (2) permeabilities, that are mainly represented by fracture permeabilities (veins) in the otherwise largely impermeable high-grade rocks. Both, the permeability of the host rock and driving forces for fluid flow are influenced by tectonic processes and deviatoric stresses in the crust. A key aspect when interpreting the formation of hydrothermal vein systems is, thus, to understand the (1) regional structural controls such as regional strain/stress fields, presence of shear zones and other first- and lower-order structures, etc. that determined (2) regional and local hydraulic heads and the permeability evolution of the host rock, i.e. the formation of vein systems (Cox et al. 1991; Ridley, 1993; Sibson and Scott, 1998; Cox et al. 2001).

8.1 Prerequisites for quartz veining: fluid pressures and effective stresses

The processes that form purely dilational (mode I) fractures in mid-crustal levels have been enigmatic in the past, since extensional fracturing at high confining pressures would require very large differential stresses of several 100 MPa that are highly unlikely to be realized in the commonly ductile mid- and lower crustal levels. The importance of high fluid pressures for the generation of extensional fractures and veins under high-confining pressures was first demonstrated by Hubbert and Rubey (1959), and later by Jaeger, (1963) and Secor, (1965) and Etheridge et al, (1984). By showing that high fluid pressures in a rock can act against and negate the lithostatic pressure, brittle, extensional failure can be induced at even high confining pressures and at deep crustal levels by simply overcoming the tensile strength of a rock. This may be optimized by the existence of favourably orientated pre-existing faults or fractures.

Under prograde metamorphic conditions, typically at greenschist- facies grades and above, near lithostatic fluid pressures prevail due to rapid sealing, infilling, and collapse of pore space through mineral deformation mechanisms (Etheridge et al., 1984; Sibson, 2001). Overpressured domains may also arise when fluids migrating along permeable pathways such as faults and shear zones are ponding against low-permeability seals

such as a shale horizon, under low-grade conditions (Sibson, 1998, 2001; Cox, 2001), or marbles at higher grades. The increase of fluid pressures to lithostatic values may produce conditions of effective tensile stress and hydraulic fractures when:

$$P_f \geq \sigma_3 + T,$$

where P_f is the fluid pressure, σ_3 is the least compressive stress and T is the tensile strength of the rock. Under these conditions, extension fractures form along planes perpendicular to σ_3 when $(\sigma_1 - \sigma_3) < 4T$, while extensional shear fractures form when $4T < (\sigma_1 - \sigma_3) < 6T$. In other words, mode I extensional fractures are favoured under low differential stresses and/or in rocks with low tensile strengths, whereas shear failure is favoured at higher differential stresses and/or in rocks of higher tensile strength. Tensile strengths and differential stresses in high-grade metamorphic, ductile rocks are commonly assumed to be low, between 1-5 Mpa (Etheridge and Wall, 1984). Thus, the formation of extensional over shear fractures, and vice versa, in the mid-crustal rocks can provide a very sensitive stress gauge in the mid-crustal rocks.

8.2 Regional controls

Rocks in the Karibib region are characterized by flattening-type strains, evidenced by e.g. the symmetrical folding and chocolate-tablet boudinage recorded in high strain zones, the consistently steep SE dipping S2 axial planar foliation, or the flattening of breccia fragments in marble breccias. This NW-SE directed subhorizontal shortening strain is also responsible for the formation of the first-order NW verging dome structures and the top-to-the-NW directed thrust transport along the MRTZ, corresponding to the main D2 collisional phase recorded in the Damara belt (Kisters et al., 2004).

The geometry and deformation of quartz veins in the Navachab open pit provide further evidence that quartz veining was controlled by the regional D2 strains. Non-coaxial fabrics that would indicate e.g. a strike-slip component during deformation are conspicuous by their absence. Non-coaxial deformation involves, by definition, a rotation of strain axes during progressive deformation. This means that earlier formed veins, or segments of veins, would undergo progressive rotation. Later veins would

cross cut earlier veins before being caught up in the deformation, The result of veining in non-coaxial shear-zone systems is documented from many shear-zone hosted lode-gold deposits (e.g. Cox, 1995; Sibson, 1998), consisting of numerous sets of variably deformed and overprinting quartz-vein generations. At Navachab, quartz veins are straight and parallel-sided, recording remarkably high aspect ratios and down-dip extents of over 300m. Fold geometries displayed by quartz veins in marble units are upright and symmetrical, pointing to post-emplacement folding of veins during vein-parallel co-axial shortening. The orientation of the strain and stress axes that can be computed from the orientation of conjugate shear veins corresponds to within 10-20° to the regional D2 strain (chapter 5.2.2; Fig. 5.8a-c). This, together with the symmetrical folding of quartz veins implies that the veins formed during co-axial D2 shortening and associated folding and thrusting.

Importantly, the conjugate set of sheeted quartz veins is developed in both the Navachab open pit and the hinge of the Usakos dome (Fig. 5.8a-c and Fig. 7.1). Both localities occupy very different structural positions with respect to the regional-scale dome structures. Quartz veins of the Navachab open pit are hosted by steep WNW dipping rocks, whereas rocks dip at shallow angles to the N and NE in the hinge of the Usakos dome. Moreover, sheeted quartz veins are developed in rocks from the Spes Bona into the Karibib Formation, across large parts of the lithological sequence. Lithological controls on quartz veining play, thus, only a subordinate role for quartz veining (see below). This illustrates the overriding importance of the regional D2 strain as the first-order control on the formation of quartz veins in the Karibib region.

The important difference between the Navachab open pit and veining recorded in the hinge of the Usakos dome lies in the thickness of the economic-grade vein swarm. Quartz veins in the Navachab pit show a close (1-1.5m) spacing over a thickness of some 150m and a cumulative thickness of veins of 6-6.5m. In contrast, quartz veining in the hinge of the Usakos dome shows, locally, a comparable spacing, but quartz veins tend to be thinner and the most prominent cluster of veins has a thickness of < 50m with a cumulative thickness of less than 1m. Given that sheeted quartz veins in the Navachab open pit and in the hinge of the Usakos dome formed during the same D2 bulk co-axial shortening, and that veining is largely independent of rock type, the main difference

that determines the abundance of veins is likely to be the amount of the finite extensional strain experienced in the two structural sites. The subvertical limb of the Karibib dome is in an orientation where subhorizontal and, thus, layer-normal shortening can only be accommodated by either lateral or vertical extrusion of the rocks. In the overall thrust regime and with the least compressive stress (σ_3) being vertical, the steep extrusion of rocks will be favoured, so that shallowly-dipping extension fractures will form. Higher extensional strains (i.e. vertical stretch) will result in more extensional fractures. It is clear that there is no linear relationship between the formation of extensional fractures and the finite vertical stretch. Minimum shortening strains in e.g. the Okawayo Formation in the open pit are > 50% (chapter 5.4), whereas the vertical extensional strain recorded by the veining is only between 0.77% - 1.4%. In contrast, the Spes Bona Formation and the Oberwasser Formation record very little shortening strain, but show consistently higher vertical extensional strains of between 0.91% and 3.52%. (chapter 5.2.4). This illustrates the ductility of particularly the marble units, where extension is largely accommodated by ductile flow, rather than veining and failure in the elastic range. The Usakos dome, in contrast is an open fold, with an interlimb angle of 80-100°. In this structural position, D2 shortening strains can be accommodated by further tightening and amplification of the fold, i.e. steepening of the fold limbs. The wall-rock sequence in the hinge of the dome does not undergo similar amounts of vertical stretch compared to that recorded in the subvertical rocks of the Navachab pit, so that fracturing and veining is delayed resulting in thinner veins and thinner veins swarms and, on a regional scale, fewer veins.

The actual timing of veining in both areas is indicated by the progressive deformation of veins and development of alteration halos. In both areas, veining has occurred at a late stage during the D2 deformation. Evidence for this is provided by e.g. the asymmetric, upward pointing alteration halos around sheeted quartz veins in the MC unit in the open pit (chapter 5.2.7, Fig. 5.12c-d.). This indicates the buoyancy-controlled, bedding-parallel fluid flow when the rocks had already attained steep attitudes and during the fold lock up of the Karibib dome. Vein sets in the hinge of the Usakos dome do not seem to have undergone a rotation during D2 folding of the strata, i.e. the vein sets have similar orientations on the SE and NW limbs as well as in the hinge of the Usakos dome.

This suggests that the veins formed at a time, when the present fold geometry of the Usakos dome was attained.

The comparison of veining in the structurally distinct areas of the open pit and the hinge of the Usakos dome demonstrates two main aspects that are important for exploration of the vein systems, namely (1) the significance of D2 coaxial shortening strains for vein formation on a regional scale and largely irrespective of lithologies and structural position, and (2) superimposed on this, the importance of structural sites within this regional strain field for the development of closely spaced vein sets. Vertical or high-angle strata record a higher finite stretch compared to shallowly-dipping strata. This favours the formation of thicker packages of closely-spaced vein sets that may result in economic-grade mineralization. Shallowly-dipping strata may show sheeted quartz veins, but a lower vertical stretch will result in thinner vein swarms.

8.3 Local controls

Vein spatial distributions at Navachab deviate from power-law behaviour ($C_v > 1$) as described by Gillespie et. al. (1999) and are more readily comparable to vein systems described for non-layered rocks. Vein spatial distributions are instead characterised by regularly spaced or anti-clustered veins. Vein clustering can only happen when the likelihood of a new vein forming close to an existing vein is higher than it being formed distantly from the existing vein (Gillespie et. al. 1999). Regularly spaced veins require a repulsive mechanism and this might be explained by a competitive vein forming mechanisms. With the increase of veins during the evolution of the vein-fracture system, neighbouring vein lobes overlap, resulting in tip-line confinement and kinematic interdependence (Olson and Pollard, 1991). This increases the effective vein lengths and thickness, and also promotes accelerated rates of vein opening. As veins grow larger, they not only interact with distant veins but also place adjacent veins into their stress shadows. The latter mechanism would inhibit further growth of smaller veins adjacent to thicker veins or vein clusters. In the open pit, thick (>10cm) veins or vein “clusters” are often surrounded by vein free zones (Fig. 5.4 and Fig. 5.5) and this might be explained by the competitive vein forming mechanisms and formation stress shadows around early veins. The stepwise nucleation and growth of veins with time is clearly illustrated in Figure 4.6a where aplite veins are cross-cut and cross-cut sheeted

quartz veins. Pre-existing or earlier formed veins may, thus, exert a significant control on quartz vein nucleation in that (1) renewed fracturing will preferentially take place along existing veins, and (2) nucleation of new veins can only occur within some distance to existing veins, i.e. outside the stress shadow of existing veins.

Lithological contrasts exert a more localized control on quartz vein development that is superimposed on the regional controls. In the study area, conjugate sets of extensional shear veins are confined to siliciclastic units of the Karibib and Usakos domes, including the Spes Bona and Oberwasser Formations as well as the central metalamprophyre sills in the open pit. In contrast, only one set of shallowly NNW dipping extensional veins is developed in marbles of the Okawayo Formation. Conjugate and extensional vein sets form part of the same swarm of sheeted quartz veins in the pit and the formation of shear versus extensional veins is a close monitor of the different tensile strengths of the heterogeneous wall-rock sequence. As such, siliciclastic rocks show higher tensile strengths, able to withstand higher differential stresses, whereas the ductile marble units show lower tensile strengths, responding by ductile flow under even low differential stresses. This competence contrasts is also reflected in the degree of post-emplacement deformation of veins, where veins in marbles are tightly folded, recording a post-emplacement shortening of up to 50%. Veins in siliciclastic units appear, in turn, largely undeformed or only gently buckled.

In the Navachab open pit, both shear and extensional veins are highly discordant and cross-cut the steeply dipping bedding and S1/S2 foliations at high angles. This indicates that the difference in tensile strength normal (T_n) and parallel (T_p) to the pre-existing anisotropy was less than the differential stress ($\sigma_1 - \sigma_3$) during veining. However, given that tensile strength and deviatoric stresses in the high-grade rocks are low and fluid pressures are close-to-lithostatic, it is conceivable that fracturing may be promoted along the pre-existing anisotropy rather than across it, since $T_n < T_p$. This condition is likely to be met first in well-bedded units, such as parts of the Oberwasser and Spes Bona Formations and may explain the presence of steeply-dipping bedding-parallel veins. These veins (chapter 5.3) are thin and relatively inconspicuous, but common, if only expressed by thin quartz stringers and associated alteration and sulphide mineralization.

The MC unit in the open pit has traditionally been regarded as a high-priority target for mineralization. It is the only unit that shows massive sulphide pods and alteration features, indicating focused fluid flow within this lower part of the Okawayo Formation in the Navachab open pit. The pervasive transposition folding and tight folding of late-stage quartz veins testify to high finite strains and ductile flow in marbles. Despite the high strain intensities, the Okawayo Formation does not constitute a shear zone in the classical sense, i.e. there is no evidence for large, across-strike lateral displacement of units, but it can be regarded as a low-displacement, mainly pure-shear dominated shear zone. The Okawayo Formation is sandwiched between the Spes Bona and Oberwasser Formations in the foot- and hanging-wall, respectively, both of which show only little evidence of pervasive ductile strains. This reflects the much lower competence of the marble units compared to the siliciclastic units during high-T deformation. It also illustrates the very confined ductile flow of the marbles between the two low-strain units. This, in turn, implies large strain rate gradients between the rapidly deforming marble units and the bounding schists and calc-silicate felses.

The MC unit represents the small-scale representation of this lithological heterogeneity. Calc-silicate felses are interlayered with marbles and the vastly different rheologies between adjacent units would, again, imply large strain-rate gradients. Ductile flow and high-strain rates in marble units can only be compensated for by brittle deformation in calc-silicate felses and the resulting fractures result in dramatically enhanced permeabilities. In essence, the sandwich situation of the Okawayo between the Spes Bona and Oberwasser Formations on a macro scale, and the calc-silicates and marbles in the MC unit create large strain-rate gradients and strain incompatibilities over short distances that can only be compensated for by microfracturing in the calc-silicates or competent units. This may also explain the higher cumulative extensional strain recorded by veining in the Spes Bona and Oberwasser Formations compared to the marble units, despite the drastically lower strain intensities of the former.

8.4 Controls on ore shoots

The flow of fluids under lithostatic pressure at the depth of formation of mesothermal gold deposits will generally be upward (Ridley, 1993; Cox, 1999). However, directional

stress-controlled permeability may deflect overpressured fluid escape pathways from the vertical (Ridley, 1993; Sibson, 1996, Cox, 1999). Fluid focusing will then occur where there is a lateral gradient in fluid pressure and flow will be towards zones of relatively low mean rock stress (Ridley, 1993). The direction of flow will be controlled by (1) the maximum hydraulic gradient, (2) existing permeability anisotropy, and (3) the superimposed structural permeability (Ridley, 1993; Sibson, 1996). Hydrothermal gold deposits will often form where a combination of these parameters led to high-volume fluid flow (Sibson, 1996).

Ore shoots in the Navachab open pit are controlled by the combination of (1) regional, strain-induced orientation of fractures, and (2) orientation of pre-existing bedding of the folded strata and the “sandwich” of the Okawayo Formation. The intersection of sheeted quartz veins with bedding (Fig. 5.13c) corresponds to the orientation of the shallow NNE plunging ore shoots identified by exploration drilling (see also Moore et al., 1998). Moreover, the intersection of conjugate fracture sets also corresponds to this plunge (Fig. 5.8a-c).

8.5 Quartz veins as strain markers

From the orientation of conjugate veins in the Usakos dome, it can be assumed that veining occurred during subhorizontal shortening, with σ_1 approximated by the acute dihedral angle between the two conjugate sets and sub-parallel to extensional veins. Continued post-emplacement (D2) sub-horizontal deformation accounts for the regionally observed folding of shallowly dipping veins and boudinage of steep veins.

The detailed mapping of quartz veins undertaken in this study also demonstrates a hitherto not documented vertical shortening strain in the Karibib region. Vertical shortening is evidenced by (1) boudinaged shallowly-dipping veins in schistose units of the Spes Bona Formation in the Karibib and Usakos domes (Fig. 5.6e and Fig. 7.3n), (2) originally boudinaged (due to vertical stretch) subvertical dykes that are subsequently shortened/folded, and (3) steep veins in schistose units that are buckled (Fig. 7.3p). Johnson (2005) first reported the collapse and vertical shortening of the granite-rich core in the SW part of the Usakos dome. Crustal thickening during regional-scale D2 fold-and-thrust tectonics, syn-D2 granite emplacement and rheological weakening of

the crustal column and the regional high-T metamorphism initiated the gravitational collapse of the crust in the CZ and saw a switch from horizontal to vertical shortening.

The deformation of quartz veins recorded in this study indicates, indeed, the temporary swap of the principal strain axes, possibly in response to the partial collapse of the crust (Fig. 8.1). Regional NW-SE directed shortening led to crustal thickening due to folding and thrusting until the high-T rocks and weak marble packages were too weak to sustain crustal thickening. Vertical shortening and orogen-parallel extension re-established the strength profile of the deforming crust, before progressive horizontal (D2) shortening could lead to a repeated swap of the principal shortening strain.

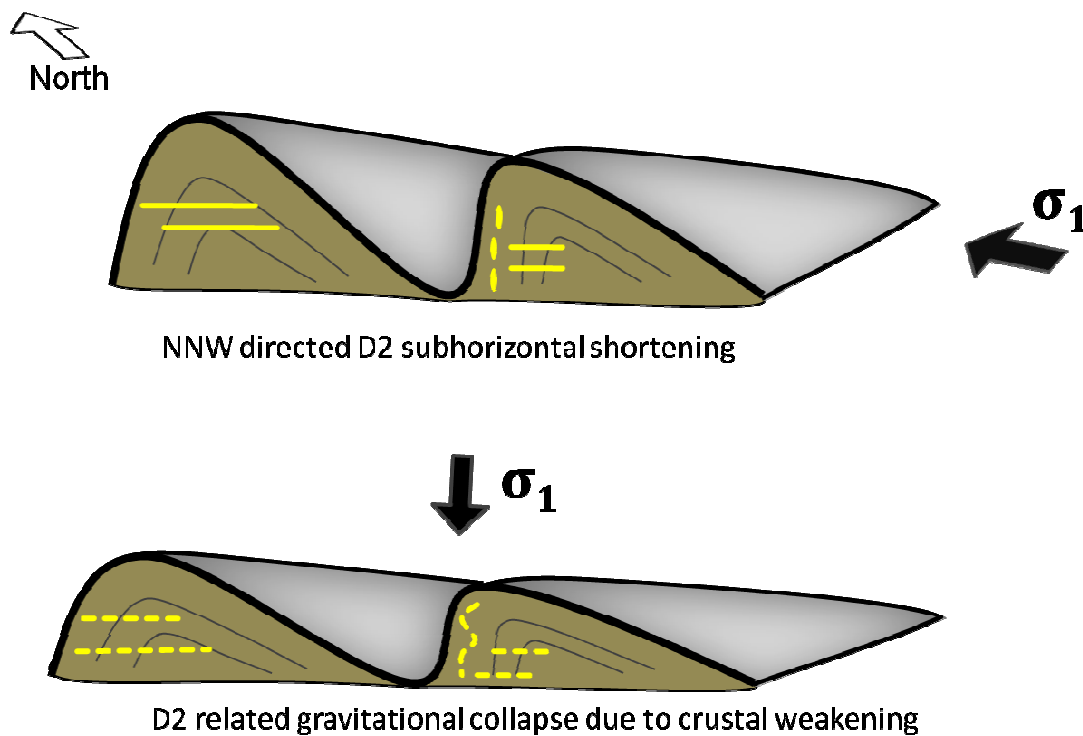


Fig. 8.1 Simplified schematic sketch showing the proposed development of boudinaged shallowly dipping quartz veins and folding of originally boudinaged (due to vertical stretch) subvertical dykes. (1) Subhorizontal shortening leads to crustal thickening, resulting in (2) the temporary swap of strain axes documenting the temporary overthickening of the crust, which leads to crustal extension and the restoration of (1). This process can be envisaged to have occurred repeatedly in the rheologically weakened crust of the CZ.

8.6 Previous models

Previous studies in the Karibib area have proposed different genetic models for the mineralisation and formation of auriferous sheeted quartz veins in the Navachab open pit:

Moore et al. (1999) proposed that auriferous quartz veins to have formed as conjugate, anti- and synthetic Riedel shears in a non-coaxial shear zone. The shear zone is represented by the steep NW limb of the Karibib dome, centered around the highly strained marbles of the Okawayo Formation. Moore et al. (1998; 1999) explained the formation of large replacement skarn lenses in the MC unit as the intersection between the vein system and the host rocks. This intersection between shallowly-dipping sheeted quartz veins and bedding would explain the shallow NNE plunge of the ore body in the Navachab pit.

Nörtemann et al. (2000) interpret the mineralisation at Navachab as a reduced skarn associated with the intrusion of a synmetamorphic lamprophyre sill, but the petrologically orientated study did not specify the actual controls of the mineralisation.

Steven et. al., (2003; 2008) suggested that the veins formed during late-stage anticlockwise rotation of the regional-scale dome structures (D4), where deformation was concentrated in NNE trending corridors that record sinistral strike-slip movement. This would explain the localization of the mineralization of the open pit on the NW limb of the Karibib Dome that is slightly oblique to the overall NE trending structural grain of the Damara Belt. Models of quartz-vein formation hosted by a strike-slip shear zone do not adequately address (1) the lack of non-coaxial structures that would indicate such a strike-slip event centered around the Okawayo Formation that is largely characterized by layer-normal flattening strains; and (2) the orientation of the shallowly-dipping sheeted quartz veins that do not correspond to a strike-slip setting, where the veins and/or Riedel shears must be expected to be subvertical.

Kisters (2005) suggested mineralization to consist of two distinct phases that developed during the progressive amplification of the Karibib Dome as the first-order controlling structure. The MC mineralization formed during flexural slip and opening of dilational

jogs. This is the first phase of mineralization during fold amplification. It is followed by sheeted quartz veins that formed when the NW fold limb of the Karibib dome reached steep attitudes, so that the fold is thought to lock up as flexural slip could no longer be resolved along the steep bedding. The sheeted quartz veins accommodate further subhorizontal shortening by subvertical fracturing. This model would account for the formation and progressive deformation of the sheeted quartz veins with respect to regional strains. However, the dilational jog model for the MC mineralization that supposedly developed during earlier bedding-parallel slip cannot be confirmed. This study rather shows that the MC mineralization is intricately associated with the sheeted quartz veins and their intersection with the basal parts of the Okawayo Formation.

8.7 Conceptual model

Previous models discuss the mineralization of the Navachab open pit to be related to the steep dips and highly strained lithologies and/or the progressive steepening of strata on the steep NW limb of the Karibib dome. As such, these models fail to explain the formation of similar sheeted quartz veins in the shallowly-plunging hinge of the Usakos dome, which represents a very different structural scenario compared to the steep limb of the Karibib dome.

This study proposes an alternative model, similar to the model proposed by Kisters (2005), but taking into account the formation of sheeted quartz vein in the hinge of the Usakos dome. The critical factors are: (1) the formation of the Usakos and Karibib domes as fault-propagation folds located at the terminations of underlying blind thrusts as proposed by Kisters et. al., (2004), (2) the asymmetry and NW vergence of the domes, (3) the localisation of D1 related high strain zones in the Okawayo Formation, evident by the thickening and internal structural complexity of the unit, (4) the restriction of the vein swarm to the ca. 150 m thick swarm around the Navachab open pit that can, with similar vein density, not be identified along the rest of the NW limb of the Karibib dome, and (5) the formation of identically orientated conjugate vein sets in different structural localities in the Karibib area.

The conceptual model envisages the formation of auriferous quartz vein systems in the Karibib and Usakos domes as part of the progressive fold amplification during late

stages of D2 dome formation. D2 shortening resulted in the progressive steepening of the NW limb of the Karibib dome to attitudes perpendicular to the shortening strain (σ_1), so that flexural slip became inactive (lock-up). Further shortening ($\sigma_3 = \sigma_v$) is accommodated by shallow dipping extensional and conjugate extensional-shear veins on the steep NW limb of the Karibib dome. Concurrently, the shallowly-dipping (30°) SE limbs of the domes were ideally orientated for continued shearing and the formation of bedding-parallel thrusts along the backlimbs of the folds. Strain localization occurred into the marble units and, in particular, into the Okawayo Formation as is evidenced by the complex intrafolial folding and deformation restricted to the marble units in the Usakos dome. Reverse slip along the shallow dipping SE limb of the Usakos dome, induced along strike dilation in hinge-line culminations, and the formation of shallowly dipping extensional and conjugate extensional-shear veins in the hinge of the Usakos dome. The actual location of economic-grade vein-swarm clusters may correspond to the presence of dilational stepovers.

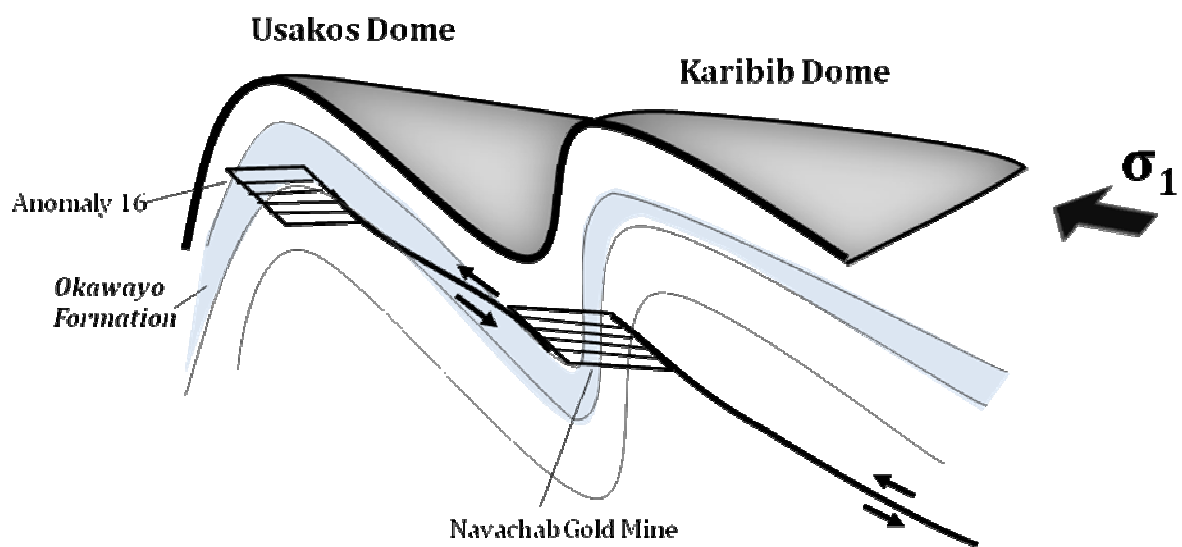


Fig 8.2 Schematic sketch illustrating the conceptual model for the formation of auriferous quartz veins on the NW limb of the Karibib dome and NE hinge of the Usakos dome.

9. Conclusions

Detailed structural and lithostratigraphic mapping combined with the analysis of auriferous quartz veins in the Navachab open pit and hinge of the Usakso dome allows for the identification of the controls of quartz veining in the area. From this study the following main conclusions can be drawn:

1. Geological mapping highlights the composite nature of strains in the first-order folds of the regional-scale D2 Karibib and Usakos domes. S1 foliation development, truncation of marker horizons and significant thickness variations in particularly the lower parts of the Damara Supergroup indicate the presence of low-angle shear zones (D1). The subsequent D2 deformation is characterized by NW-SE directed shortening strains. Non-coaxial fabrics that may point to the oblique collisional history of the Damara belt are conspicuous by their absence. On a regional scale, D2 strains find their manifestation in the NW-verging folding of the Karibib and Usakos domes and associated top-to-the-NW thrusting. On a local scale, D2 strains are heterogeneous and two distinct types of D2 related high-strain zones can be distinguished. NW-SE trending subvertical high-strain zones have an axial planar (S2) orientation with respect to first-order folds. Low-angle (30-40°) shear zones are preferentially developed on the shallowly-dipping SE limbs of D2 folds, recording top-to-the-NW kinematics. Both high-angle flattening zones and low-angle thrust zones are preferentially developed in marble units, highlighting the significance of strain localization into incompetent units.
2. Mineralized quartz veins can be shown to occur in structurally very diverse settings. In the Navachab open pit, auriferous quartz veins are developed in steeply dipping rocks on the NW limb of the Karibib dome. In the Usakos dome, veining is abundant in the shallow NE plunging NE hinge of the Usakos dome. Quartz veins occur as mainly shallowly NE and NW dipping sets in siliceous units of the Navachab open pit as well as in the NE hinge of the Usakos dome. Together with the symmetrical folding of veins, this implies that the veins formed during co-axial NW-SE subhorizontal shortening during the late stages of D2 folding and thrusting. The occurrence of these quartz vein sets irrespective of the regional structural position

with respect to first-order structures demonstrates that the regional stress field represents the first-order control of quartz-vein formation in the area

3. The difference between the economic-grade mineralization of the Navachab open pit and sub-economic veining recorded in the hinge of the Usakos dome lies in the thickness of the vein swarm. The subvertical limb of the Karibib dome is in an optimal orientation for the formation of shallowly-dipping extension fractures during subhorizontal shortening, whereas shortening in the Usakos dome is an open fold, and D2 shortening strains can still be accommodated by further tightening and amplification of the fold. The two structural locations therefore undergo different amounts of vertical stretch resulting in fewer veins and thinner quartz-vein packages in the hinge of the Usakos dome.
4. Conjugate quartz-vein sets and extensional quartz veins form part of the same set of shallowly dipping quartz veins. The formation of conjugate over extensional quartz veins is merely controlled by lithology and, more specifically, the tensile strength (competence) of wall-rock lithologies.
5. Quartz veins show, in general, a regular to anti-clustered spacing. Veins have very high aspect ratios (> 1: 1000), continuous down-dip extents (> 300m) and straight, parallel-sided geometries. This is consistent with the growth of veins during (1) co-axial bulk shortening (D2), and (2) a competitive growth process where vein growth is determined by a balance between fracture nucleation along existing or earlier formed veins and fracture nucleation in intact wall rock outside the stress shadow of existing veins.
6. The massive sulphide lenses in the MC unit of the Navachab open pit are the alteration/mineralization products of shallow dipping sheeted quartz veins as they cross-cut the intercalated marbles and calc-silicates. The orientation of massive sulphide ore shoots corresponds to the intersection of the shallow dipping quartz veins with the steeply dipping bedding. Interfingering and upward pointing alteration halos point to the buoyancy-assisted, bedding-parallel fluid flow in the upright host-rock sequence.

7. Lithological controls exert a more localized control on quartz-vein formation. Competent, siliceous units or dolomitic marbles show higher fracture densities compared to ductile, e.g. calcitic marbles, where fracturing and veining is delayed due to the ductility of wall rocks undergoing high-temperature metamorphism.

8. Quartz-vein formation is controlled by regional D2 flattening strains, but this study suggests that the actual location of economic-grade vein clusters seems to be controlled by dilational stepovers between overlapping D2 related shear zones (thrusts). The low-angle shear zones are preferentially localized in rheologically weak marble units, particularly of the highly deformed Okawayo Formation in the stratigraphically central parts of the Damara Sequence.

References

Badenhorst, F.P. (1987). Lithostratigraphy of the Damara Sequence in the Omaruru Area of the northern Central Zone of the Damaran Orogen and a proposed correlation across the Omaruru Lineament. *Communications of the Geological Survey of South West Africa*, 3, 3-8.

Badenhorst, F.P. (1992). The Lithostratigraphy of area 2115B and D in the Central Zone of the Damara Orogen in Namibia: with emphasis on facies changes and correlation. Unpublished MSc thesis, University of Port Elizabeth, p. 124.

Brandt, R. (1985). Preliminary report on the stratigraphy of the Damara Sequence and the geology and geochemistry of Damaran granites in an area between Walvis Bay and Karibib. *Communications of the Geological Survey of Namibia*, 1, 31-43.

Brandt, R. (1987). A revised stratigraphy for the Abbabis Complex in the Abbabis inlier Namibia. *South African Journal of Geology*, 90, 314-323.

Cox, S., Wall, V.J., Etheridge, M.A., and Potter T.F. (1991). Deformation and metamorphic processes in the formation of mesothermal vein-hosted gold deposits – examples from the Lachlan fold belt in central Victoria, Australia. *Ore Geology Reviews*, 6, 391-423.

Cox, S. (1995). Faulting processes at high fluid pressures: An example of fault-valve behavior from the Wattle Gully Fault, Victoria, Australia: *Journal of Geophysical Research*, v. 100, p. 12,841-12859.

Cox, S.F., Sun, S.-S., Etheridge, M.A., Wall, V.J., and Potter T.F. (1995). Structural and geochemical controls on the development of turbidite-hosted gold quartz vein deposits, Wattle Gully mine, central Victoria, Australia. *Economic Geology*, 90, 1722-1746.

Cox, S.F., (1999). Deformational controls on the dynamics of fluid flow in mesothermal gold systems. In: McCaffrey, K.J.W., Lonergan, L. and Wilkinson, J.J. (Eds.) *Fractures, Fluid Flow and Mineralization*. Geological Society, London, Special Publications, 155, 123-140.

Cox, S.F., Knackstedt, M.A., Braun, J., (2001). Principles of structural control on permeability and fluid flow in hydrothermal systems. In: Richards, J.P., Tosdal, R.M. (Eds.), *Structural Controls on Ore Genesis. Reviews in Economic Geology*, p. 1–24.

De Kock, G.S., Eglinton B., Armstrong R.A., Harmer, R.E. and Walraven, F. (2000). U-Pb and Pb-Pb ages on the Naaupoort rhyolite, Kawakeup leptite and Okangava Diorite: implication for the onset of rifting and orogenesis in the Damara belt Namibia. *Communications of the Geological Survey of Namibia*, 12, 81-88.

Etheridge, M.A., (1983). Differential stress magnitudes during regional deformation and metamorphism: upper bound imposed by tensile fracturing. *Geology*, 1, 231–234.

Etheridge, M.A., Wall, V.J., Cox, S.F., Vernon, M.H., (1984). High fluid pressures during regional metamorphism and deformation: implications for mass transport and deformation mechanisms. *Journal of Geophysical Research*, 100, 4344–4358.

Gevers, T.W. (1931). Fundamental Complex of Western Damaraland, South West Africa- Unpublished. Doctor of Science thesis, University of Cape Town, p. 163.

Gillespie, P.A., Johnston, J.D., Loriga, E., McCaffrey, K.J.W., Walsh, J.J., Watterson, J., (1999). Influence of layering on vein systematics in line samples. In: McCaffrey, K.J.W., Lonegran, L., Wilkinson, J.J. (Eds.), *Fractures, Fluid Flow and Mineralization*, Geological Society Special Publication, 155, p. 35-56.

Goldfarb, R.J., Groves, D.I., Gardoll, S., (2001). Orogenic gold and geological time: a global synthesis. *Ore Geology Reviews*, 18, 1-75.

Gray, D.R., Foster, D.A., Goscombe, B., Passchier, C.W. & Trouw, R.A.J. (2006). $^{40}\text{Ar}/^{39}\text{Ar}$ thermochronology of the Pan-African Damara Orogen, Namibia, with implications for tectonothermal and geodynamic evolution. *Precambrian Research*, 150, 49–72.

Groves, D.I., Goldfarb, R.J., Gebre-Mariuam, M., Hagemann, S., Robert, F. (1998). Orogenic gold deposits: A proposed classification in the context of the crustal distribution and relationship to other gold deposit types. *Ore Geology Reviews*, 13, 7-28.

Groves, D.I., Goldfarb, R.J., Robert, F., Hart, C.J.R. (2003). Gold deposits in metamorphic belts: overview of current understanding, outstanding problems, future research and exploration significance. *Economic Geology*, 98, 1-29.

Hodgson, C.J. (1989). The structure of shear-related, vein-type gold deposits: a review. *Ore Geology Reviews*, 4, 231-273.

Hoffman, P.F., Hawkins, D.P., Isachsen, C.E. and Bowring, S.A. (1996). Precise U-Pb zircon ages for early Damaran magmatism in the Summas Mountains and Welwitschia inlier, northern Damara belt, Namibia. *Communications of the Geological Survey of Namibia*, 11, 47-52.

Hoffmann, K.-H., Condon, D.J., Bowring, S.A. and Crowley, J.L. (2004). U-Pb zircon date from the Neoproterozoic Ghaub Formation, Namibia: Constraints on Marinoan glaciation. *Geology*, 32, 817-820.

Hubbert, M.K., and Rubey W.W., (1959). Role of fluid pressure in mechanics of overthrust faulting. *Geol. Soc. America Bull*, 70, 115-166.

Jacob, R.E. (1974). Geology and metamorphic petrology of part of the Damara Orogen along the lower Swakop River, South West Africa. *Bull. Precambrian Res. Unit*, Univ. Cape Town, 17, p. 184.

Jacob, R.E., Kröner, A. and Burger, A.J. (1978). Areal extent and first U-Pb age of Pre-Damaran Abbabis Complex in the Central Damaran belt of South West Africa. *Geologische Rundschau*, 67, 706-718.

- Jacob, R.E., Snowden, P.A. and Bunting, F.J.L. (1983). Geology and structural development of the Tumas Basement Dome and its cover rocks. In: Miller, R.McG. (Ed), Evolution of the Damara Orogen of South West Africa. *Special Publication of the Geological Society of South Africa*, 11, 157-172.
- Jacob, R.E., Moore, J.M. and Armstrong, R.A. (2000). Zircon and titanite age determinations from igneous rocks in the Karibib District, Namibia: implications for Navachab vein-style gold mineralization. *Communications of the Geological Survey of Namibia*, 12, 157-166.
- Jaeger, J.C. (1963). Extension failures in rocks subject to fluid pressure. *Journal of Geophysical Research*, 68, 6066-6067.
- Johnson, S.D. (2005). Structural geology of the Usakos dome, Damara Belt, central Namibia. Unpublished MSc thesis, University of Stellenbosch, p. 159.
- Johnson, S.D., Poujol, M., Kisters, A.F.M. (2006). Constraining the timing and migration of collisional tectonics in the Damara Belt, Namibia: U-Pb zircon ages for the syntectonic Salem-type Stinkbank granite. *South African Journal of Geology*, 109, 427-440.
- Jung, S., Hoernes, S. and Mezger, K. (2001). Trace element and isotopic (Sr, Nd, Pb, O) arguments for a mid-crustal origin of Pan-African garnet-bearing S-type granites from the Damara orogen (Namibia). *Precambrian Research*, 110, 325-355.
- Jung, S. and Mezger, K. (2003). Petrology of basement-dominated terranes: I Regional metamorphic T-t path from U-Pb monazite and Sm-Nd garnet geochronology (Central Damara orogen, Namibia). *Chemical Geology*, 198, 223-247.
- Kerrick, R., Goldfarb, R.J., Groves, D.I., Garwin, S. (2000). The geodynamics of world-class gold deposits: Characteristics, space-time distribution and origins. In: Hagemann, S. and Brown, P.E. (eds.) Gold in 2000. *Reviews in Economic Geology*, pp.501-551.
- Kisters, A.F.M., Smith Jordaan, L. and Neumaier, K. (2004). Thrust-related dome structures in the Karibib district and the origin of orthogonal fabric domains in the south Central Zone of the Pan-African Damara belt, Namibia. *Precambrian Research*, 133, 283-303.
- Kisters, A.F.M. (2005). Controls of gold-quartz vein formation during regional folding in amphibolite-facies, marble-dominated metasediments of the Navachab Gold Mine, in the Pan-African Damara Belt, Namibia. *South African Journal of Geology*. 108, 365-380.
- Kretz, R. (1983). Symbols for rock-forming minerals. *American Mineralogist*, 68, 277-279.
- Kröner, A., Retief, E.A., Compston, W., Jacob, R.E. and Burger, A.J. (1991). Single-grain and conventional zircon dating of remobilized basement gneisses in the central Damara Belt of Namibia. *South African Journal of Geology*, 94, 279-387.

Masberg, H.P., Hoffer, E., Hoernes, S. (1992). Microfabrics indicating granulite-facies metamorphism in the low-pressure central Damara orogen Namibia. *Precambrian Research*, 55, 243–257.

Masberg, H.P. (2000). Garnet growth in medium pressure granulite-facies metapelites from the central Damara Orogen: igneous versus metamorphic history. *Communications of the Geological Survey of Namibia*, 12, 115-124.

Miller, R. McG. (1983). The Pan-African Damara Orogen of South West Africa/ Namibia. In: Miller, R.McG. (Ed.), Evolution of the Damara Orogen of South West Africa. *Geological Society of South Africa, Special Publication*, 11, 431-515.

Moore, J.M. and Jacob, R.E. (1998). The Navachab sheeted vein/skarn Au deposit, Namibia. *Abstract volume, Annual Conference of the Geological and Mineralogical Associations of Canada*, A125-A126.

Moore, J.M., Jacob, R.E., Harris, C. and Armstrong, R.A. (1999). The Navachab gold deposit, Namibia: a mesothermal sheeted-vein/skarn system related to the Pan-African Damara Orogen. *Journal of African Earth Sciences*, 28, 50-51.

Neumaier, K. (2002). Structural and lithological mapping of the Usakos dome, central Namibia, Unpublished Diploma mapping project. Ludwigs-Maximilians University, p. 70.

Nex P.A.M., Oliver, G.J.H. and Kinnaird, J. (2001). Spinel-bearing assemblages and P-T-t evolution of the Central Zone of the Damara Orogen, Namibia. *Journal of African Earth Sciences*, 32, 471-489.

Nörtemann, M.F.-J., Mücke, A., Weber, K., Meinert, L.D., (2000). Mineralogy of the Navachab skarn deposit, Namibia: an unusual Au-bearing skarn in highgrade metamorphic rocks. *Communications of the Geological Survey of Namibia*, 12, 149–156.

Olson, J.E., Pollard, D.D. (1991). The initiation and growth of en-echelon veins. *Journal of Structural Geology*, 13, 595-608.

Piranjo, F. and Jacob, R.E, (1991). Gold mineralization in the intracontinental branch of the Damara orogen, Namibia: a preliminary survey. *Journal of African Earth Sciences*, 13, 305-311.

Porada, H. (1989). Pan-African rifting and orogenesis in southern to equatorial Africa and eastern Brazil, *Precambrian Research*, 44, 103-138.

Prave, A.R. (1996). Tale of three cratons: Tectonostratigraphic anatomy of the Damara orogen in northwestern Namibia and the assembly of Gondwana. *Geology*, 24, 1115-1118.

Puhan, D. (1983). Temperature and pressure of metamorphism in the central Damara orogen. In: Miller, R. McG. (Ed.), Evolution of the Damara Orogen of South West Africa/Namibia. *Geological Society of South Africa, Special Publication*, vol. 11, 219–223.

Ridley, J.R. (1993). The relations between mean rock stress and fluid flow in the crust: With reference to vein- and lode-style gold deposits. *Ore Geology Reviews*, 8, 23-37.

Ridley, J. and Mengler, F. (2000). Lithological and structural controls on the form and setting of vein stockwork orebodies at the Mount Charlotte gold deposit, Kalgoorlie. *Economic Geology*, 95, 85-98.

Robert, F. and Poulsen, K.H. (2001). Vein Formation and deformation in greenstone gold deposits. *Reviews in Economic Geology*, 14, 111-155.

Schaubs, P.M. and Wilson, C.J.L. (2002). The relative roles of folding and faulting in controlling gold mineralization along the Deborah anticline, Bendigo, Victoria, Australia. *Economic Geology*, 97, 351-370.

Secor, D.T. (1965). Role of fluid pressure in jointing. *American Journal of Science*, 263, 633-646.

Sibson, R.H., Robert, F. and Poulsen, K.H. (1988). High-angle reverse faults, fluid pressure cycling and mesothermal gold-quartz deposits. *Geology*, 16, 551-555.

Sibson, R.H. (1996). Structural permeability of fluid-driven fault-fracture meshes. *Journal of Structural Geology*, 18, 1031-1042.

Sibson, R.H. and Scott, J. (1998). Stress/fault controls on the containment and release of overpressurized fluids: Examples from gold-quartz vein systems in Juneau, Alaska; Victoria, Australia; and Otago, New Zealand. *Ore Geology Reviews*, 13, 293-306.

Sibson, R.H. (2001). Seismogenic framework for hydrothermal transport and ore deposition. *Reviews in Economic Geology*, 14, 25-50.

Smith, D.A.M. (1965). The geology of an area around the Khan and Swakop Rivers in South West Africa. *Geological Society of South Africa Memoir, South West Africa Series*, 3, p. 113.

Stanistreet, I.G., Kukla, P.A. and Henry, G. (1991). Sedimentary basinal responses to a Late Precambrian Wilson Cycle: The Damara Orogen and Nama Foreland, Namibia. *Journal of African Earth Science*, 13, 141-156.

Steven, N.M. (1993). A study of Epigenetic Mineralization in the Central Zone of the Damara Orogen, Namibia, with special reference to gold, tungsten, tin and rare elements. *Memoirs of the Geological Survey of Namibia*, 16, p. 166.

Steven, N.M. and Badenhorst, F.P. (2002). Mesothermal gold deposits of the Damara Orogen. Excursion guidebook, 11th Quadrennial IAGOD Symposium and Geocongress, Windhoek, p. 225.

Steven, N.M. (2002). Report on the 1:10,000 geological mapping of the Navachab Corridor in 2002. Rockwater Consulting report for AngloGold Namibia Pty. Ltd., p. 34.

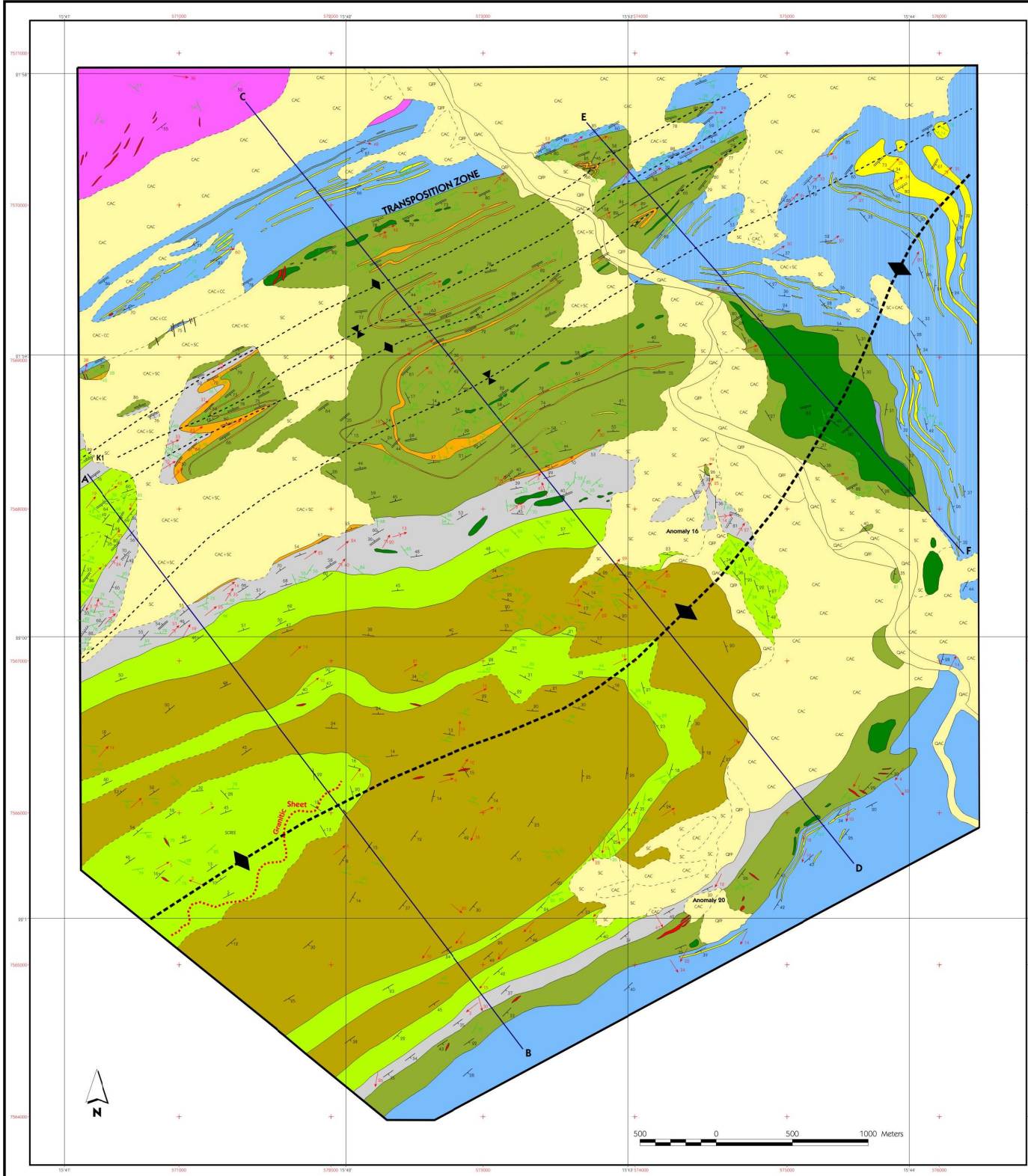
Steven, N.M., Badenhorst, F.P., Kitt, S. and Wulff, K. (2008). The Navachab gold deposit, Namibia: the largest non-Witwatersrand-type gold deposit in southern Africa. Extended Abstracts, SEG-GSSA Conference, Misty Hills, South Africa.

Trompette, R. (1997). Neoproterozoic (~600 Ma) aggregation of western Gondwana:

a tentative scenario. *Precambrian Research*. 82, 101–112.

Windh, J. (1995). Saddle reef and related gold mineralization, Hill End gold field, Australia: evolution of an auriferous vein system during progressive deformation. *Economic Geology*, 90, 1764-1774.

Wulff, K. (2008). Petrography, geochemistry and stable isotope characteristics of the Navachab gold deposit, Namibia. Unpublished Phd thesis, RWTH Aachen, Germany, p. 190.



- Quaternary and Tertiary legend**
- QTP Unconsolidated flood plain sediments
 - QAC Unconsolidated active channel sediments
 - SC Unconsolidated scree (colluvial)
 - CC Calcrite (in situ)
 - CAC Alluvial conglomerate with calcareous cement (consolidated)
- Structural Legend**
- Strike and dip of S0/S1 Foliation
 - Strike and dip of inverted S0
 - Strike and dip of S8 Foliation
 - Strike and dip of quartz vein
 - Strike and dip of fold axial plane
 - Plunge and plunge direction of fold axis
 - Plunge and plunge direction of all lineations
 - ∇ Cross sections
- Geological Contacts**
- - - Inferred
 - Observed
- Lithological legend (with Mine Lithological coding in brackets)**
- Pegmatite, apatite, granitic dyke
 - Kuabab fm ■ Biotite-concordite schist, metapsammites and calc-silicates felses
 - Dolomitic marble
 - Kaibab fm ■ Intraformational marble breccias
 - Calcareous marble
 - Amphibolites, mafic volcanics
 - Oberwasser fm ■ Calc-silicate felses
 - Biotite-concordite schists with intercalated calc-silicate felses and intraformational breccias
 - Olavayo fm ■ Intercalated calcareous marble and calc-silicate felses (WC), calcareous and spilitic marble (MBM) and amphibolites
 - Spies Bona fm ■ Metapsammites, biotite schists, calc-silicate felses
 - Biotite schist, calc-silicates felses

Geological Map of the NE part of the Usakos Dome

Compiled by : Shawn Kitt
 Date : June 2008
 Scale : 1 : 10 000
 Drafted by : SK

Appendix II
Navachab open pit sampling line vein data

Sampling Line 1		Area: Eastern Wall level 1050				
Sample no	At (m)	Vein Orientation		Thickness (cm)	Cumulative thickness (cm)	Spacing (m)
		Dip	Dip Direction			
1	0	28	47	2	2	0.8
2	3	42	58	3	5	0.5
3	5	35	46	3	8	5.2
4	25	42	69	1	9	0.3
5	26	50	75	1	10	0.5
6	28	50	66	2	12	1.0
7	32	48	58	2	14	1.6
8	38	45	72	2	16	2.1
9	46	36	60	1	17	0.3
10	47	54	84	1	18	1.0
11	51	33	77	3	21	2.3
12	60	46	90	2	23	0.5
13	62	47	82	1	24	2.1
14	70	34	50	1	25	2.1
15	78	37	73	1	26	0.3
16	79	19	65	1	27	1.3
17	84	35	79	1	28	0.5
18	86	24	76	1	29	1.0
19	90	30	75	1	30	0.5
20	92	14	32	5	35	2.1
21	100	40	75	2	37	1.3
22	105	57	88	2	39	3.1
23	117	41	60	2	41	1.3
24	122	20	45	5	46	1.8
25	129	24	348	20	66	1.8
26	136	13	10	5	71	1.0
27	140	18	57	5	76	3.4
28	153	22	71	3	79	0.5
29	155	30	50	3	82	0.8
30	158	14	53	4	86	2.6
31	168	16	360	5	91	1.3
32	173	25	55	3	94	3.1
33	185	34	330	4	98	0.3
34	186	36	77	3	101	3.6
35	200	26	333	4	105	1.3
36	205	24	334	2	107	1.3
37	210	26	76	5	112	0.5
38	212	21	40	2	114	0.5
39	214	16	340	8	122	1.6
40	220	22	320	7	129	3.4
41	233	26	56	4	133	3.6
42	247	10	310	2	135	6.5
43	272	23	360	2	137	0.8

44	275	22	2	5	142	0.8
45	278	21	325	2	144	5.7
46	300	10	320	2	146	

Sampling Line 2		Area: Eastern Wall level 1010				
Sample no	At (m)	Vein Orientation		Thickness (cm)	Cumulative thickness (cm)	Spacing (m)
		Dip	Dip Direction			
1	2	20	340	5	5	1.3
2	7	12	10	5	10	1.3
3	12	14	15	5	15	1.3
4	17	22	330	5	20	0.3
5	18	20	20	5	25	4.1
6	34	22	348	5	30	2.3
7	43	24	350	10	40	0.8
8	46	20	63	5	45	2.1
9	54	14	65	5	50	3.9
10	69	10	52	5	55	0.5
11	71	12	5	5	60	2.3
12	80	14	6	5	65	2.6
13	90	16	8	5	70	2.1
14	98	19	3	5	75	2.1
15	106	25	42	3	78	2.1
16	114	22	8	10	88	0.8
17	117	26	332	7	95	1.6
18	123	31	41	10	105	0.5
19	125	27	23	3	108	1.3
20	130	26	70	3	111	1.3
21	135	30	28	5	116	0.5
22	137	10	350	15	131	1.0
23	141	14	347	3	134	2.3
24	150	27	54	10	144	0.3
25	151	30	72	10	154	1.6
26	157	26	50	10	164	3.4
27	170	20	38	4	168	0.5
28	172	14	351	5	173	0.5
29	174	19	22	3	176	5.4
30	195	13	348	8	184	3.9
31	210	20	31	3	187	1.6
32	216	16	28	5	192	0.8
33	219	21	344	5	197	3.4
34	232	20	353	5	202	2.1
35	240	12	28	4	206	0.8
36	243	21	22	4	210	0.3
37	244	26	341	3	213	4.1
38	260	19	28	4	217	0.8
39	263	20	349	5	222	

Sampling Line 3		Area: Eastern Wall level 970				
Sample no	At (m)	Vein Orientation		Thickness (cm)	Cumulative thickness (cm)	Spacing (m)
		Dip	Dip Direction			
1	20	17	342	4	4	0.8
2	23	18	347	6	10	3.1
3	35	12	65	3	13	4.7
4	53	17	340	5	18	0.5
5	55	17	340	5	23	0.8
6	58	17	340	5	28	0.3
7	59	17	340	5	33	7.0
8	86	22	35	5	38	0.3
9	87	24	328	5	43	1.3
10	92	30	40	7	50	4.1
11	108	34	328	8	58	2.8
12	119	20	336	10	68	0.5
13	121	18	57	7	75	0.3
14	122	15	337	7	82	0.3
15	123	12	3	7	89	2.3
16	132	15	348	3	92	0.8
17	135	22	24	8	100	2.6
18	145	20	340	5	105	3.4
19	158	28	320	10	115	1.3
20	163	20	335	7	122	1.8
21	170	20	335	5	127	2.6
22	180	34	338	12	139	1.8
23	187	26	323	10	149	1.3
24	192	32	318	10	159	4.4
25	209	19	324	10	169	2.1
26	217	20	320	8	177	2.6
27	227	15	350	5	182	1.8
28	234	17	50	7	189	1.0
29	238	30	347	8	197	0.3
30	239	19	350	5	202	1.6
31	245	25	323	3	205	1.8
32	252	31	330	7	212	1.3
33	257	30	320	5	217	1.8
34	264	32	320	5	222	1.3
35	269	30	320	5	227	

Sampling Line 4		Area: Northern wall level 980				
Sample no	At (m)	Vein Orientation		Thickness (cm)	Cumulative thickness (cm)	Spacing (m)
		Dip	Dip Direction			
1	1	11	32	2	2	1.5
2	4	27	8	12	14	3
3	10	20	347	8	22	1
4	12	27	320	8	30	1.5
5	15	10	28	6	36	1.5
6	18	14	355	5	41	1.5
7	21	42	357	4	45	

Sampling Line 5		Area: Western wall: west ramp				
Sample no	At (m)	Vein Orientation		Thickness (cm)	Cumulative thickness (cm)	Spacing (m)
		Dip	Dip Direction			
1	4	24	355	4	4	2.8
2	15			1	5	1.8
3	22	28	345	7	12	0.3
4	23			5	17	0.3
5	24			5	22	1.3
6	29			3	25	4.9
7	48			3	28	4.4
8	65			2	30	1.6
9	71	19	20	1	31	0.8
10	74			2	33	0.5
11	76			1	34	0.3
12	77			1	35	0.5
13	79			3	38	0.5
14	81			5	43	0.5
15	83			1	44	0.5
16	85			1	45	2.1
17	93			3	48	1.0
18	97	28	50	3	51	0.8
19	100			1	52	0.5
20	102			2	54	4.9
21	121			1	55	1.3
22	126			3	58	0.3
23	127			3	61	0.1

24	127.5			1	62	0.1
25	128			3	65	0.1
26	128.5			2	67	0.1
27	129	12	45	1	68	0.1
28	129.5			5	73	0.1
29	130			1	74	0.3
30	131			2	76	0.1
31	131.5			2	78	14.6
32	188			5	83	4.4
33	205			3	86	1.3
34	210			1	87	1.3
35	215			2	89	4.7
36	233			3	92	4.9
37	252			2	94	4.7
38	270			2	96	0.5
39	272			2	98	3.4
40	285			3	101	1.0
41	289			2	103	

Sampling Line 6		Area: Western wall: west ramp				
Sample no	At (m)	Vein Orientation		Thickness (cm)	Cumulative thickness (cm)	Spacing (m)
		Dip	Dip Direction			
1	5	38	318	13	13	1.6
2	11	35	310	15	28	1.0
3	15	14	3	3	31	0.5
4	17	20	345	5	36	0.5
5	19	20	330	5	41	0.5
6	21	19	323	5	46	0.3
7	22	20	340	5	51	1.3
8	27	20	335	5	56	0.8
9	30	15	333	10	66	2.1
10	38	14	13	10	76	3.1
11	50	33	350	2	78	0.3
12	51	38	315	2	80	2.1
13	59	25	350	2	82	4.4
14	76	30	318	5	87	1.3
15	81	25	335	5	92	1.3
16	86	18	85	5	97	0.5
17	88	25	37	5	102	2.3
18	97	16	8	2	104	1.6
19	103	20	3	2	106	5.2
20	123	23	356	5	111	0.5
21	125	20	52	8	119	1.0

22	129	20	40	2	121	0.3
23	130	30	38	2	123	1.3
24	135	55	36	2	125	3.9
25	150	15	10	10	135	1.0
26	154	28	66	1	136	2.8
27	165	10	350	2	138	1.3
28	170	15	355	2	140	2.1
29	178	24	340	5	145	0.5
30	180	30	38	5	150	2.8
31	191	28	50	10	160	1.6
32	197	20	55	7	167	0.8
33	200	24	66	8	175	1.0
34	204	11	357	7	182	3.4
35	217	13	346	10	192	5.4
36	238	15	22	5	197	1.0
37	242	21	30	5	202	1.8
38	249	23	22	5	207	1.0
39	253	16	27	6	213	2.6
40	263	23	28	4	217	1.3
41	268	15	20	5	222	0.5
42	270	13	22	5	227	3.4
43	309	15	15	4	231	2.6
44	316	20	34	5	236	5.2
45	335	28	352	1	237	2.6
46	345	24	70	3	240	3.1
47	357	21	15	10	250	1.8
48	367	28	22	10	260	

Appendix III
Navachab open pit diamond drillhole data

N271		Okawayo Formation marbles		
Sample no	Sheeted quartz veins			
	At (m)	Thickness (cm)	Cumulative thickness (cm)	Spacing (m)
1	7.42	1	1	1.73
2	9.15	1	2	9.13
3	18.28	1	3	10.01
4	28.29	1	4	2.04
5	30.33	1	5	4.83
6	35.16	5	10	5.34
7	40.5	2	12	3.5
8	44	1	13	0.19
9	44.19	0	13	2.35
10	46.54	1	14	17.04
11	63.58	0.5	14.5	0.85
12	64.43	0.5	15	3.18
13	67.61	1	16	2.83
14	70.44	2	18	12.45
15	82.89	1	19	0.46
16	83.35	2	21	1.34
17	84.69	2	23	2.38
18	87.07	2	25	7.47
19	94.54	1	26	0.57
20	95.11	1	27	5.78
21	100.89	1	28	2.04
22	102.93	1	29	0.96
23	103.89	1	30	1.18
24	105.07	1	31	2.55
25	107.62	1	32	3.35
26	110.97	1	33	5.3
27	116.27	15	48	1.53
28	117.8	10	58	14.17
29	131.97	10	68	3.91
30	135.88	5	73	2.98
31	138.86	3	76	21.99
32	160.85	1	77	1.04
33	161.89	1	78	0.96
34	162.85	1	79	4.95
35	167.8	5	84	0.16
36	167.96	1	85	1.4

37	169.36	0.5	85.5	0.83
38	170.19	0.5	86	2.58
39	172.77	0.5	86.5	1.17
40	173.94	0.5	87	0.4
41	174.34	0.5	87.5	0.34
42	174.68	0.5	88	0.86
43	175.54	0.5	88.5	1.38
44	176.92	1	89.5	0.28
45	177.2	1	90.5	2.07
46	179.27	2	92.5	2
47	181.27	1	93.5	1.6
48	182.87	1	94.5	0.58
49	183.45	1	95.5	2.43
50	185.88	0.5	96	1.52
51	187.4	2	98	1.32
52	188.72	22	120	0.95
53	189.67	1	121	3.63
54	193.3	0.5	121.5	0.4
55	193.7	1	122.5	3.54
56	197.24	1	123.5	1.43
57	198.67	0.5	124	1.2
58	199.87	3	127	1.61
59	201.48	1	128	3.42
60	204.9	10	138	2.8
61	207.7	10	148	1.71
62	209.41	20	168	2.1
63	211.51	2	170	0.41
64	211.92	0.5	170.5	1.17
65	213.09	2	172.5	2.34
66	215.43	1	173.5	1.03
67	216.46	1	174.5	0.98
68	217.44	1	175.5	0.43
69	217.87	0.5	176	1.73
70	219.6	0.5	176.5	0.67
71	220.27	10	186.5	0.46
72	220.73	10	196.5	1.86
73	222.59	5	201.5	1.38
74	223.97	2	203.5	0.84
75	224.81	1	204.5	10.98
76	235.79	1	205.5	1.96
77	237.75	2	207.5	5.88
78	243.63	1	208.5	7.97
79	251.6	0.5	209	1.03
80	252.63	1	210	1.02
81	253.65	0.5	210.5	1.37

82	255.02	0.5	211	2.17
83	257.19	1	212	2.2
84	259.39	1	213	2.71
85	262.1	2	215	0.35
86	262.45	0.5	215.5	0.74
87	263.19	0.5	216	0.31
88	263.5	2	218	0.52
89	264.02	1	219	2.87
90	266.89	0.5	219.5	1.08
91	267.97	0.5	220	1.6
92	269.57	1	221	5.46
93	275.03	0.5	221.5	11.12
94	286.15	1	222.5	1.05
95	287.2	2	224.5	2.69
96	289.89	4	228.5	8.96
97	298.85	1	229.5	1.84
98	300.69	1	230.5	2.04
99	302.73	3	233.5	7.36
100	310.09	4	237.5	1.47
101	311.56	1	238.5	3.69
102	315.25	2	240.5	2.83
103	318.08	2	242.5	1.71
104	319.79	5	247.5	3.12
105	322.91	2	249.5	1.81
106	324.72	3	252.5	4.82
107	329.54	3	255.5	5.65
108	335.19	2	257.5	2.68
109	337.87	2	259.5	1.11
110	338.98	1	260.5	2.02
111	341	0.5	261	8.44
112	349.44	1	262	

N527		Spes Bona Formation schist		
Sample no	Sheeted quartz veins			
	At (m)	Thickness (cm)	Cumulative thickness (cm)	Spacing (m)
1	2.57	1	1	0.37
2	2.94	1	2	3.16
3	6.1	6	8	4.8
4	10.9	7	15	2.61
5	13.51	1	16	2.32
6	15.83	6	22	1.5
7	17.33	1	23	6.12
8	23.45	2	25	0.8
9	24.25	21	46	2.68

10	26.93	1	47	0.22
11	27.15	2	49	0.95
12	28.1	5	54	0.67
13	28.77	8	62	0.89
14	29.66	8	70	4.23
15	33.89	16	86	2.57
16	36.46	7	93	0.64
17	37.1	5	97	0.15
18	37.25	3	100	0.25
19	37.5	2	102	2.15
20	39.65	20	122	1.13
21	40.78	1	123	0.77
22	41.55	2	125	2.38
23	43.93	3	128	1.29
24	45.22	12	140	2.55
25	47.77	15	155	2.83
26	50.6	5	160	3.05
27	53.65	15	175	0.8
28	54.45	14	189	1.87
29	56.32	8	197	1.69
30	58.01	10	207	1.79
31	59.8	14	221	2.27
32	62.07	7	228	0.55
33	62.62	9	237	2.52
34	65.14	2	239	2.34
35	67.48	5	244	1.77
36	69.25	5	249	0.93
37	70.18	4	253	1.88
38	72.06	6	259	2.6
39	74.66	10	268	1.15
40	75.81	4	272	5.54
41	81.35	8	279	1.06
42	82.41	4	283	1.09
43	83.5	0	284	0.13
44	83.63	0	284	0.93
45	84.56	2	286	0.44
46	85	1	287	0.75
47	85.75	6	293	1.67
48	87.42	6	298	0.98
49	88.4	2	300	0.17
50	88.57	3	303	0.08
51	88.65	2	305	0.1
52	88.75	3	308	3.4
53	92.15	2	310	2
54	94.15	3	313	2.8

55	96.95	11	324	1.05
56	98	1	326	0.38
57	98.38	0	326	0.04
58	98.42	0	326	0.16
59	98.58	1	327	0.1
60	98.68	1	327	2.47
61	101.15	1	328	0.2
62	101.35	1	329	0.12
63	101.47	2	331	1.08
64	102.55	3	333	1.86
65	104.41	1	334	1.01
66	105.42	2	337	1.63
67	107.05	2	338	1.65
68	108.7	9	347	6.05
69	114.75	2	349	3.1
70	117.85	7	356	5.37
71	123.22	2	357	0.16
72	123.38	2	360	0.62
73	124	0	360	0.35
74	124.35	3	363	0.28
75	124.63	3	365	0.87
76	125.5	4	369	0.1
77	125.6	4	373	0.5
78	126.1	5	378	0.45
79	126.55	1	379	3.71
80	130.26	3	382	6.84
81	137.1	3	386	1.06
82	138.16	4	389	0.49
83	138.65	2	391	1.68
84	140.33	4	395	3.55
85	143.88	4	399	0.66
86	144.54	13	412	4.87
87	149.41	4	416	1.69
88	151.1	12	428	4.75
89	155.85	2	430	1.06
90	156.91	15	445	1.06
91	157.97	4	449	1.18
92	159.15	4	453	0.27
93	159.42	4	457	0.33
94	159.75	1	458	1.63
95	161.38	11	469	7.64
96	169.02	9	478	2.58
97	171.6	12	490	0.05
98	171.65	3	492	1.35
99	173	2	494	2.46

100	175.46	12	506	0.27
101	175.73	3	509	1.27
102	177	7	515	2.15
103	179.15	1	517	0.25
104	179.4	8	525	0.08
105	179.48	2	526	0.12
106	179.6	2	528	0.86
107	180.46	4	532	2.64
108	183.1	9	541	1.12
109	184.22	2	543	2.48
110	186.7	4	546	4.74
111	191.44	3	549	2.96
112	194.4	2	551	0.78
113	195.18	1	552	4.14
114	199.32	2	555	3.68
115	203	6	561	1.95
116	204.95	2	562	1.7
117	206.65	1	563	0.34
118	206.99	1	564	2.09
119	209.08	1	565	0.38
120	209.46	5	570	0.74
121	210.2	4	574	0.75
122	210.95	10	584	0.31
123	211.26	16	600	3.15
124	214.41	12	611	1.07
125	215.48	1	613	1.14
126	216.62	4	616	0.74
127	217.36	16	632	3.46
128	220.82	3	635	0.65
129	221.47	5	639	1.13
130	222.6	1	640	0.86
131	223.46	5	645	

N550		Spes Bona Formation schist		
Sample no	Sheeted quartz veins			
	At (m)	Thickness (cm)	Cumulative thickness (cm)	Spacing (m)
1	4.07	2	1.8	0.78
2	4.85	3	5	2.9
3	7.75	3	8	2.83
4	10.58	1	9.2	1.96
5	12.54	3	12.4	1.8
6	14.34	8	20.4	2.78
7	17.12	7	27.4	0.14

8	17.26	1	28.4	1.07
9	18.33	6	34.4	1.5
10	19.83	3	37.4	1.07
11	20.9	4	40.9	1.73
12	22.63	1	41.9	1.37
13	24	9	50.9	6.27
14	30.27	10	60.9	0.53
15	30.8	2	62.4	5.93
16	36.73	9	71.4	6.22
17	42.95	2	72.9	1.49
18	44.44	14	86.9	1.16
19	45.6	3	90	6.06
20	51.66	8	98	0.56
21	52.22	8	106	5.31
22	57.53	7	112.5	5.29
23	62.82	12	124.5	0.73
24	63.55	11	135.5	2.2
25	65.75	12	147.5	1.45
26	67.2	1	148.5	0.86
27	68.06	1	149.5	1.21
28	69.27	2	151.6	2.88
29	72.15	12	163.6	6.7
30	78.85	9	172.6	0.65
31	79.5	6	178.1	0.1
32	79.6	11	189.1	0.15
33	79.75	5	194.1	1.3
34	81.05	4	198.1	4.57
35	85.62	3	201.2	2.74
36	88.36	1	202.2	0.83
37	89.19	4	205.7	1.61
38	90.8	5	210.2	0.15
39	90.95	3	212.7	0.38
40	91.33	2	214.2	0.09
41	91.42	1	215.4	0.04
42	91.46	1	216.6	2.2
43	93.66	1	217.1	0.04
44	93.7	1	218	0.6
45	94.3	0	218.4	0.04
46	94.34	0	218.8	0.33
47	94.67	2	220.8	4.18
48	98.85	15	235.8	0.45
49	99.3	6	241.8	0.39
50	99.69	6	247.3	0.71
51	100.4	3	250.3	2.69
52	103.09	3	252.8	0.99

53	104.08	8	260.8	1.62
54	105.7	2	262.3	0.94
55	106.64	7	269.3	1.18
56	107.82	3	271.8	1.21
57	109.03	1	272.7	0.31
58	109.34	4	276.2	0.51
59	109.85	1	277	1.08
60	110.93	18	295	1.07
61	112	4	298.8	2.02
62	114.02	5	303.3	3.62
63	117.64	25	328.3	3.81
64	121.45	4	332.3	1.08
65	122.53	3	335.3	0.87
66	123.4	8	343.3	3.45
67	126.85	4	347.3	8.1
68	134.95	8	355.3	3.95
69	138.9	2	357.3	1.26
70	140.16	5	361.8	0.16
71	140.32	1	363	1.43
72	141.75	3	366	2.51
73	144.26	4	370	6.92
74	151.18	4	374	4.08
75	155.26	9	382.5	

N554		Okawayo Formation marbles		
Sample no	Sheeted quartz veins			
	At (m)	Thickness (cm)	Cumulative thickness (cm)	Spacing (m)
1	5.2	1	1	2.28
2	7.48	1	2	8.71
3	16.19	3	5	4.83
4	21.02	1	6	9.86
5	30.88	3	9	9.77
6	40.65	1	10	12.19
7	52.84	2	12	2.7
8	55.54	1	13	6.38
9	61.92	1	14	4.47
10	66.39	2	16	7.77
11	74.16	1	17	11.71
12	85.87	2	19	5.45
13	91.32	1	20	2.65
14	93.97	1	21	1.75
15	95.72	1	22	0.2
16	95.92	1	23	1.77

17	97.69	1	24	0.55
18	98.24	1	25	5.88
19	104.12	1	26	4.49
20	108.61	2	28	0.95
21	109.56	2	30	2.65
22	112.21	1	31	1.43
23	113.64	4	35	2.77
24	116.41	1	36	5.91
25	122.32	1	37	1.89
26	124.21	3	40	0.76
27	124.97	1	41	2.03
28	127	1	42	1.63
29	128.63	1	43	1.82
30	130.45	1	44	1.44
31	131.89	1	45	2.13
32	134.02	1	46	0.98
33	135	1	47	1.29
34	136.29	1	48	1.52
35	137.81	1	49	1.1
36	138.91	1	50	4.88
37	143.79	3	53	1.87
38	145.66	5	58	0.61
39	146.27	5	63	1.73
40	148	1	64	0.91
41	148.91	1	65	1.06
42	149.97	1	66	1.49
43	151.46	1	67	1.33
44	152.79	2	69	2.21
45	155	2	71	1.06
46	156.06	2	73	0.08
47	156.14	3	76	1.49
48	157.63	1	77	0.43
49	158.06	10	87	0.94
50	159	10	97	0.28
51	159.28	3	100	1.17
52	160.45	10	110	1.35
53	161.8	1	111	1.04
54	162.84	1	112	2.66
55	165.5	1	113	1.47
56	166.97	1	114	2.81
57	169.78	1	115	1.53
58	171.31	1	116	1.12
59	172.43	1	117	0.15
60	172.58	20	137	1.09
61	173.67	1	138	1.38

62	175.05	1	139	0.65
63	175.7	15	154	2.59
64	178.29	5	159	3.21
65	181.5	4	163	0.28
66	181.78	4	167	2.44
67	184.22	1	168	1.08
68	185.3	5	173	2.18
69	187.48	11	184	0.58
70	188.06	3	187	1.54
71	189.6	1	188	1.4
72	191	5	193	1.96
73	192.96	4	197	0.58
74	193.54	1	198	

N556		Okawayo Formation marbles		
Sample no	Sheeted quartz veins			
	At (m)	Thickness (cm)	Cumulative thickness (cm)	Spacing (m)
1	6.35	2	2	2.7
2	9.05	1	3	4.55
3	13.6	3	6	6.4
4	20	0.5	6.5	0.6
5	20.6	1	7.5	1.85
6	22.45	5	12.5	2.25
7	24.7	1	13.5	0.48
8	25.18	5	18.5	0.65
9	25.83	2	20.5	1.32
10	27.15	2	22.5	12.35
11	39.5	2	24.5	0.7
12	40.2	2	26.5	1.55
13	41.75	10	36.5	1.4
14	43.15	3	39.5	2.5
15	45.65	3	42.5	0.25
16	45.9	3	45.5	0.3
17	46.2	1	46.5	2.05
18	48.25	1	47.5	0.4
19	48.65	1	48.5	2.9
20	51.55	15	63.5	0.93
21	52.48	1	64.5	3.92
22	56.4	10	74.5	1.43
23	57.83	1	75.5	0.72
24	58.55	10	85.5	5.2
25	63.75	15	100.5	5.55
26	69.3	0.5	101	0.75
27	70.05	0.5	101.5	0.78

28	70.83	0.5	102	0.27
29	71.1	0.5	102.5	0.73
30	71.83	0.5	103	4
31	75.83	0.5	103.5	0.36
32	76.19	0.5	104	0.17
33	76.36	0.5	104.5	1.54
34	77.9	2	106.5	0.25
35	78.15	2	108.5	0.55
36	78.7	2	110.5	1.42
37	80.12	0.5	111	0.52
38	80.64	0.5	111.5	0.86
39	81.5	1	112.5	0.37
40	81.87	1	113.5	0.13
41	82	0.5	114	0.3
42	82.3	0.5	114.5	0.37
43	82.67	0.5	115	0.73
44	83.4	1	116	0.65
45	84.05	0.5	116.5	0.72
46	84.77	0.5	117	0.16
47	84.93	1	118	0.67
48	85.6	1	119	0.51
49	86.11	0.5	119.5	0.39
50	86.5	0.5	120	0.22
51	86.72	0.5	120.5	0.58
52	87.3	1	121.5	0.76
53	88.06	0.5	122	0.88
54	88.94	0.5	122.5	0.16
55	89.1	1	123.5	0.5
56	89.6	1	124.5	3
57	92.6	2	126.5	1.5
58	94.1	3	129.5	6.85
59	100.95	3	132.5	4.83
60	105.78	3	135.5	7.15
61	112.93	3	138.5	5.12
62	118.05	1	139.5	3.03
63	121.08	1	140.5	3.07
64	124.15	2	142.5	2.35
65	126.5	0.5	143	3.7
66	130.2	1	144	2.93
67	133.13	1	145	4.12
68	137.25	1	146	4.1
69	141.35	1	147	2.15
70	143.5	1	148	6.2
71	149.7	1	149	0.2
72	149.9	2	151	0.25

73	150.15	1	152	0.95
74	151.1	3	155	0.6
75	151.7	2	157	0.78
76	152.48	2	159	0.17
77	152.65	1	160	0.23
78	152.88	3	163	0.92
79	153.8	1	164	0.4
80	154.2	1	165	0.55
81	154.75	3	168	2.75
82	157.5	2	170	0.2
83	157.7	1	171	5.39
84	163.09	1	172	0.94
85	164.03	1	173	0.02
86	164.05	0.5	173.5	1.05
87	165.1	1	174.5	0.8
88	165.9	0.5	175	0.3
89	166.2	0.5	175.5	1.9
90	168.1	1	176.5	0.25
91	168.35	1	177.5	0.27
92	168.62	0.5	178	0.24
93	168.86	1	179	2.14
94	171	1	180	7.75
95	178.75	0.5	180.5	0.52
96	179.27	1	181.5	2.03
97	181.3	1	182.5	1
98	182.3	1	183.5	1.3
99	183.6	0.5	184	0.95
100	184.55	1	185	2.45
101	187	1	186	0.3
102	187.3	1	187	0.88
103	188.18	1	188	2.42
104	190.6	1	189	10.55
105	201.15	2	191	0.75
106	201.9	3	194	2.55
107	204.45	5	199	2.72
108	207.17	2	201	2.83
109	210	1	202	3.65
110	213.65	3	205	0.51
111	214.16	2	207	0.69
112	214.85	1	208	2.45
113	217.3	1	209	0.33
114	217.63	1	210	1.14
115	218.77	3	213	5.15
116	223.92	5	218	2.03
117	225.95	5	223	5.21

118	231.16	1	224	1.64
119	232.8	1	225	1.05
120	233.85	5	230	2.42
121	236.27	5	235	

N570		Oberwasser Formation schist		
Sample no	Sheeted quartz veins			
	At (m)	Thickness (cm)	Cumulative thickness (cm)	Spacing (m)
1	53.13	4	4	1.17
2	54.3	5	9	4.88
3	59.18	1	10	1.46
4	60.64	1	11	1.38
5	62.02	2	13	0.9
6	62.92	1	14	5.27
7	68.19	1	15	0.34
8	68.53	1	16	2.7
9	71.23	2	18	9.27
10	80.5	5	23	4.71
11	85.21	2	25	0.85
12	86.06	2	27	5.12
13	91.18	1	28	2.16
14	93.34	1	29	5.34
15	98.68	5	34	2.41
16	101.09	2	36	3.06
17	104.15	1	37	3.13
18	107.28	1	38	1.99
19	109.27	1	39	0.85
20	110.12	2	41	0.48
21	110.6	1	42	3.42
22	114.02	5	47	1.3
23	115.32	1	48	1.2
24	116.52	3	51	7.74
25	124.26	1	52	2.89
26	127.15	1	53	3.89
27	131.04	2	55	2.51
28	133.55	5	60	3.94
29	137.49	5	65	0.09
30	137.58	1	66	1.56
31	139.14	1	67	0.63
32	139.77	5	72	3.03
33	142.8	5	77	4
34	146.8	1	78	1.36
35	148.16	5	83	4.55
36	152.71	1	84	6.37

37	159.08	2	86	3.63
38	162.71	1	87	0.15
39	162.86	1	88	8.06
40	170.92	5	93	2.94
41	173.86	4	97	0.1
42	173.96	2	99	1.62
43	175.58	2	101	3.85
44	179.43	5	106	1.76
45	181.19	3	109	6.91
46	188.1	2	111	14.45
47	202.55	4	115	21.23
48	223.78	2	117	1.8
49	225.58	1	118	2.76
50	228.34	1	119	6.97
51	235.31	5	124	2.55
52	237.86	5	129	1.52
53	239.38	10	139	7
54	246.38	5	144	1.21
55	247.59	2	146	3.57
56	251.16	4	150	2.89
57	254.05	4	154	6.33
58	260.38	10	164	3.38
59	263.76	7	171	4.87
60	268.63	2	173	1.02
61	269.65	3	176	3.62
62	273.27	4	180	1.86
63	275.13	3	183	3.25
64	278.38	2	185	1.3
65	279.68	8	193	2.09
66	281.77	2	195	0.15
67	281.92	2	197	2.62
68	284.54	2	199	1.63
69	286.17	10	209	10.6
70	296.77	10	219	1.96
71	298.73	5	224	6.96
72	305.69	4	228	2.37
73	308.06	5	233	14.64
74	322.7	5	238	

N573		Spes Bona Formation schist		
Sample no	Sheeted quartz veins			
	At (m)	Thickness (cm)	Cumulative thickness (cm)	Spacing (m)

1	86.5	4	4	1.79
2	88.29	2	6	3.84
3	92.13	5	11	13.07
4	105.2	2	13	2.14
5	107.34	1	14	1.79
6	109.13	5	19	5.52
7	114.65	2	21	2.91
8	117.56	1	22	2.33
9	119.89	2	24	3.01
10	122.9	6	30	4.07
11	126.97	1	31	2.88
12	129.85	3	34	1.65
13	131.5	1	35	0.67
14	132.17	2	37	6.01
15	138.18	5	42	0.37
16	138.55	13	55	1.67
17	140.22	6	61	2.08
18	142.3	6	67	1.56
19	143.86	2	69	1.78
20	145.64	3	72	3.09
21	148.73	6	78	1.8
22	150.53	2	80	1.43
23	151.96	4	84	1.61
24	153.57	2	86	2.3
25	155.87	5	91	1.23
26	157.1	3	94	3.28
27	160.38	5	99	1.88
28	162.26	20	119	0.51
29	162.77	5	124	0.11
30	162.88	1	125	1.02
31	163.9	10	135	2.2
32	166.1	5	140	0.34
33	166.44	4	144	2.51
34	168.95	2	146	3.41
35	172.36	1	147	3.71
36	176.07	6	153	8.85
37	184.92	5	158	1.89
38	186.81	3	161	0.82
39	187.63	6	167	1.54
40	189.17	2	169	0.23
41	189.4	7	176	2.46
42	191.86	20	196	0.86
43	192.72	10	206	0.59
44	193.31	5	211	0.32
45	193.63	2	213	0.4

46	194.03	4	217	2.99
47	197.02	10	227	0.23
48	197.25	2	229	1.42
49	198.67	20	249	1.53
50	200.2	15	264	0.28
51	200.48	1	265	3.65
52	204.13	5	270	0.97
53	205.1	4	274	0.18
54	205.28	3	277	1.74
55	207.02	4	281	0.28
56	207.3	2	283	1.25
57	208.55	3	286	0.51
58	209.06	1	287	0.8
59	209.86	2	289	6.17
60	216.03	1	290	1.12
61	217.15	3	293	1.3
62	218.45	3	296	3.28
63	221.73	6	302	1.59
64	223.32	3	305	1.14
65	224.46	6	311	4.17
66	228.63	6	317	2.93
67	231.56	4	321	1.57
68	233.13	2	323	0.85
69	233.98	2	325	0.47
70	234.45	2	327	0.51
71	234.96	7	334	2.24
72	237.2	3	337	0.86
73	238.06	5	342	1.67
74	239.73	2	344	1.84
75	241.57	7	351	0.1
76	241.67	5	356	

Appendix IV
Anomaly 16 diamond drillhole data

Area: Anomaly 16			ND 10		
At	Dip	Vein Orientation		Cumulative thickness (cm)	Spacing (m)
		Dip direction	Thickness (cm)		
37.7	37	55	3	3	1.25
38.95	35	55	2	5	0.2
39.15	28	60	3	8	1.71
40.86	30	68	3	11	2.06
42.92	41	78	1	12	2.5
45.42	41	35	1	13	1.54
46.96	36	53	2	15	0.24
47.2	42	60	2	17	1.25
48.45	31	60	3	20	1.59
50.04	35	60	1	21	1.56
51.6	25	56	7	28	1.3
52.9	25	62	3	31	0.58
53.48	36	52	2	33	1.94
55.42	28	20	1	34	1.61
57.03	30	58	0.5	34.5	1.44
58.47	46	55	0.5	35	0.26
58.73	31	57	1	36	1.02
59.75	29	77	1	37	0.05
59.8	32	54	2	39	1.91
61.71	34	56	1	40	0.12
61.83	30	55	1	41	0.87
62.7	20	40	1	42	0.35
63.05	23	58	1	43	0.4
63.45	20	59	2	45	1.15
64.6	36	67	1	46	0.3
64.9	29	58	1	47	0.73
65.63	34	67	4	51	1.17
66.8	37	64	1	52	0.17
66.97	38	52	1	53	0.71
67.68	29	63	1	54	0.74
68.42	38	72	1	55	0.28
68.7	34	60	2	57	

Area: Anomaly 16			ND 16		
At	Dip	Vein Orientation		Cummulative thickness (cm)	Spacing (m)
		Dip direction	Thickness (cm)		
42.2	24	50	1	1	1.4
43.6	15	60	0.5	1.5	0.1
43.7	12	53	0.5	2	1.24
44.94	6	48	1	3	1.11
46.05	14	55	2	5	0.38
46.43	28	72	1	6	0.19
46.62	25	72	0.5	6.5	1.28
47.9	37	54	1	7.5	0.5
48.4	29	60	3	10.5	3.1
51.5	42	50	2	12.5	2.97
54.47	30	53	5	17.5	6.08
60.55	30	50	4	21.5	4
64.55	29	47	2	23.5	2.3
66.85	30	50	3	26.5	

Area: Anomaly 16			ND 17		
At	Dip	Vein Orientation		Cummulative thickness (cm)	Spacing (m)
		Dip direction	Thickness (cm)		
40.34	34	58	1	1	4.07
44.41	29	79	2	3	1.04
45.45	37	51	0.5	3.5	1.59
47.04	19	78	0.5	4	0.16
47.2	12	70	1	5	0.68
47.88	20	52	4	9	0.35
48.23	21	46	1	10	0.18
48.41	20	55	0.5	10.5	1.89
50.3	24	48	0.5	11	0.8
51.1	27	48	1	12	1.86
52.96	26	73	2	14	0.24
53.2	21	46	2	16	2

55.2	23	38	2	18	1.2
56.4	32	80	0.5	18.5	2.33
58.73	18	53	3	21.5	0.75
59.48	31	57	3	24.5	3.57
63.05	14	48	1	25.5	0.67
63.72	21	44	1	26.5	0.76
64.48	30	44	1	27.5	1.29
65.77	25	38	0.5	28	2.59
68.36	17	45	0.5	28.5	0.66
69.02	22	50	3	31.5	

Area: Anomaly 16			ND 18		
At	Dip	Vein Orientation		Cummulative thickness (cm)	Spacing (m)
		Dip direction	Thickness (cm)		
31.72	20	40	1.5	1.5	1.07
32.79	14	50	1	2.5	1.98
34.77	13	64	2	4.5	0.61
35.38	20	50	0.5	5	4.37
39.75	12	27	5	10	2.33
42.08	17	48	1	11	3.72
45.8	14	57	3	14	0.17
45.97	22	50	3	17	4.45
50.42	14	35	0.5	17.5	0.2
50.62	18	60	5	22.5	0.17
50.79	10	42	1	23.5	0.06
50.85	15	39	1	24.5	0.26
51.11	15	45	0.5	25	0.08
51.19	22	76	0.5	25.5	0.4
51.59	11	51	0.5	26	0.93
52.52	20	87	2	28	0.33
52.85	21	83	10	38	1.15
54	22	48	1	39	0.09
54.09	20	55	1	40	0.11
54.2	17	52	1	41	0.5
54.7	22	82	0.5	41.5	0.05
54.75	21	73	0.5	42	4.16
58.91	26	93	2	44	0.95
59.86	28	64	0.5	44.5	0.96
60.82	15	58	3	47.5	1.08
61.9	21	77	0.5	48	1.9

63.8	15	76	2	50	0.12
63.92	24	83	1	51	0.35
64.27	15	30	2	53	0.48
64.75	22	49	0.5	53.5	1.03
65.78	49	100	4	57.5	1.02
66.8	30	74	2	59.5	0.63
67.43	27	61	3	62.5	2.01
69.44	20	80	2	64.5	